CATALYST DEVELOPMENT FOR THE CATALYTIC WET

AIR OXIDATION (CWAO) OF PHENOL

Thesis for the degree of Doctor of Philosophy in
"Chemical Technologies and Innovative Processes"

Candidate:
Dr. Giuseppe TRUNFIO

Supervisor:
Prof. Francesco ARENA

CYCLE XXI (2006-2008)   Area 03- Scienze Chimiche (CHIM 04)

"He was leaned on the banister over the creek, wondering at the big fishes swimming happily five meters beyond him on the small stream, bridled between two rows of cherry trees…"

CATALYST DEVELOPMENT FOR THE CATALYTIC WET AIR OXIDATION (CWAO) OF PHENOL

Dissertation presented by

Giuseppe Trunfio

To obtain the degree:

Doctor in Philosophy
of the University of Messina

Faculty of Science

Department of Industrial Chemistry and Material Engineering

Acknowledgements

This work owes a lot to the ideas, suggestions, help and encouragement of many people, to whom I would like to express my sincere gratitude.

In the first place, to my supervisor Prof. Francesco Arena for his guidance and critical spirit throughout this time. Definitely, he gave me the passion for catalysis and science, which I was close to lose.

Within the Department of Industrial Chemistry and Materials Engineering to other students and researchers with whom I shared laboratory and, through numerous discussions (and appetizers) clarified many of my doubts. Moreover, people working in other Institutions, as CNR Institutes, for information I could not obtain by myself. Particular thanks to Prof. A. Parmaliana, father of this PhD course, who cannot see the conclusion of my studies.

Evidently, I have to dedicate particular gratitude to my mother and my brother for their continuous support and encouragement. And to my father who saw my efforts from the sky.

Finally, to the special person who taught me the real simple sense of the life.

Abstract

Wastewater treatment and reuse of industrial process water is a critical issue for the suitable development of human activities. The need for an effective water recycling has reinforced the research on tailored low cost pollution abatement since the existing solutions are not already universal. The Catalytic Wet Air Oxidation (CWAO) of organic compounds represents to date the most reliable technique for the abatement of pollutants from wastewater streams. In fact, among the various methods developed during last decades, it is the unique one able to process flows with large range of both pollutant load and feed. It can be carried out in absence of catalysts at severe operating conditions in terms of temperature and pressure, which can be highly decreased using appropriate catalysts.

Many compounds were employed in CWAO studies, but phenol has attracted lot of attention, due to its presence in various industrial wastewater streama. Noble metal supported on various systems, as inhert oxides or active carbons, are the most used catalysts in this process but their expensive costs and their tendency to deactivate because of poisoning forced researchers to find out new cheaper and more active systems. Among various metals able to catalyze the mineralization of organic pollutants, copper is one of the most active and it was employed in the formu only when dissolved into the reacting solution, that is when acidic intermediates are formed, lessening the pH and allowing copper to dissolve. The metal leaching from the solid catalyst represents a subsequent source of pollution, given the toxicity of copper and other heavy metals even at low concentrations. Moreover, heterogeneous Cu-based catalyst are not stable because their inability to restore the initial oxidation state of the active phase, that is at the base of oxidative catalysis, as demonstrated by redox characterization tests.

The reactor optimization is compulsory in the CWAO process development due to metal dissolution from the reactor wall, probably being the cause of literature data poor reproducibility of blank test results. Basic correlations among conversion, selectivity and pH of homogeneous tests signal that both catalytic and non-catalytic homogeneous wet air oxidations progress *via* a

poorly selective *free-radical* reaction path, leading to the ultimate formation of acetic, oxalic and formic acids and CO_2. While, a typical surface L-H mechanism accounts for a superior water decontamination efficiency and mineralization selectivity of the heterogeneous $MnCeO_x$ system.

Given the high number of oxidation states, manganese represents a valid alternative to Cu-based catalysts and many attempts were performed in order to develop the suitable system for the CWAO process. Systematic studies conducted on catalysts formed of manganese and cerium oxides prepared by means of the classic co-precipitation method confirm their efficiency in removing phenol from aqueous solutions even at very mild conditions and indicate the basic requirements of the optimum CWAO catalyst. The mineralization of phenol on the $MnCeO_x$ system proceed through the fast adsorption of the substrate on the catalyst surface and then the catalyst lattice oxygen slowly oxidize it to carbon dioxide. This reaction mechanism indicates in the enhancement of the surface exposure and in the improvement of redox properties the key features to improve the system.

The exploitation of a new synthesis route which allows the intimate mixing of Mn and Ce precursors allows to obtain a novel $MnCeO_x$ system with improved features. This new catalyst shows a higher surface area exposure, an amorphous structure, a greater active phase surface dispersion, a stabilization of the manganese at high oxidation number, improved redox featuresand a strong ability to restore the initial redox features in comparison to the classic co-precipitated system. Catalytic tests confirm the higher activity towards the phenol abatement at mild conditions. In particular, the substrate is effectively converted to CO_2 at 423K, showing an incipient carbon dioxide production at 373K, yet, in contrast with a sensible slower rate presented by the previous system. The absence of any intermediates into the reacting solution during reaction time and the high stability after several runs, make the new system "clean" and suitable for the development of the process at industrial scale.

Contents

Chapter I

Wastewater Treatments

I.1. Water and global policies

Up to date, only 14.000 of the 42.700 km³ of worldwide annual renewable available freshwater is appropriated for human uses [1], indicating a high degree of exploitation of the existing water resources [2]. Anyway, due to the widely accepted foreseen population and industrial growth, coupled with climate changes, in the close future the water resources may even suffer drastic variations on a local and/or global level. Nevertheless, while the actual world requirement is about 7.000 km³, 69% of which for agricultural needs, 23% for industrial uses and 8% for civil wants, corresponding to ca. 50% of total available resources, the increasing of the quality of life for an ever bigger population will drastically amplify the above percentage [1,2]. In fact, at the actual industrial rate and for a world population evaluated on $8 \cdot 10^9$ inhabitants, this value will grow at 90% on 2025 [1].

Moreover, the huge variety of organic compounds made available by the continuous development of chemical, food, pharmaceutical and petrochemical industries reflects an incessant improvement of the quality of life, whose improper handling and release on the environment can result in serious damages to the ecosystem and human health [3]. Besides, the disposal of waste streams containing toxic and/or bio-refractory organic pollutants generated by many industrial processes or deriving from civil uses, deserves a proper concern to accomplish more and more stringent legislative targets aimed at preserving natural resources and environment [1,2,4-8]. In this context, it is nowadays worldwide recognised the need of decisive actions for preserving natural resources and ensuring a sustainable development to future generations and wastewater remediation assumes an outmost importance in the modern society. However, one should keep in mind that, from a global point of view, the recycling of water is not environmentally benign if high energy input technologies are used for this purpose [2]. Thus, the development of efficient wastewater technologies with low energetic and operation costs is essential for all types of wastewater [2].

Environmental state and human health are inseparable aspects of the same problem, as clearly stated by the "World Health Organization" (WHO),

supporter of the Program *"Health and the Environment".* Following this important statement, with a series of mandatory directives the governments of developed and, in the very recent years, developing countries have then fixed the actions and the activities that all the members must achieve by 2020. In particular, EU's members are pressed to accomplish radical actions in terms of energy consumption/supply and pollutant emissions reduction/control, to overall reduce the impact of human activities on the ecosystem. An ever-increasing exploitation of renewable energies and advance of new "environmental-friendly" technologies with "zero emission" target are under scrutiny. In this context, new effective technologies for control and treatment of gaseous and liquid pollutant emissions are necessary, also considering that their preservation could lead to new sources of profit for entrepreneurs.

Finally, nowadays wastewater treatments are characterized by continuous evolutions targeted to the improvement of existing tecnologies and the introduction of new ecofriendly processes. Moreover, new highly skinned figures are required, as engineers, chemists physics and biologists involved in the entire management [9].

I.2. Water pollution

Wastewater, except the natural ones of non-anthropic nature, can be divided into five broad categories, according to its origin, namely domestic and agricultural, industrial, public service and system loss/leakage [2]. Among these, industrial wastewaters occupy a 42.4% of the total volume and domestic the 36.4% [2].

Domestic pollution derives from urban sewer systems, which contain huge amounts of organic moieties subjected to the anaerobic demolition, so consuming the water oxygen and producing gases noxious to the aquatic wildlife as NH_3, CH_4, H_2, etc. [10].

Agricultural pollution is due to the employement of fertilizers and, most dangerous and even more used, of herbicides, insecticides and so on. Many of this compounds results very toxic to the eco-system and their uncontrolled

employement can cause serious damages, particularly in concomitance with driving rains [10].

Factories of different nature produce the industrial pollution which constitutes the most noxious one, both for nature and human health. Typically, it is dumped directly onto rivers and seas or, sometimes, on damaged sewer systems and contains many substancies, which result refractory to subsequent treatments [10].

Finally, public services and system loss/leakage cause serious damages to the ecosystem because of the presence of particular toxic compounds which can severely pollute soils, rivers or seas. Nowadays, increasing quantities of wastewater with a high organic load result from numerous industrial and domestic applications because of the increasing demand of new products. The delocalization and the industrialization of developing countries are moving the sources of pollution spreading worldwide numerous toxic compounds [2].

Types of contaminants can be summarised as:

- Suspended solids, dissolved inorganics;
- Biodegradable organics & nutrients;
- Priority pollutants (carcinogeneous etc.), pathogens, Refractory (non-biodegradable) organics, heavy metals.

I.3. Wastewater treatments

Wastewaters treatment is become strictly necessary before their admission into the receiving basins in order to abate the concentration of polluting compounds below the limits of laws (Table 1). In fact, governments of even more numerous countries are issuing very restricting laws in the attempt to agree with claims of the civil society, pressing industries and academies to develop new suitable strategies to abate these pollutant agents in a profitable way.

At the moment there is a large number of process for the treatment wastewater containing organic pollutants and all of them take advantage of their oxidation to carbon dioxide. Inorganic pollutants, such as heavy metals

are set away by separating it with other chemical reactions, such as precipitation with the appropriate agent, before admitting the polluted flow to organic depolluting section. Among the most common organic compound demolishing technologies available nowadays (Figure 1), the conventional **_biological treatment_** is the most used all over the world.

Table 1. Limit values of some pollutants in waters.

PARAMETER	LIMIT IN SURFACE WATERS	LIMIT IN SEWAGE SYSTEM
pH	5,5-9,5	5,5-9,5
BOD_5 (as O_2)	≤40 mg/L	≤250 mg/L
COD (as O_2)	≤160 mg/L	≤500 mg/L
Alluminium	≤1 mg/L	≤2 mg/L
Arsenicum	≤0,5 mg/L	≤0,5 mg/L
Barium	≤20 mg/L	-
Borus	≤2 mg/L	≤4 mg/L
Cadmium	≤0,02 mg/L	≤0,02 mg/L
Chromium (total)	≤2 mg/L	≤4 mg/L
Chromium VI	≤0,2 mg/L	≤0,2 mg/L
Iron	≤2 mg/L	≤4 mg/L
Manganese	≤2 mg/L	≤4 mg/L
Mercury	≤0,005 mg/L	≤0,005 mg/L
Nichel	≤2 mg/L	≤4 mg/L
Lead	≤0,2 mg/L	≤0,3 mg/L
Copper	≤0,1 mg/L	≤0,4 mg/L
Selenium	≤0,03 mg/L	≤0,03 mg/L
Tin	≤10 mg/L	-
Zincum	≤0,5 mg/L	≤1 mg/L
CN^-	≤0,5 mg/L	≤1 mg/L
Sulphides (as H_2S)	≤1 mg/L	≤2 mg/L
Sulphites (as SO_3)	≤1 mg/L	≤2 mg/L
Sulphates (as SO_4)	≤1000 mg/L	≤1000 mg/L
Clorides	≤1200 mg/L	≤1200 mg/L
Fluorides	≤6 mg/L	≤12 mg/L
Fats	≤20 mg/L	≤40 mg/L
Idrocarbons	≤5 mg/L	≤10 mg/L
Phenols	≤0,5 mg/L	≤1 mg/L
Aldeydes	≤1 mg/L	≤2 mg/L
Organic solventes	≤0,2 mg/L	≤0,4 mg/L
Pesticides	≤0,1 mg/L	≤0,1 mg/L

However, as can be seen from Figure 1, its application becomes impossible when streams containing high organic load and/or bio-toxic compounds which kill the active sludges necessary to the biological oxidation [11]. For example, aqueous phenol solutions with concentrations exceeding 0.5 g/L should not be treated in biological plants, even though acclimatized cultives in laboratory tests have performed the depollution of solutions with up to 2 g/L of phenol [2]. Phenol and phenol-like compounds are frequently present in many streams of several chemical industries, such as petrochemical, pharmaceutical, etc. [1,3,11-17].
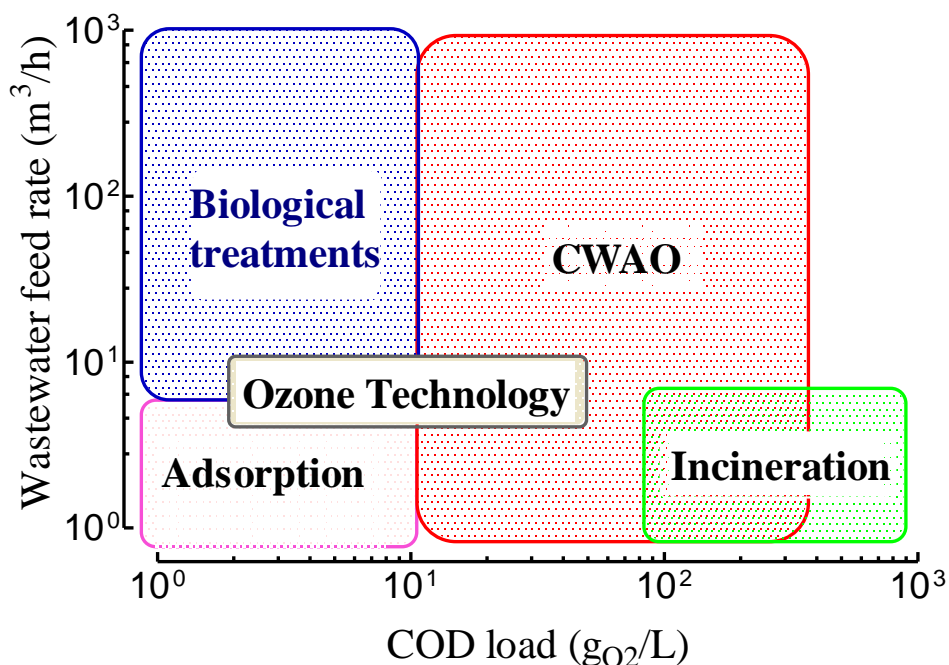
Figure 1. Load and feed rate limits of the most used wastewater depolluting technologies.

Alternative methods have been developed for the remediation of these effluents, the most important being the adsorption on activated carbon, the thermal incineration and the liquid phase chemical oxidation (Figure 1).

The **_Adsorption on activated carbons_** is very effective for a broad range of organic pollutants thanks to their large surface area which make them adsorbing significant quantities of pollutants [18]. Unfortunately, they do not ultimately destroy them, so implying an adequate strategy for their required disposal or regeneration in additional plants, strongly harming the operating costs of the method. Adsorption takes place both in batch, and in continuous operations with the employment of powder catalysts (40-80 mesh). The pollutant load constitutes its main limit due to the very low feed concentration which increases remarkably the reaction time and costs [18].

Incineration is the other well established technology for the treatment of concentrated and toxic organic waste streams. Organic pollutants are burnt at atmospheric pressure and high temperatures between 1000°C and 1700°C [11]. Incineration can offer almost complete pollutant destruction, although at very high energy costs, because of an organic load above 300mg/l and the low feed rate that is necessary to guarantee the autothermal oxidation. Thus, it represents an important limit for its employment at industrial scale [7]. Furthermore, this technique has been accused for the emission of toxic by-products such as dioxins and furans [11].

I.3.1. Liquid phase oxidation

Liquid phase chemical oxidation methods promise to overcome the existing drawbacks of the above mentioned treatment methods by destroying the pollutant while being dissolved in the liquid phase. Several emerging liquid phase oxidation methods can be distinguished in terms of the different oxidants, catalysts and selected operating conditions and can be divided in two main groups [11]:

1) Advanced Oxidation Processes **(AOP)**

2) Wet Air Oxidation **(WAO)**

The first ones are conducted in presence of O_3, H_2O_2 or other activated oxygen species produced by means of special techniques as UV radiation, while the

seconds utilize molecular oxygen to demolish organic compounds to CO_2 [11]. WAO processes can be further subdivided in [11]:

a)   *Thermic Wet Air Oxidation* (TWAO),
b)   *Supercritical Wet Air Oxidation* (SWAO) and
c)   *Catalytic Wet Air Oxidation* (CWAO).

In all the processes, molecular oxygen is dissolved in the water phase and oxidizes dissolved organic pollutants to carbon dioxide.

I.3.1A. Thermic wet air oxidation processes (TWAO)

TWAO processes are performed at high pressure and temperature. High pressure increases solubility of oxygen in water and makes it more available for the reaction, while high temperature enhances reaction rate. Therefore, the process is typically run at 0.5-20 MPa and 400-700 K, with residence time ranging from 10 to 120 min [11].

The oxidation proceeds through a radical mechanism, and two paths occur simultaneously: degradation to lower carboxylic acids (acetic acid is considered to be the most refractory to oxidation) and elimination of CO_2 during the reaction [7].

For nitrogen-containing compounds, the oxidation leads to ammonia, nitrate, dinitrogen gas, and nitrous oxide depending on the pollutant and reaction conditions. For most cyanide- and amine-containing compounds, ammonia is the end product of the TWAO. The process becomes energetically self-sustaining when the COD exceeds 20 g/dm³ [19,20].

The important drawback of TWAO is the high capital costs due to the severe operating conditions (high temperature and pressure) conducted in a hostile environment (the formed oxygenated compounds are highly corrosive under these conditions, demanding the use of special alloys). The capital costs of TWAO are higher than those for incineration but the operating costs are lower, mainly because of the lower energy requirements of the process [20]. However, TWAO is a proven technology with more than 200 full-scale

installations operating by 1996, with the first commercial unit for the treatment of sulfite liquors being started in the late 1950s [21,22].

I.3.1B. Supercritical wet air oxydation (SWAO)

Severe process conditions necessary to conduct the WAO process stimulated researchers to investigate for techniques operating at milder conditions. An alternative to conventional TWAO is SWAO, i.e., oxidizing organic pollutants in supercritical water at elevated temperatures and pressures, possibly in the presence of a catalyst [11]. Under supercritical conditions (T>374°C and P>253 atm), organic compounds become completely miscible with water, while inorganic salts become insoluble in water. This let the process to show destruction efficiencies exceeding 99.99% in 1-10min. However, the operating costs for SWAO process are 2-4 times higher than those for the WAO process. Because of the very high cost, SWAO technique should only be used for very toxic and/or refractory pollutants [11].

I.3.1C. Photocatalytic processes

Photocatalytic processes uses photocatalytic systems as TiO_2, also in combination with H_2O_2 or Fe^{3+}/H_2O_2, which have potential application in the abatement of clorophenols, solvent as chlorides and cyanides. Unfortunately, they show low conversion rates and they need low pollutant load in the wastewater streams. Moreover, the pollutant complexity can interfere on the reaction mechanism or with chromophore groups which promote the photo-oxidation, so seriously affecting the overall efficiency. It must be stressed also the high cost of catalysts and materials, as well evidenced in literature data, which, together with low reaction rate, compromise the industrial development of the process [11,23]. All these drawbacks make the AOPs ideal only for wastewater streams with very low pollutant load (≤ 5 g/L) and containing particular types of pollutants [23].

On this account, AOPs need specific and strong improvements, in order to make catalysts able to take advantage of visible light instead of expansive UV ray sources [11,23].

I.3.2. Industrial non-catalytic wet oxidation processes

The wet air oxidation process was originally developed by F. J. Zimmermann and its first industrial applications appeared in the late 1950s [24]. Currently, there are more than 200 plants operating around the world, the majority being dedicated to the treatment of sewage sludge. Other main fields of application consist in the regeneration of activated carbon and the treatment of industrial wastewaters [2,20].

Up to now, only few industrial processes are being practiced widely. Some industrial applications are summarised on the works of Kolaczkowski et al. [20], Luck [25,26] and Debellefontaine and Foussard [27]. The main differences between the distinct processes consist in the reactor type used and the incorporation, or not, of a catalyst.

The major industrial non-catalytic wet oxidation processes are reported in Table 2. Anyway, in this work only the Zimpro and the Vertech process are discussed in more detail.

Table 2. Industrial WAO Processes.

PROCESS	Reactor	Temperature (°C)	Pressure (MPa)	Time (min)
ZIMPRO	Bubble Column	150-325	2-12	20-240
WETOX	Stirred Tank	200-250	4	30-60
VERTECH	Deep Shaft	180-280	8.5-11	60
KENOX	Recirculating	200-240	4.1-4.7	40
OXYJET	Jet-Mixer	140-300		<5

I.3.2A. The Zimpro Process

This process is one of the oldest and most widely used industrial WAO processes, with more than 200 units built to date for the treatment of a large spectrum of wastes (for example, municipal sludges, ethylene caustics, various refinery caustics, pharmaceutical wastes, pesticides, and other industrial wastewaters) with the main goals of (i) pretreatment to produce biodegradable wastes, (ii) process liquor treatment for recycle or recovery, (iii) the reduction of COD in general, (iv) the destruction of specific components, and (v) the elimination of toxicity.
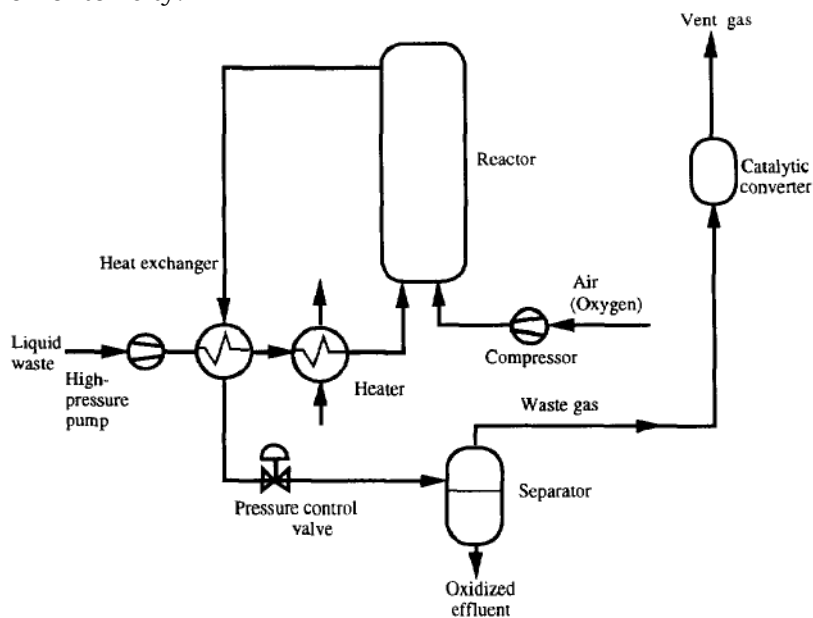
Figure 2. Simplified Zimpro process flow diagram.

The process uses air as oxidant at temperatures of 100-320 °C and pressures of 2-20 MPa. Co-current bubble column reactors with height-to-diameter ratios in the range of 5-20 with or without internal baffles are commonly used. The detailed operating parameters are largely dependent on the type of waste to be treated and the degree of oxidation required. For example, refinery caustics and pharmaceutical wastewaters generally require

more severe treatment conditions, compared to ethylene caustics and cyanide wastes. For municipal sludges, the conditions vary, depending on the aim of the treatment. Sludge dewatering occurs in the range of 150-200°C, while the regeneration of spent activcarbons and the conversion of refractory wastes to biodegradable substances is performed at temperatures of 200-250°C. If higher degrees of destruction are required, temperatures up to 325°C are necessary [13].

Reactors are operated with retention times between 20 min to 4 h, but, most commonly, the design aims to achieve 60 min of retention [13]. As with all bubble columns, both axial and longitudinal mixing of the waste can occur, resulting in the decrease of the wastewater residence time. Thus, the required degree of conversion may not be achieved, which would make further downstream treatment processes necessary to complete the conversion [13].

I.3.2B. The Vertech Process

The process uses pure oxygen to destroy the sludge in a subsurface vertical reactor that consists of two concentric tubes. The inner one acts as a downcomer and conveys the waste and oxygen to the bottom of the reactor. The outer tube, the upcomer, brings the reacted effluent back to the surface. These tubes descend to a depth of 1200÷1500 m and, at this depth, the waste and gas, with its liquid-gas static head above, is under sufficient pressure for the WO process to proceed [13]. This leads to considerable savings in power consumption. In fact, pumps are used only to overcome frictional losses. The pressures attained in the reactor are dependent on the depth of the shaft and the fluid density. For shafts that extend to depths of 1200-1500 m, pressures in the range of 8.5-11 MPa are developped [13,20].

The concentric tubes also act as heat exchangers, where the influent flow down the downcomer is heated with the hot effluent in the upcomer. The oxidation starts at 177°C and increases further through the heat released by the oxidation reaction. The heat-exchange system maintains a temperature of ~280 °C at the bottom of the reactor. After the waste passes from the bottom of the downcomer to the upcomer, its pressure and temperature decreases, until,
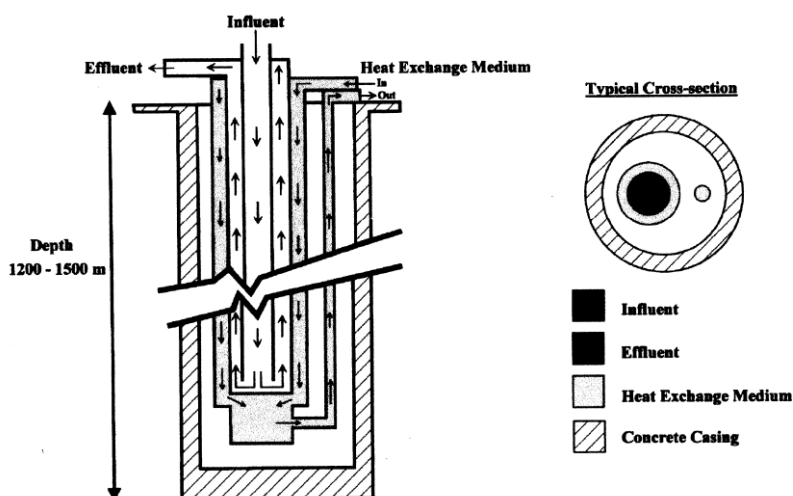
Figure 3. Simplified Vertech process flow diagram.

upon exit from the system, the effluent is at a temperature of ~50 °C [13]. The heat-exchange medium enters the system via the jacket surrounding the upcomer and leaves, heated, via a separate insulated tube and is used to generate electricity. When the system is started, the flow of the heat-exchange medium is reversed, so that the preheated medium in the insulated tube flows to the bottom of the reactor, heating it. This procedure allows for good temperature control of the system [13,20].

The turbulent oxygen and waste flow down the downcomer allows for exceptional mass transfer between the two components and good heat transfer between the downcomer and the upcomer. The waste and the oxygen progress in a plug flow regime, enabling a high conversion per unit volume. Residence times within the Vertech reactor are of about 1h, with 30-40min of this time spent in the oxidative reaction zone [13,20].

Maintenance involves regular nitric acid washes, to remove scale buildup along its walls. Typically, this is performed every 10 days and takes ~8 h. Inhibitors added to the feed can reduce the formation of scale [13,20].

The subsurface treatment of waste, while saving space above ground, does pose environmental concerns (possible contamination of drinking water aquifers). Precautions that are taken to prevent contamination include (i)

careful site selection (only geologically stable sites are selected) and (ii) double concrete lining of the reactor when there are drinking water aquifers at the top of the reactor.

I.3.3. Catalitic wet oxidation (CWAO)

Catalytic wet oxidation processes demolish the organic pollutants present in the wastewater stream by oxidazing them with the help of homogeneous or heterogeneous catalysts at milder reaction conditions. It is evident the sensible decrease of operative costs even if many important drawbacks have to be overcome, yet, such as catalyst recovery in the homogeneous CWAO [2,13] and catalyst deactivation by active phase leaching or fouling in the heterogeneous CWAO [1,2,6,11-17,25-47]

I.3.3A. Homogeneous processes (HoCWAO)

Homogeneous catalysts in WO systems have been reported to significantly enhance the destruction of organics, with copper salts showing high reaction rates [11,13]. Reactors chosen for a homogeneous catalytic system (two-phase regime) are similar to noncatalyzed WO ones. The major issue of the homogeneous catalytic system however, is the need to recover/remove the catalyst from the effluent after treatment. This necessitates an additional processing step and increased capital cost of the system.

Homogeneous catalysis has been used with co-oxidation (where an easily oxidized material promotes the rate of oxidation of a more refractory material), as well as with radical promoters working in combination with transition metals. Examples are hydrogen peroxide with Fe^{2+} as a catalyst. Hydrogen peroxide has been associated with the generation of free radicals that are able to catalyze the reaction, especially when used with iron or copper salts. Often two or more metal salts act in a synergistic mode [48-50].

I.3.3B. Bayer LoProx Process

This process is mainly used as a pretreatment step to biological treatment methods. Wastewaters containing compounds not easily amenable to biological oxidation are treated under mild conditions to render them suitable for biological treatment methods [13]. The process is ideally suited for wastes with a COD of 5-100 g/L. Typical reaction conditions used are temperatures lower than 200 °C, pressures of 0.5-2 MPa, and reactor residence times in the range of 1-3 h. The process has been used to treat wastes from paper mills, landfills, and municipal waste sludge. A scheme of the process is reported in Figure 4. The reaction is catalyzed by Fe^{2+} ions and organic quinone-forming substances [13].

During the formation of quinone, hydrogen peroxide forms as a reaction intermediate. The combination of hydrogen peroxide and Fe^{2+} ions is potently oxidizing, with the decomposition of the hydrogen peroxide providing hydroxyl radicals for easy oxidation of organic compounds [13].
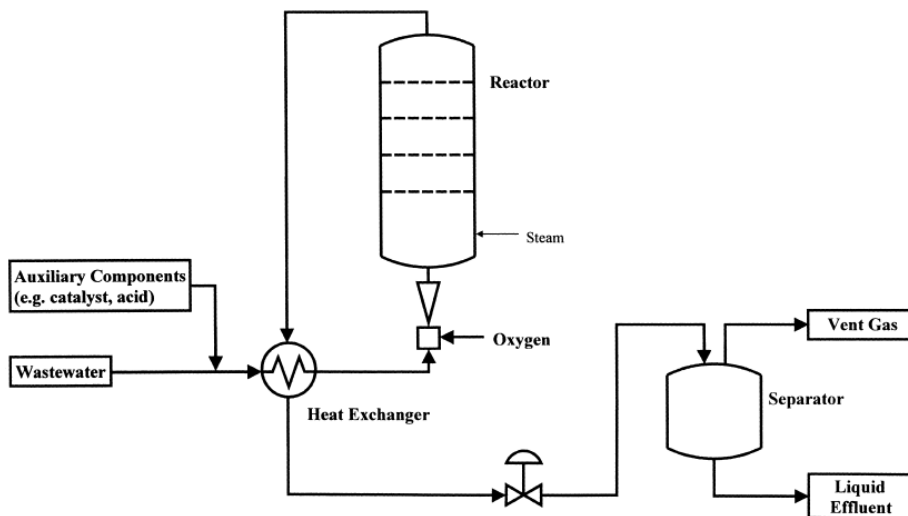
Figure 4. Bayer Loprox Schematic Process.

I.3.3C. ATHOS Process

16

This process has been designed for the treatment of residual sludges and includes the steps of sludge preparation, oxidation, heat recovery, and dewatering of residual solids [13]. The reaction is conducted in a recirculation reactor (ensures complete mixing), with oxygen as oxidant, at temperatures of 235-250 °C and pressures of 4.5-5.5 MPa. The plant design is intended to achieve residence times of ca. 1h. Effective processes for the treatment of residual sludges are gaining in importance, because sludges are byproducts of most wastewater treatment plants [13].

I.3.3D. Wet peroxide oxidation (WPO) process

Wet peroxide oxidation (WPO) uses hydrogen peroxide as oxidant [13] and compares very favorably to processes using gaseous oxygen. The lack of a gas/liquid boundary removes mass-transfer limitations, and the hydrogen peroxide acts as a free-radical initiator, providing OH• radicals that promote the degradation of the organic polluting compounds. This leads to reduced residence times and enables conversion under milder conditions. For example, in the removal of TOC and color from dyeing wastewater concentrate, WPO allowed much shorter reaction times to be realized and yielded a dramatic reduction in TOC and color, compared to WAO. In fact, with WAO, only 15% TOC removal and no color reduction occurred in 2h at 6MPa and 200°C. When hydrogen peroxide was used as oxidant, at a pressure of only 50 kPa, and at a temperature of 110 °C, 80% of the TOC was removed and 90% of the color was reduced in just 30 min.

The use of metal salt combinations with hydrogen peroxide greatly increases TOC removal, even for refractory low molecular weight organic acids. For example, through treatment of a mixture of acetic, oxalic, succinic, and malonic acids for 60 min at 100 °C with hydrogen peroxide and a combination of Fe^{2+}, Cu^{2+}, and Mn^{2+} ions in a weight ratio of 23:50:27,14,175 an 89% reduction in TOC was attained. A similar mechanism to Fenton's reaction has been proposed, with the exception that the OH• radicals are generated by the thermo-scission of hydrogen peroxide in WPO and by Fe^{2+} ion catalysis in Fenton's reaction [13].

17

I.3.4. Heterogeneous catalytic wet oxidation

The major advantage of a heterogeneous over a homogeneous catalytic system is the easy catalyst retrieval from the reaction media. However, the stability and durability of the catalyst under CWAO operating conditions is severely tested. Catalyst deactivation occurs by the following causes:

1)   *poisoning* (active phase poisoning),

2)   *sintering* (active phase agglomeration),

3)   *fouling* (catalyst surface covering by carbonaceous deposits),

4)   *leaching* (active phase dissolution into the reacting medium).

Moreover, in fixed-bed reactors, pressure drops occur inside the reactor and the catalyst can deactivate easily by fouling and plugging. For these reasons, interparticle and intraparticle mass transport limitations must be minimized [13].

The pressure drop across the catalyst bed in FBRs is determined by catalyst particle size (the pressure drop increases with decreasing pellet size). In fact, the increase of the catalyst particles diameter reduces the pressure drop, while, using larger pellets, reaction rates become diffusion-limited. Sadana and Katzer [51] have reported that reaction rates were lower with large catalyst particles (dp ~ 0.4 mm) than with catalysts of smaller (dp ~ 0.06 mm) pellet sizes, and they attributed this phenomenon to oxygen intraparticle diffusion limitations in the larger pellets. In addition, as interfacial contact area between catalyst and solution is reduced with larger pellet size, a considerable portion of catalyst may not be effectively utilized [13]. Suspended solid materials in the wastestream cause clogging of the reactor bed, eventually resulting in a large pressure drop. This can be prevented by the use of a two-stage reactor, [13,51] where, in the first stage (noncatalytic), the solid matter is

dissolved and then the waste is transferred to the second (catalytic) stage for oxidation.

A monolith catalyst structure may be used as an alternative to a fixed bed. The monolith is comprised of several parallel channels, oriented in the direction of fluid flow. The catalyst is fixed onto the walls of these channels, so that intimate contact is established as the waste flows through the channels. The channel size, cell density, and wall thickness are fabricated to a designed cross-sectional area [13]. Provided that this area is larger than the particulate size in the waste, there is little impediment to the solution flow through the channel, minimizing pressure losses and catalyst plugging [13]. The shape of the channel cross-section can also be varied, with circular, rectangular, hexagonal, and sinusoidal forms being available. In addition, when operated in the slug flow regime (with gas and liquid plugs sandwiching each other), a recirculation pattern within each liquid plug is created, further improving mass transfer. This regime ensures formation of a thick liquid film between the channel wall and the gas, which promotes high mass-transfer rates and keeps the catalyst continuously wetted [13].

Heterogeneous catalytic processes include the Nippon Shokubai process and the Osaka Gas process.

I.3.4A. The Nippon Shokubai Process

The Nippon Shokubai Kagaku Company Limited had installed ten catalytic systems by 1996 and developed numerous heterogeneous catalysts in both pellet and honeycomb form for use in wet air oxidation processes [13]. For example their European Patent [52] covers a heterogeneous catalyst capable of converting organic and inorganic substances present in the wastewater to nitrogen, carbon dioxide and water.

The catalyst is comprised of titanium dioxide, an oxide of an element of the lanthanide series and one metal from the group consisting of manganese, iron, cobalt, nickel, tungsten, copper, silver, gold, platinum, palladium, rhodium, ruthenium and iridium or a water insoluble or sparingly water

soluble compound of the metal [53]. Although the use of titania or zirconia as carriers increased catalyst strength compared with alumina supports, both their catalytic activity and durability was not satisfactory. In contrast to this, oxides of elements of the lanthanide series were found to exhibit catalytic activity, but could not be easily moulded and in the long term degraded in physical strength. In the Nippon Shokubai catalyst the combination of titanium dioxide with oxides of elements of the lanthanide series resulted in a mouldable, physically stable catalyst, exhibiting only a slight loss in strength and catalytic activity, while being capable of withstanding long term use [53].

The Nippon Shokubai process operates over a temperature range of 433 K to 543 K and at pressures of between 0.9 to 8.0 MPa, with typical residence times in the region of about 1 h [53]. The effectiveness of the catalyst to remove compounds refractory to non-catalytic oxidation was illustrated by the treatment of a waste containing acetic acid and ammonia at a temperature of 503 K and a pressure of 5.0 MPa [53]. A further catalyst from Nippon Shokubai contains a main "A component" comprising an oxide of iron together with an oxide from at least one of titanium, silicon and zirconium, plus an active "B component" consisting of one or more of cobalt, nickel, cerium, silver, gold, platinum, rhodium, ruthenium and iridium. The A component makes up 90% to 99.95% by weight of the catalyst with the B component making up the balance.

The catalyst is capable of treating organic wastes, including compounds that contain nitrogen, sulfur, or halogens, with lasting catalytic activity. Also, any nitrogen in the compound is decomposed to nitrogen gas. The use of this catalyst for the treatment of sulfur and halogen-containing organics is best performed under basic conditions, because acidic conditions shorten the life of the equipment used [13,20].

I.3.4B. The Osaka Gas Process

The patented Osaka Gas Process is similar to the Zimpro process except for the inclusion of a heterogeneous catalyst in the reactor, supplied in the

form of spheres or a honeycomb support. The catalyst uses titania, zirconia or similar oxides (as either a one-element or two-element system) as the carrier together with a mixture of two or more precious or base metals such as iron, cobalt, nickel, ruthenium, palladium, platinum, copper, gold, tungsten and compounds thereof [13].

The operating conditions including temperature, pressure and initial pH vary depending on the composition of the waste and required destruction efficiency, with the catalyst retaining activity for a long service life. For example, in the treatment of gas liquor wastewater from coke ovens over 11.000 hours of continuous operation was obtained at 523 K and 6.86 MPa, with no change in catalytic activity. After a residence time of 24 min the waste was decomposed from an initial chemical oxygen demand (COD) of 5,87 g/L to a value of less than 0,01 g/L [13].

Further, the process can be used to destroy a variety of wastewaters and sludge including sewage sludge, ammonium nitrate wastewater, domestic wastes and pharmaceutical waste. In addition, catalysts used for the treatment of various nitrogen containing compounds (e.g. ammonia, ammonium salts and nitrates) will achieve a virtually complete conversion of nitrogen content to nitrogen gas [13,52].

I.3.4C. The NS-LC process

The NS-LC process employs an honeycomb catalyst based on Pt-Pd/TiO_2-ZrO_2. The flow rate of liquid and gas phases into the vertical catalyst monolith channels can be varied in a large operative range, optimizing the so-called "segment" model for an efficient contact between phases [25]. At typical operative conditions the process works at 220°C, 4 MPa and a SV of 2 h^{-1}, and oxidation of compounds like phenol, acetic acid, glucose etc. exceed the value of 99%, while in absence of catalyst the efficiency get lower for values of 5 and 50% [25].

1.4 Catalytic Wet Air Oxidation Catalysts

Heterogeneous catalysts employed in the catalytic wet oxidation can be divided in two main groups: metal oxides (as well as mixtures of them) and supported noble metals [7,8]. Besides, active carbons, without any deposited active phase, exhibits appreciable catalytic activity [54].

1.4.1 Noble metal catalysts

Noble metals have demonstrated high efficiency in the treatment of different pollutants present in wastewater treatment such as phenols [1,7,8,11,13,55,56,], carboxylic acids, including refractory acetic acid, [7,8,11,13,57,58], ammonia [59-61] and kraft effluents [62-66]. In particular, in the last two decades of last century, palladium, platinum and ruthenium received most attention although iridium or rhodium were tested [11,13]. From Table 3, which summarizes the applications of noble metal catalysts in the CWAO it can be deduced that numerous noble metal catalysts are available, but different pollutants need different metals to be efficiently demolished. For example, in the case of acetic acid oxidation, Barbier et al. [57] state that the catalytic activity decreases in the order Ru > Ir > Pd, while for the oxidation of p-chlorophenol, Qin et al. [67] found out that catalytic activity decreases in a reverse order Pt > Pd > Ru [2].

Occasionally, synergistic effects in bimetallic catalysts improve catalyst activity and/or selectivity. For example, during ammonia oxidation the higher N_2 selectivity was achieved using a mixed Ru−Pd/CeO_2 catalyst [59]. Moreover, promoters have also been used with noble metal catalysts. An Ag promoted Pt/MnO_2/CeO_2 system, in fact showed an enhanced CWAO of phenol in comparison with the non promoted catalyst [2].

The noble metal support also influences significantly the catalyst performance. Metal oxides, like alumina, ceria, titania and zirconia, as well as active carbon or high specific area graphite have been mainly studied with appreciable results and important information (Table 3). In fact, In the treatment of Kraft bleach effluents the support surface area increasing had a

Table 3. CWAO using noble metal catalysts. Adapted from reference [11].

Catalyst	Reactor[a]	T (K)	P (atmosphere) (MPa)
Pt, Pd, Ru *on* CeO_2	SR	393-503	2.0 (O_2)
Pt, Pd on AC *and* γAl_2O_3	SR	473	0.42 (O_2)
Pt, Pd, Ru *on* CeO_2	SR	443	2.0 (O_2)
Pt, Ru *on* CBS, SM	TBR	393-473	5.0-8.0 (air)
Pt/TiO_2 *and* Pt/ γAl_2O_3	SR	403-473	2.5-4.3 (air)
Pt_xAg_{1-x}/MnO_2-CeO_2	SR	353-403	0.5 (O_2)
Pt/graphite	SR	393-453	0.01-0.8 (O_2)
Ru/CeO_2	SR	473	
Ru/AC	SR	433	2.0 (O_2)
Pt/ γAl_2O_3	SR	353-448	0.5-1.5 (O_2)
Pt/TiO_2	SR	423-473	3.4-8.2 (O_2)
Pt, Pd, Ru *on* CBC	TBR	393-433	5.0-8.0 (air)
Pd on ZSM_5, MCM-41, ZrO_2, TiO_2	SR		
Ru/TiO_2	SR	448-473	0.34-1.38 (O_2)
RuO_2/ γAl_2O_3, RuO_2-CeO_2/ γAl_2O_3	SR	423	3.0 (air)
Ru/TiO_2	SR	373-413	0.1 (O_2)

[a] BR, (semi)Batch Reactor. TBR, Trickle Bed Reactor.

positive effect on catalyst activity [65]. While the active phase dispersion was proved to be essential for the CWAO of phenol, as indicated by a comparative study of Pt/Al_2O_3 catalysts prepared with different synthesis methods [56].

1.4.2. Metal oxides

The other group of catalysts employed in the CWAO of organic compounds is represented by pure or mixed metal oxides, as can be seen on Table 4, where are reported some of works reported on literature. Their catalytic activity had received the interest of many researchers, as witnessed by the huge amount of scientific papers published worldwide and summarized in many reviews appeared in the very recent years [1,7,8,11,13].

The activity of these catalysts was evaluated using batch or semibatch operated stirred-tank reactors with slurry (SR) or spinning basket reactors (SBR), and continuously operated fixed-bed reactors with upflow or downflow of reactants, with the latter usually operated in a trickle-flow regime (TBR). [11]

In particular, copper oxide, alone or combined with other oxides, has received special attention in the CWAO of aqueous effluents [1,2,7,8,11,13,28-31,38-41].

Table 4. CWAO using metal oxide catalysts. Adapted from reference [11].

Catalyst	Reactor[a]	T (K)	P (atmosphere) (MPa)
CoMo/AC, Mo/AC, Mn/AC	SR	473	0.42 (O_2)
Mn-Ce oxide composites	SR	383	0.5 (O_2)
MnO_2/CeO_2	SR	353	0.5 (O_2)
Mn-Ce oxides, cryptomelane	TBR	373	1.0 (O_2)
Ni.Mn oxides	SR	308	Atm. Press.
NiO_2	SR	308	Atm. Press.
NiO_2	SR	288-328	Atm. Press.
Fe/AC	TBR	373-400	0.8 (O_2)
CeO_2	SR	413-453	0.5-1.0 (O_2)
CeO_2	SR	433-453	0.5-1.0 (O_2)
CeO_2/γ-Al_2O_3, CeO_2/TiO_2, CeO_2/SiO_2, $CeO_2/AlPO_4$[5-]	SR	453	1.5 (O_2)
CeO_2/γ-Al_2O_3	SR	453	0.5-2.0 (O_2)

[a] BR, (semi)Batch Reactor. TBR, Trickle Bed Reactor.

Phenol was successfully oxidized by a commercial Harshaw catalyst, comprising 10% copper oxide supported over alumina [51]. Baldi et al. [68] and Goto and Smith [69] tested a commercial CuO/ZnO catalyst to oxidize Formic acid while Levec et al. [2] used a catalyst combining Cu, Mn and La oxides supported on Al_2O_3 and ZnO to oxidize acetic acid.

In the early nineties, other commercial catalysts comprising CuO, ZnO, CoO or Al_2O_3 alone or in combination [2] were patented and dealed and successfully employed in many oxidation reactions such as the CWAO. Ceria oxide, manganese-ceria mixed oxides and promoted ceria catalysts have also exhibited high activities [28-37,42-47].

In the eighties, Imamura and co-workers (as summarised by [7]) developed Mn/Ce oxide catalysts for the CWAO of ammonia, and demonstrated they are very effective for most organic compounds. De Leitenburg et al. [70] reported that ternary mixed oxides with ceria zirconia and MnO_x or CuO performed better than ceria, or ceria-zirconia catalysts alone. Hamoudi et al. found that that CeO/MnO catalysts can effectively oxidize phenol [15] while,

Chen et al. [14] showed that a Mn/Ce ratio of 6/4 was the most active for phenol oxidation.

Metal oxide catalyst were then improved by the incorporation of alkaline metals [16,17], although this modification mainly affected catalyst stability. However, metal oxide catalysts not based on copper or cerium have been tested in fewer cases. For example, nickel oxide catalysts have been used to effectively remove phenol under atmospheric pressure conditions [71].

1.4.3. Active carbons

Most commonly, active carbons have been used as catalyst support because of its high adsorptivity toward various organics [2,13,58] while, only in the very recent years they were used without any additional active phase and showed appreciable long term catalytic activity in the oxidation of phenol [51], that could even surpass that of a conventional copper oxide catalyst, which suffer of active phase leaching [2,28,29,51].

Active carbons are resistant to acidic pH that is inherent to the CWAO process. For instance, active carbon used as a catalyst support in CWAO caused a significant reduction of copper leaching [2,54]. In fact, copper catalyst supported by active carbon performed better than the commercial G-66A catalyst, and copper leaching from CuO/AC catalyst was lower than that from the commercial oxide catalysts (G-66A). Moreover, it shows catalytic activity without the presence of any active metal. However, in typical CWAO conditions (140 °C and 0.9 MPa of oxygen partial pressure), there is a substantial loss of active carbon by combustion and, consequently, the catalyst deactivated for that reason. Partial combustion of active carbon was also observed even at temperatures as low as 120 °C. The combustion of active carbon can be significantly reduced (but not eliminated), e.g., by decreasing the oxygen partial pressure from 9 to 2 bar. [11]

1.4.4. Catalyst deactivation

Unfortunately, all studied catalysts present some drawbacks, such as the partial combustion of active carbons mentioned in the precedent paragraph, which face researchers to the necessity of strong efforts in order to make the process feasible at industrial scale [2].

The stability and possible deactivation of a heterogeneous catalyst has a significant impact on the cost of the CWAO process. It is also important to say, from an environmental and process point of view, that components leached from a catalyst sometimes can result more toxic or hazardous than organic pollutants and lead to catalyst deactivation. Therefore, investigations on catalyst stability (and ways to improve stability through catalyst preparation methods) and catalyst deactivation is an important part of many studies conducted on the CWAO process.

Catalyst deactivation can occur via several mechanisms, such as sintering, poisoning of active sites, fouling and metal and support leaching. Many researchers have investigated the stability and/or deactivation of various CWAO catalysts by varying reaction conditions [11] and optimizing the catalyst stability. Maintaining a high level of activity is a significant challenge for researchers investigating CWAO systems, primarily because of the harsh conditions in most CWAO processes (high temperature, acidic conditions).

Catalyst containing noble metals, though exhibiting higher activity than copper and other base metal catalysts and not reporting some leaching of precious active phase in the reacting solution, are strongly sensitive to poisons such as halogen-, sulfur-, and phosphorus-containing compounds [11]. The sensitivity of noble metals to these poisons can be reduced by the proper choice of metal oxide support. For instance, alkali and alkaline-earth-metals are known to be appropriate for this purpose. Noble metals can also lose their catalytic activity because of oxidation under CWAO conditions and can deactivate because of the deposition of polymers that are formed on the catalyst surface during the CWAO processes [11].

Polymeric substances can be formed on the catalyst surface because of condensation reactions between phenolic compounds and oxidation

intermediates adsorbed on the catalyst surface. According to Pintar and Levec, [72] polymers are formed in two reactions taking place in the liquid phase: (a) stepwise addition polymerization of C-2 aldehyde (glyoxal), which is an intermediate in phenol oxidation, to phenol, and (b) polymerization of C-2 aldehyde. Benzoquinones were also considered to be precursors of polymeric deposits. In the case of Cu-based systems, Alvarez et al. suggested that organo-cupric polymers can be responsible for catalyst fouling [73]. The formation of polymers is high when oxidation is performed in (semi)batch reactors (BR), while it is significantly suppressed when operated in continuous reactors such as trickle bed reactors (TBR). In fact, Cu-spinels were relatively stable in a TBR, while they lost their activity in SR (probably because of polymer formation). On the other hand Cu-Ni-spinel catalyst do not present that phenomenon. Evidently, the residence time of the liquid phase in TBRs is much shorter than in BRs and the catalyst surface accessibility for intermediates that can either polymerize or be oxidized to carbon dioxide is higher. Moreover, no condensation products were found in the final solution or deposited on the Cu catalysts in the TBR, recovered at the end of the reation [11,74]

Besides, Pintar and Levec observed copper leaching (phenol conversion dropped to ca. 40% and the Cu ion concentration in the effluent was 150 mg/L), but they claimed that the Cu catalyst deactivation was mainly due to formation of polymeric deposits [72].

During phenol oxidation, some acidic intermediates, such as short chain carboxylic acids, with acetic acid being the most resistant to the subsequent oxidation can be formed [74-75]. Refractory carboxylic acids are aggressive toward catalyst components under oxidation conditions, and some catalyst components leach out, resulting detrimental for the catalyst and for the toxicity of the solution [28-31]. In fact, some eluted substances can be harmful for aquatic systems [38-41]. Obviously, the leaching rate of copper is strongly enhanced by the acidic conditions [28,29].

It was demonstrated that Cu-based systems lifetime is depending on the amount of copper oxide on the support, implying that the catalyst still remain active until the active phase is present on the system. The calcinations

treatment allows a decrease in the catalyst lifetime, proving again that it is able to oxidize the substrate only when surface Cu is accessible, the thermal treatment hindering some active phase on the system [75].

According to the vast majority of papers, copper oxide reacts in acidic conditions with carboxylic acids to produce compounds that are soluble in the reaction medium. Santos et al. claimed that soluble copper salts react with oxalic acid, which is one of the intermediates, and the resulting copper oxalate complex is deposited on the catalyst surface. This make phenol conversion decrease because of a drop in the concentration of the homogeneous catalyst. The rate of leaching depends on operating conditions such as the stream composition and pH and the catalyst composition [38-41].

There have been carried out many attempts to eliminate or decrease copper leaching: by the modification of operating conditions of the CWAO, by the search for appropriate ways for catalyst preparation and pretreatment, the selection of the best catalyst support, and the search for the best composition of catalytic species. The oxidation of phenol in the presence of bicarbonate buffer (pH ~ 8) by using a heterogeneous copper catalyst significantly decreases the copper leaching since the pH of the reaction mixture is maintained in a narrow interval [29,38-41].

Moreover, toxic intermediates as hydroquinone, benzoquinone, and catechol are not produced at pH 8, while these were found in the catalytic phenol oxidation at acidic conditions [38-41]. However, the rate of oxidation in basic conditions is lower than that in acidic ones [29], up to 1 order of magnitude. Basic conditions are also useful to prevent catalyst fouling. Operating conditions were also modified by modulation of the liquid flow rate. It had a minor effect on phenol conversion but it also affected product distribution, favoring the total oxidation process and, hence, reducing refractory compounds. No Cu leaching was observed for the fresh catalyst when the concentration of phenol was <1.5 kg/m^3 [11]. The concentration of pollutants in wastewaters cannot be, however, easily controlled. Copper leaching was found to be independent of temperature [29].

Modification of the catalyst composition is among the most effective means to prevent or decrease leaching of copper from the catalyst. An attempt to limit copper leaching by the modification of the catalyst composition was made by Hocevar et al. [30,31]. They prepared the mixed $Ce_{1-x}Cu_xO_{2-\delta}$ catalysts support, using the precipitation and sol-gel methods, which are much less soluble in hot acidic solutions. If prepared in the form with highly dispersed copper oxide phases on CeO_2, they are catalytically very active under mild reaction conditions and are selective toward the CO_2 formation. Arena et al. also studied coprecipitated $CuCeO_x$ and their finding was, however, that copper is still significantly leached from the Cu/Ce catalyst [28,29].

Kim and Ihm found carbonaceous deposits on the used transition metal catalysts for the wet oxidation of phenol and observed a substantial variation in the amount and nature of the carbonaceous deposits [49]. On this context, supported manganese oxide catalysts showed the highest amount of carbonaceous species on the catalyst surface. Cerium addition to the transition metal oxide catalysts was proved to increase the amount of carbonaceous deposits, leading at the same time to the enhancement of catalytic activity for phenol abatement. The nature of the carbonaceous deposits was mostly aromatic, and the aliphatic carbon appeared only for the Cu loaded systems [49].

The fouling of the catalyst representing the major cause of deactivation for Mn-based catalyst, due to the carbon deposition on the catalyst surface, Hussain et al. tried to enhance its features by doping the system with various promoters (Pt, Pd, Ag, K, etc.), founding that potassium addition (4 wt%) enhances both activity and resistance to fouling, allowing, thus, for a subsequent substantial mitigation of CWAO reaction conditions [16,17]. They also stressed the influence of the redox properties, reaction conditions and Mn/Ce atomic ratio on their activity and stability in the CWAO of phenol improving the complete oxidation of the substrate and founded the system active even at low temperatures (383K) getting a quasi total conversion of phenol and TOC just after 30 minutes for a catalyst to substrate ratio of 5 (wt/wt) [1,14-17]. They also observed no leaching of the active phase [1,14-17].

Abecassis-Wolfowitz et al., instead, stressed the ability of this system to adsorb phenol, in terms of Surface Reaction Adsorption (SRA) and Carbon Adsorption Capacity (CAC) [33]. Namely, they tried to take advantage of this drawback by enhancing it and indicated in the regeneration of the catalyst at temperatures higher than that of adsorption the way to really mineralize the organic noxious compounds [33,34]. This would imply the development of a suitable reactor for burning the carbonaceous deposits at relatively high temperatures and the appropriate layout of the industrial plant, that is a sensible increase of the operative costs of the process.

I.5. Model compounds employed in the CWAO of phenol

Various organic compounds have been used in the CWAO, taken as model substances for the study of mechanistic and kinetic evidences. Carboxylic acids, alcohols, aldehydes, chetones, amides, etc. represents the most common substrates employed, as summarized on Table 5 toghether with experimental data reported [11,13]. The above mentioned compounds received so much attention because of their resistance to mineralization, and, among them, carboxylic acids show the high resistance to oxidation [11,13]. Evidently, the catalytic system able to oxidize them would allow the total oxidation of every compound.

Carboxylic acids/salts are structurally similar but do not necessarily undergo WO (in terms of % TOC/COD conversion) to a similar extent under the same reaction conditions. An example, which clearly illustrates, it is the difference in TOC conversion between 1,3-benzenedicarboxylic acid (sodium salt) and 1,4-benzenedicarboxylic acid (sodium salt), where the latter compound undergoes only 3.2% TOC conversion, compared to 21.0% for the former compound, under the same reaction conditions [72].

Solution pH can have a significant effect on the WO of carboxylic acids/salts. This is clearly demonstrated by the differences in WO (in terms of TOC conversion) between oxalic acid and the sodium salt of oxalic acid under similar physical reaction conditions (90% TOC conversion at pH 2.5 after 20 min at 160 °C, compared with <2% TOC conversion at pH >14 after 2 h at 165 °C) [11,13].

On this account, the pH can affect the catalytic activity, due to the different stability between acids and salts. In fact, the resonance energy stabilize the salt making it more refractory to total oxidation. It is evident that the pH control any intermediate formation and, as a consequence, the overall TOC removal [11].

P-cumaric acid was chosen by some groups of scientists as a representative model compound of the biologically recalcitrant polyphenolic fraction in olive processing and wine distilleries wastewaters. It belongs to a group of phenolic components of these streams comprising gallic, caffeic, and

31

vanillic acids that are known to inhibit biological treatment of wastewaters of agricultural origin. Poly- (ethylene glycol)s (PEGs) are an important group of nonionic water-soluble polymers that are commonly used in the production of surfactants, lubricants, pharmaceuticals, etc. The rate of their biodegradation substantially decreases with the increasing of molecular weight [13].

Table 5. Model compounds generally studied in the CWAO of phenol. Reaction conditions and results.

Compound	Reaction conditions	Results
alkylbenzene sulfonate	P_{O_2}=1.5Mpa, T=200-240°C	TOC,60%;COD,70%(2h, pH 8.5,240°C)
methyl, ethyl alcohol, diethyl malonate, diethylene glycol	P_{O_2}=3Mpa, T=220°C	TOC,30-38%;COD,29-38%(2h)
formaldehyde, dioxane	P_{O_2}=3Mpa, T=220°C	TOC,39-45%;COD,41-45%(2h)
propionaldehyde, methyl ethyl ketone, acetylacetone	P_{O_2}=3MPa, T=220°C	TOC,43-54%;COD,58-61%(2h)
acrylonitrile	T=275-320°C	acrylonitrile,99.00%(275°C)
1,2-diphenyl-hydrazine	T=275-320°C	1,2- hydrazine,99.98%(275°C)
poly(vinyl alcohol), PVA	P_{O_2}=0.53-2.11Mpa T=175-275°C	TOC,80%(4h,250°C,1.4MPa); COD,88%(4h,250°C,0.7MPa)
PEG	P_{O_2}=2-3Mpa, T=110-240°C	TOC,55%(1h,240°C)
Monoazo dye Orange II	P_{O_2}=1Mpa, T=180-240°C	TOC,70%(1.5h,230°C)
Azo dye Orange II	P_{O_2}=1Mpa, T=130-190°C	Azo dye, 100%(1h,190°C)
thiocyanate	P_{O_2}=7.1-10.1Mpa T=170-210°C	Tiocyanates,99% (210min,210°C)
n-butylamine	P_{O_2}=1Mpa, T=220°C	TOC,3.5%(1h)
pyridine	P_{O_2}=1Mpa, T=270°C	TOC,10.7%(1h)
p-cumaric acid	P_{O_2}=2.0-5.0 Mpa,T=160-190°C	p-cumaric acid, 90%
phenol	P_{O_2}=0.5-2.0 Mpa,T=80-170°C	phenol, 75-100%
acetic acid	P_{O_2}=1.2 Mpa,T=190°C	Acetic acid, 96%

Imamura et al. compared the activities of various noble metals (5 wt % metal) or metal oxide supported on γ-Al$_2$O$_3$, CeO$_2$, TiO$_2$, ZrO$_2$ catalysts, and NaY-zeolite in the oxidation of PEG-200. The activity on TOC removal was as follows [76]:

$$a_{Ru} = a_{Rh} = a_{Pt} > a_{Ir} > a_{Pd} > a_{MnO}$$

32

Tests performed using Ru on ceria demonstrated it is the most effective catalyst among the ones investigated and is even better than homogeneous catalyst $Cu(NO_3)_2$. The reactivity of intermediates such as ethylene glycol, formic acid, and formaldehyde toward this catalyst was also investigated by Imamura et al. Again, the activity of Ru/CeO_2 catalyst was higher than that of copper nitrate [77]. The lower the pH, the higher was the TOC removal.

Imamura et al. also studied the decomposition of PEG 200 in the presence of Mn/Ce (7:3) and Co/Bi (5:1) composite oxides. Both catalysts were fairly active in oxidation, with ~60% in TOC removal in 60 min [78].

Mantzavinos et al. found that a Co/Bi composite oxide was the most effective for the degradation of *p*-coumaric acid with its almost total conversion and 75% TOC removal in 10 min at 403 K [79]. The possible leaching of cobalt, a toxic metal, excludes application of this catalyst, since it could inhibit the microorganisms in the after-CWAO biological treatment. $CuO\text{-}ZnO/Al_2O_3$ and $CuO\text{-}CoO\text{-}ZnO/Al_2O_3$ catalysts performed similarly (TOC removal ~ 80% in 90 min), but leaching of Cu and Zn occurred at acidic conditions, while at alkaline conditions Al was dissolved. The same authors also oxidized PEG in the presence of base and noble metal catalysts proving that Pt catalyst shows the better TOC removal (97% after 90 min) while Pd performed slightly worse. Metal oxides catalysts efficiency was much lower [79].

I.5.1. Phenol

Finally, numerous studies have been conducted in the catalytic wet oxidation of phenol, due to its presence in many wastewaters deriving from important industrial sites such as petro-chemistry, plastic, paper mills etc. Besides, phenol is a strong bactericide and at concentration higher than 200ppm can deactivate plants for the removal of BOD killing bacteria in biological processes [1,7,11,13].

Regarding sea plants, phenol can be toxic even at concentrations of 1÷100 ppm and, as a consequence, it must be abated under the level of 1ppm

(see Table 2). Phenols can also interfere in the oxidation of sulfides to sulfates and tiosulfates.

From a chemical point of view, phenol is a very stable compound, really refractory to oxidation. All such characteristics allow phenol to be elected as the model compound for the catalytic wet oxidation process both in presence and absence of catalysts [1,7,11,13].

Phenol oxidation is strongly affected by temperature, oxygen partial pressure and pH. Many intermediates can generate during its degradation such as more oxygenated organic compounds, aldehydes, ketones, or acetic, formic and oxalic acids (see schemes 1, 2, and 3), some of which results more refractory to the subsequent oxidation to carbon dioxide, representing, thus a crucial limit for the CWAO process [1,7,11,13].

I.6. Reaction mechanism

In spite of the numerous efforts carried out to evaluate the catalytic efficiency (substrate and TOC conversion) of the catalytic wet oxidation of organic pollutants present in various wastewaters, the chemistry taking place during the reaction is still unclear. In fact, due to the presence of many compounds in the stream coupled with the occurrence of different reactions pathways relative to each compound, many reaction mechanisms can be proposed. Slight differences in molecular structure can have significant effects on the type of intermediates formed during WO of a carboxylic acid/salt. This, in turn, influences the achieved degree of TOC conversion. A very slight change in molecular structure can lead to the formation of intermediates that are either more or less susceptible to WO. Therefore, this can lead to a higher or lower degree of TOC conversion. [13]

Different types of chemical reactions leading to oxidation of organic compounds under typical WO conditions include auto-oxidation (free radical reactions involving oxygen), heterolytic/homolytic cleavage (oxidative or non-oxidative thermal degradation), hydrolysis, decarboxylation, alkoxide formation followed by subsequent oxidation (alkaline solution), and carbanion formation followed by subsequent oxidation (alkaline solution). Other phenomena can influence and/or cause the WO of an organic compound, such as co-oxidation (oxidation of an organic compound via a free-radical intermediate produced during oxidation of another compound) and so on [13].

The total number of reactions occuring during the WO of a single organic compound can be extremely high, even for a simple low molecular- weight organic compound such as propionic acid. For example, Day et al. proposed a 16-step free-radical reaction mechanism for the WO of propionic acid [80].

The wet oxidation of an organic compound involves two main stages: (i) a physical stage, which involves the oxygen transfer from the gas phase to the liquid phase, and (ii) a chemical stage, involving the reaction between the transferred oxygen (or an active oxygenated species formed during degradation) and the organic compound.

Essentially, the physical stage of WO involves the oxygen transfer from gas to the liquid phase, for which the only significant resistance to transfer is located at the gas/liquid interface (film model), with the following three limiting cases:
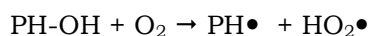
(i)   oxygen reaction within the film because of a rapid chemical reaction (oxygen transfer rate is enhanced);

(ii)   rapid oxygen reaction within the bulk liquid, where its concentration is close to zero (the overall rate is equal to the rate at which oxygen is transferred);

(iii)   oxygen concentration within the bulk liquid equal to the interface (or equilibrium) concentration (the overall rate is the *chemical* step rate, and it is usually low).

According to Debellefontaine et al., the effect that the rate of oxygen transfer on the overall reaction rate can often be eliminated through high mixing efficiency, which then enables unencumbered chemical kinetic rates to be determined [13,27].

On the other hand, many factors can influence the rate/extent of the chemical reaction stage. The most important factors include temperature, oxygen partial pressure (dissolved oxygen concentration), reactor geometry, the composition of the reactor walls, pH of the reacting solution, and the "nature" of the organic compounds (and intermediates formed)/kind of occurring chemical reactions.
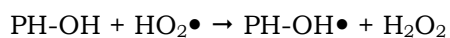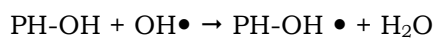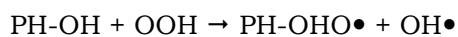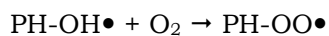
Phenol is first oxidized to polyphenols that are converted into benzoquinones. The rings of benzoquinones are then opened with the formation of appropriate acids, which are oxidized to low molecular wight carboxylic acids. Decarboxylation and/or oxidation of diacids leads to monocarboxylic acids that are most refractory to oxidation, particularly acetic acid. The difficulty of oxidation of acetic acid could be due to a low adsorption coefficient of the molecule on the catalyst surface or to a weak reactivity in the adsorbed state, or to a combination of both. The mechanism of phenol oxidation is that important because many other organic compounds are oxidized to (poly)phenols in the first reaction stages [13].

Initiation

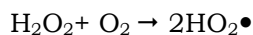PH-OH + O_2 → PH• + HO_2•

$k = 7*10^{12} \, exp^{(-150.000/RT)}$

Propagation

PH-OH• + O_2 → PH-OO•

PH-OH + PH-OHOO• → PH• + PH-OOH•

PH-OH + OOH → PH-OHO• + OH•

PH-OH + OH• → PH-OH • + H_2O

PH-OH + HO_2• → PH-OH• + H_2O_2

$k = 1.2*10^7 \, exp^{(-25.000/RT)}$

H_2O_2 + O_2 → $2HO_2$•

$k = 5.4*10^{10} \, exp^{(-166.200/RT)}$

H_2O_2 + OH• → H_2O + HO_2•

Termination

$2HO_2$• → H_2O_2 + O_2

OH• + intermediates or reactor walls → products

HO_2• + intermediates or reactor walls → products

PH-OO• + intermediates or reactor walls → products
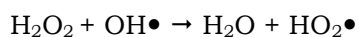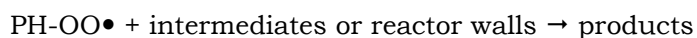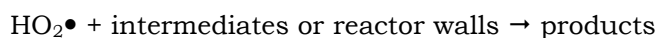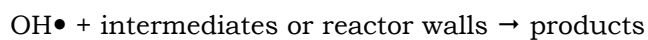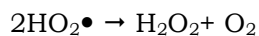
Scheme 1. Reaction scheme for the WO of phenol [81].

Rivas et al proposed a detailed reaction mechanism (Scheme 1), based predominantly on free-radical reactions, for the WO of phenol for which the bimolecular reaction between phenol and oxygen is considered to be the sole radical initiation step [81].

Very few detailed reaction pathways are proposed for the WO of phenol in contrast to the CWAO for which several reaction pathways have been proposed. The lack of proposed reaction pathways for the WO of phenol may be due to the fact that Devlin and Harris published an extremely comprehensive reaction pathway almost 20 years ago [82]. A less-detailed version is schematized in Scheme 2.

Reaction pathways for the CWAO of phenol have been studied by several researchers over the last two or three decades. A sum of the proposed reaction pathways are given in Scheme 3 [82]. Evidently, many different intermediates from the CWAO of phenol on various catalysts can be produced during the reaction. These intermediates can have a significant effect on the final phenol and TOC conversion.
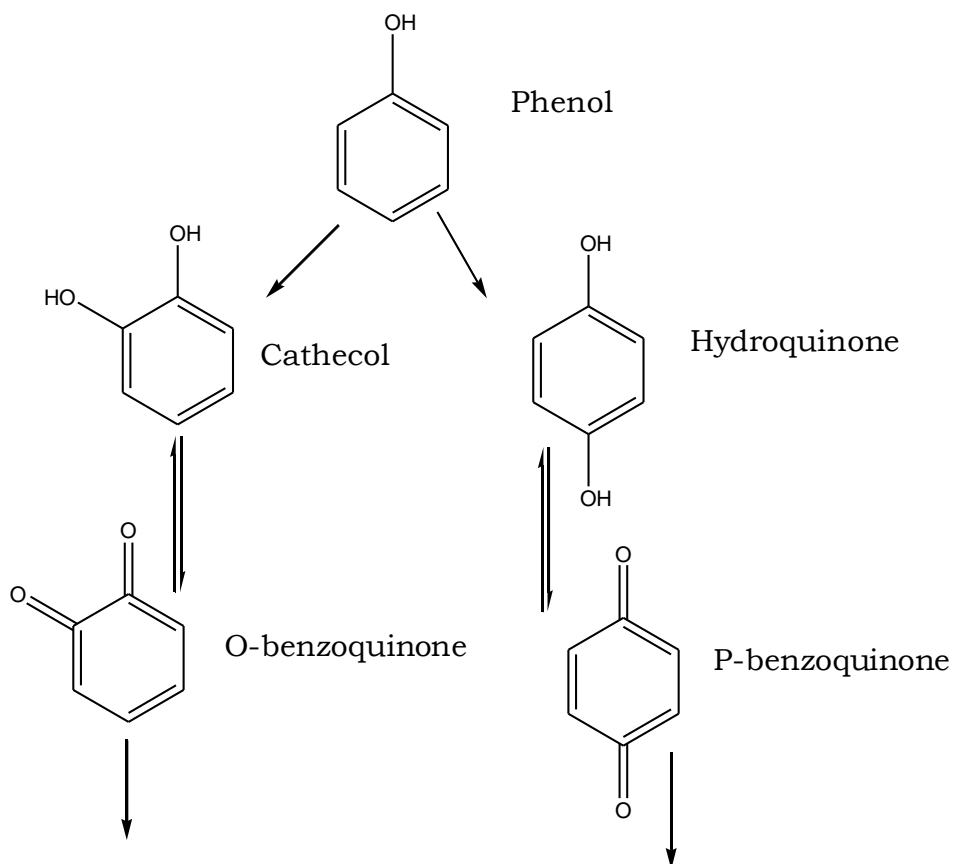
4-oxo-butenoic acid
Muconic acid
Maleic acid
Glyoxylic acid
Glyoxal
Acrylic acid
Succinic acid
3-hydroxy propionic acid
3-oxo-propionic acid
Propionic acid
Malonic acid
Formic acid

2,5-dioxo-3-hexendioic acid
1,4-dioxo-2-butene
4-oxo-2-butenoic acid
Maleic acid
Glyoxal
Acrylic acid
Formic acid
Succinic acid
3-hydroxy propionic acid
3-oxo-propionic acid
Propionic acid
Malonic acid
Formic acid

Scheme 2. Reaction scheme for the WO of phenol [81].
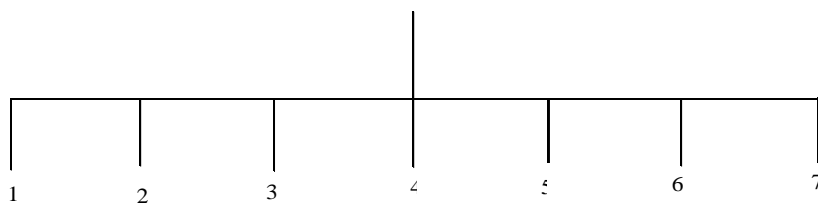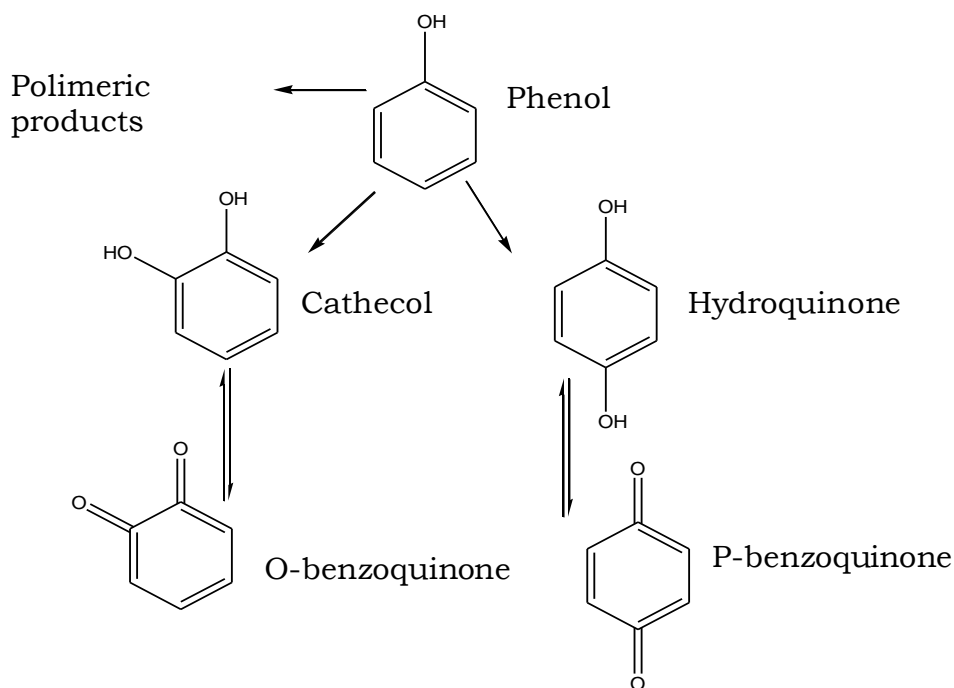
1= maleic, succinic, malonic, glyoxylic, oxalic, acetic acid
2= maleic, oxalic acid
3= maleic, succinic, acrylic, oxo and hydroxyl propionic, oxalic, acetic, formic acid
4= 2,5 dioxo-3-hexendioic, maleic, acrylic, malonic, oxalic, acetic, formic acid
5= maleic, fumaric, malonic, acetic, oxalic, formic acid
6= succinic, acetic, oxalic, formic acid
7= C4-products

Scheme 3. Reaction scheme for the CWAO of phenol [82].

40

I.7. Reactors suitable for the catalytic wet air oxidation

The effectiveness and economical feasibility of the CWAO process is highly influenced by the choice of reactor and its design. Thus, chemical reactor engineering and design pose significant challenges because of many factors:

(i)   the multiphase nature of CWAO reactions (two-phase for homogeneous reactions and three-phase for heterogeneous reactions),

(ii)   the temperatures and pressures of the reaction,

(iii)   the radical reaction mechanism.

In multiphase reactors, complex relationships between parameters such as chemical kinetics, thermodynamics, interphase, intraphase, intraparticle mass transport, flow patterns and hydrodynamics influence reactant mass transfer. Complex models have been developed to assess the influence of catalyst wetting, the interface masstransfer coefficients, the intraparticle effective diffusion coefficient, and the axial dispersion coefficient on CWAO [11]. Thus, multiphase reactions are greatly influenced by diffusion kinetics
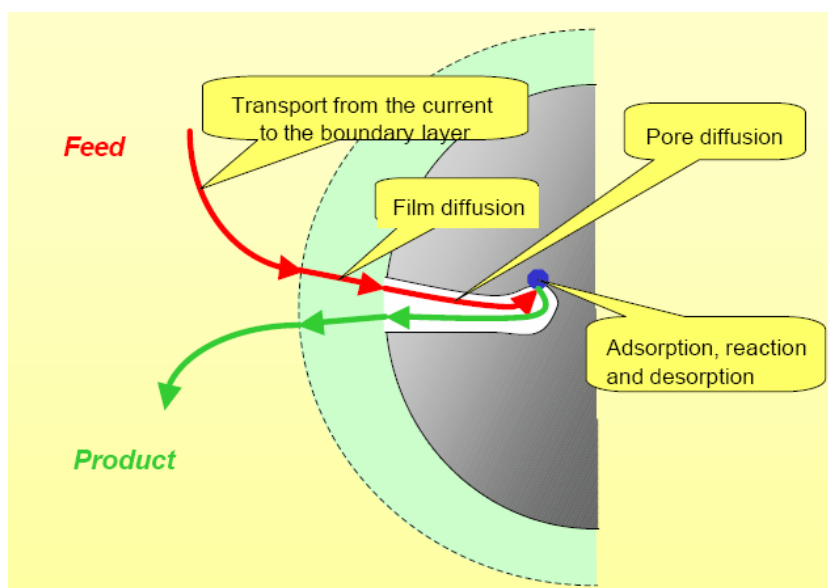
Figue 5. Reaction steps of catalytic multiphase reactions.

because of the various interfaces which represent the resistances into the reacting solution as evidenced in Figure 5 and schematized in Figure 6.
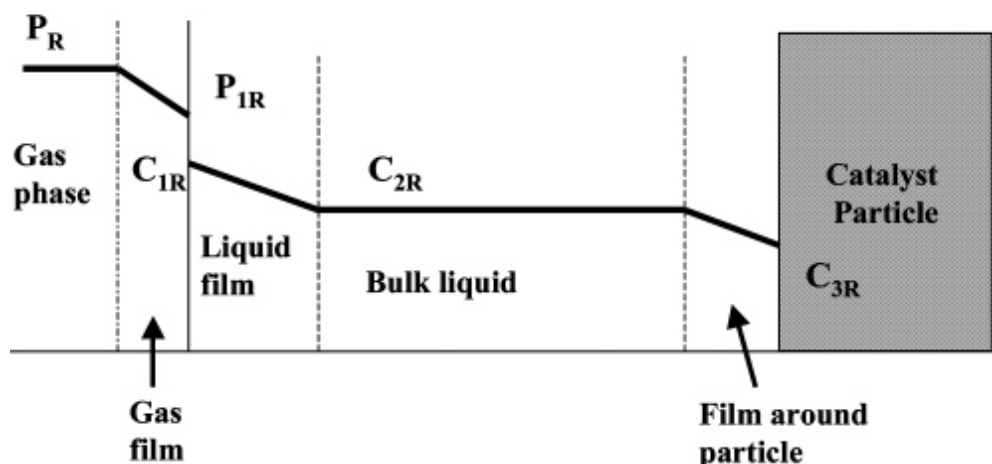
Figure 6. Path of gaseous reactant to catalyst surface in slurry reactor (adapted from reference [13]).

Mechanistically, a three-phase reaction involves the following steps:

(i)   mass transfer of the gaseous species to the gas/liquid interface,

(ii)   mass transfer of the gaseous species from the gas/liquid interface to the bulk liquid,

(iii)   mass transfer of gaseous and liquid species to the catalyst surface,

(iv)   intraparticle diffusion of the reactant species to catalyst-active sites,

(v)   adsorption of species on active sites and surface reaction,

(vi)   desorption and diffusion into the liquid phase.

The eventual homogeneous-heterogeneous radical reaction mechanism, with its initiation, propagation, and termination reactions, can add further complexity.

Common two-phase reactor types used in CWAO (Figure 7) are divided in:

1. TRICKLE BED REACTOR (TBR);

2. PACKED BUBBLE COLUMN (PBC);

3. THREE-PHASE FLUDIZED BED (TPFB);

4. SLURRY BUBBLE COLUMN (SBC),
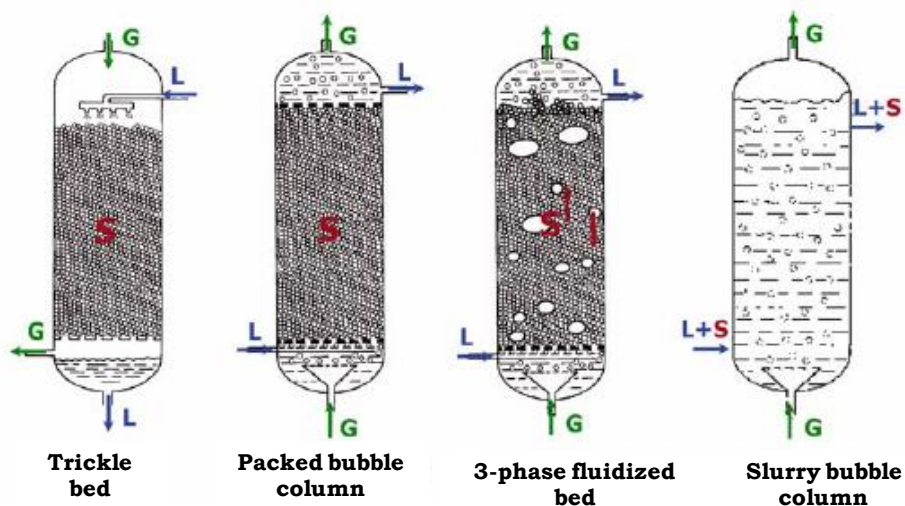
Figure 7. Typical reactor configurations used in the CWAO process (adapted from reference [1]).

Huge amount of detailed studies on the aspects of wet oxidation reactor design, and, in particular, the influence of reaction kinetics and mass transfer, are present in literature [13,20,83,84]. Extensive kinetic models have been developed for CWAO reactions from simple lumped schemes to very detailed reaction schemes, including simple empirical power laws to mechanistic Langmuir-Hinshelwood kinetics [13]. Kinetic data are often measured in differential reactor mode (low conversion), so to have simple information, not affected by complex reactions and other drawbacks. However, the increases in computer power and efficiency allows the use of integral reactor models with nonlinear kinetic parameter estimation giving more accurate representation of

the industrial reactor operations [13]. Unfortunately, only a few published studies have predicted the performance of integral reactors.

It must be also stated that the extrapolation of kinetic data collected in one reactor type can be very difficult and may lead to erroneous conclusions. For example, measurements of reaction rates in stirred slurry reactors, which are generally characterized by a high liquid-to-catalyst ratio, may not yield true oxidation rates, because of the enhanced homogeneous condensation reactions that lead to catalyst deactivation [13].

A reactor design with minimal mass-transfer limitations must carefully consider [11]:

> (i)   the gas-liquid interfacial area (a),
>
> (ii)   the gas holdup,
>
> (iii)   the bubble diameter,
>
> (iv)   the liquid mass-transfer coefficient (k_L),
>
> (v)   the flow regime,
>
> (vi)   the reactor geometry, and
>
> (vii) the material of construction.

The economics of the WO process is largely determined by reaction rates and the demanded oxidation degree with both parameters controlling the reaction time for wastewater conversion and, thus, the reactor volume. Increased pressure and temperature leads to increased reaction rates and, thus, reduced reactor size. However, some of the advantages may be offset by the increased materials costs for a high-pressure-high-temperature reactor [11].

I.7.1. Effect of gas-liquid interfacial area, gas holdup, and bubble size

The overall mass-transfer coefficient is dependent on the interfacial area available between the gas and liquid phases. In bubble systems, the specific gas-liquid interfacial area a is defined as:

$$a = \frac{6\epsilon}{d_{vs}}$$

where d_{vs} is the mean bubble diameter and ϵ is the gas holdup [13].

The gas holdup, gas volume to fluid volume ratio, determines the extent of interfacial area available for mass transfer, and is controlled by the gas flow rate (increased flow rate increases the efficiency, but also increases capital and operating costs, because of the increased pumping requirement) and the rise velocity of bubbles which is linked to bubble size (smaller bubbles have a slower rise velocity and offer a greater area for mass transfer).

Bubble size is controlled by the type of sparger, the flow regime, the fluid properties, and the operating conditions. An increase in gas delivery pressure to the sparger also leads to smaller bubble sizes, smaller rise velocities, and, thus, a greater $ê$ value. With increasing pressure, however, the influence of sparger type diminishes quickly and became insignificant at pressures of >10 MPa [13].

I.7.2. Effect of oxygen partial pressure

Oxygen pressure is one of the critical driving force for oxygen mass transfer from the gas phase to the liquid phase, and some pressure drops due to the CO_2 formation during the reaction or to the vapor pressure due to the high operating temperature, can affect the efficiency with which oxygen is transferred and, thus, results in a declining reaction rate as the reaction progresses [20]. Thus, reactors switched in series, with the ability to remove carbon dioxide between them, result in a more effective reduction of COD than a single reactor with the same residence time [13].

I.7.3. Effect of reactor geometry and construction materials

Presenting the CWAO process a heterogeneous-homogeneous radical reaction mechanism involving radical initiation, propagation, and termination reactions, the kinetics and selectivity of such reactions can be controlled by the reactor geometry and construction material. For example, metallic surfaces, can promote some radicalic reaction changing global reaction rates and reaction selectivity. Similarly, Kolaczkowski et al. found in a laboratory-scale experiment that the rate of phenol removal was faster in a glass-lined vessel than in a stainless-steel one [20]. However, in a full-scale industrial reactor, the ratio of the surface area to the volume of the vessel is far smaller and, hence, the wall effects in such a system are far less pronounced than in the laboratory [20]. This is a significant issue when scaling up processes from the laboratory scale to plant scale and when comparing results from different reactor configurations [13].

I.7.4. Co-current packed bed

Phenol conversion achieved in the packed bubble column (PBC) exceed that in the trickle bed reactor (TBR) at any phenol concentration mainly because of the degree of catalyst wetting achieved by the different reactor configurations.

Wetting is defined as the fraction of the external particle surface covered by liquid (the internal particle surface is generally fully wetted, because of capillary forces). The wetting efficiency in the TBR was ca.80%, showing that operation in this reactor mode occurs with only partially wetted catalyst pellets. However, with a PBC, especially in an up-flow configuration, almost complete catalyst wetting can be achieved [84].

The wetting efficiency is also improved by increasing the gas superficial velocity or, in a down-flow configuration, by increasing the pressure. However, the diffusion diminishes faster than the increased wetting efficiency in a downward flow, and, thus, the up-flow configuration is preferred when the

pressure is increased. Increasing the pressure and temperature increased the solubility of oxygen and, hence, its transfer flux to the catalyst [84].

I.7.5. Fluidized bed

Three-phase fluidized bed reactors (FBRs) are ideal for adiabatic operations and wastewaters with very high organic loads. Catalyst particle size directly influences the phase holdups, solids mixing pattern (ranging between no solids mixing and complete solids mixing), mass transfer, and chemical reaction rates. However, Iliuta and Larachi found that phenol conversion initially increases with particle size, reaches a maximum with pellets of 1mm, and then decreases with larger pellets [84]. This behavior in fluidized beds was attributed to the competing effects of increasing solids holdup (beneficial) and decreasing η (detrimental). Debellefontaine et al. also showed that increased liquid backmixing resulted in decreased solids holdup and, thus, reduced the conversion of pollutants in domestic and industrial wastewaters in bubble columns [27]. Axial mixing generally only affects TBRs at the bench and pilot levels but not in fullscale commercial reactors, because, according to Mears criteria, axial dispersion becomes negligible for beds 20 times longer than the catalyst pellet size [13].

I.7.5. Monolith reactor

A new class of reactor suitable for the CWAO process is represented by the monolith reactors which uses monolithic catalysts *(honeycomb catalysts)* produced as continuous unitary structures containing small straight passages. These structures are of large void fraction ranging from 0.7 to >0.9. Catalytic species are incorporated either into a very thin layer of a porous catalyst support deposited on the channel or incorporated into the thin walls [11].

The short diffusion distance inside the thin layer of the structured catalysts results in higher catalyst utilization. The regular structure of the arranged catalysts prevents the formation of the random misdistributions characteristic of
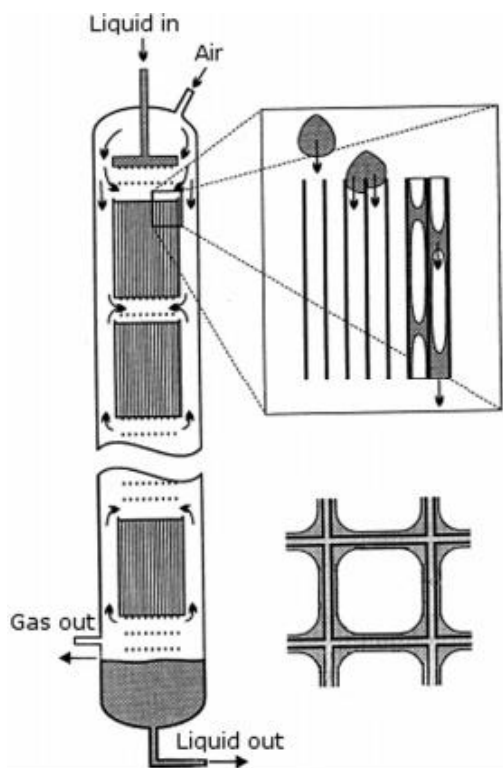
Figure 8. Monolith reactor. Adapted from reference [11].

randomly packed particles beds. This contributes to the better yield than that in conventional packed-bed reactors. Scale-up of monolithic reactors can be expected to be straightforward, since the conditions within the individual channels are scale invariant. Important advantages offered by monolithic catalysts for catalytic wet air oxidation (CWAO), such as the low pressure drop (large volumetric liquid flow rates), short internal diffusion distances (oxygen transport rate limiting), and the low tendency for bed plugging in the uniform and straight channels (wastewaters often contain solid particles or the particles can be formed through oxidation of metal containing pollutants), have attracted the attention of scientists and practitioners [11]. In Figure 8 a typical monolithic reactor is represented.

Finally, advantages and disadvantages of batch, trickle bed and monolith reactors are briefly summarized in Table 6.

Table 6. Advantages and disadvantages of various reactor configurations.

Reactor	Advantages	Disadvantages
Trickle bed	high conversion low liquid hold-up high catalyst loading low pressure drop	low distribution in the liquid partial catalyst wetting high intraparticle resistence low radial mixing low masstransfer coefficient bad temperature control
Slurry	high external mass low intraparticle resistence easy catalyst addition and easy temperature control	catalyst separation high radial mixing low catalyst load high liquid/solid ratio
Monolith	Low pressure drop High liquid velocity Short internal diffusion distances Very low bed flooding High mass transfer	Low radial transfer High costs Low scal-up

I.8. References

[1]. F. Larachi, *Top. Catal.* **33** (2005) 109.

[2]. A. Eftaxias, *PhD Thesys* Universitat Rovira i Virgili, Tarragona, Spain, December 2002

[3]. J. Levec, A. Pintar, *Catal. Today* **124** (2007) 172

[4]. G. Busca, S. Berardinelli, C. Resini, L. Arrighi, *J. Hazard. Mater.* **160** (2008) 265.

[5]. K. Pirkanniemi, K. Sillanpää, *Chemosphere* **48** (2002) 1047.

[6]. S.K. Bhargava, J. Tardio, J. Prasad, K. Foger, D.B. Akolekar, S.C. Grocott, *Ind. Eng. Chem. Res.* **45** (2006) 1221.

[7]. S. Imamura, *Ind. Eng. Chem. Res.* **38** (1999) 1743.

[8]. Yu.I. Matatov-Meytal, M. Sheintuch, *Ind. Eng. Chem. Res.* **37** (1998) 309.

[9]. R.S. Ramalho, *Introduction to wastewater treatment processes*, 2nd edition, Academic Press, New York, USA, 1952.

[10]. P. Berbenni, G. Bianucci, *Trattamento delle acque di scarico*, ET/AS KOMPASS, Milan, ITALY, (1965).

[11]. A. Cybulski, *Ind. Eng. Chem. Res.*, **46**, (2007) 4007.

[12]. A. Pintar, G. Bercic, M. Besson, P. Gallezot, *Appl. Catal. B* **47** (2004) 143.

[13]. S.K. Bhargava, J. Tardio, J. Prasad, K. Foger, D.B. Akolekar, S.C. Grocott, *Ind. Eng. Chem. Res.* **45** (2006) 1221

[14]. H.Chen, A. Sayari, A. Adnot, F. Larachi, *Appl. Catal. B* **2** (2001) 195.

[15]. S. Hamoudi, F. Larachi, A. Sayari, *J. Catal.,* **177 (**1998) 247.

[16]. S.T. Hussain, A. Sayari, F. Larachi, *Appl. Catal. B* **34** (2001) 1.

[17]. S.T. Hussain, A. Sayari, F. Larachi, *J. Catal.* **201** (2001) 153.

[18]. Lenntech, *Catalytic wet air oxidation, http://www.lenntech.com/zcwao.htm.*

[19]. R. Andreozzi, V. Caprio, A. Insola, R. Marotta, *Catal. Today* **1999**, *53* (1), 51-59.

[20]. S.T. Kolaczkowski, P. Plucuiski, F.J. Beltran, F.J. Rivas, D.B. Melurgh, *Chem. Eng. J.* **73** (1999) 149.

[21]. V.S. Mishra, V.V. Mahajani, J.B. Joshi, *Ind. Eng. Chem. Res.*, **34** (1995) 2.

[22]. C.B. Maugans, C. Ellis, Proceeding of the IT3'02 Conference, New Orleans, LA, May 13-17, (2002).

[23]. R. Andreozzi, V. Caprio, A. Insola, R. Marotta, *Catal. Today*, **53** (1999) 51.

[24]. F.J. Zimmermann, *Chem. Eng.* **25** (1958) 117.

[25]. F. Luck, *Catal. Today* **53** (1999) 81.

[26]. F. Luck, *Catal. Today* **27** (1996) 195.

[27]. H. Debellefontaine, J. N. Foussard, *Waste Management* **20** (2000) 2.

[28]. F. Arena, R. Giovenco, T. Torre, A. Venuto, A. Parmaliana, *Appl. Catal. B* **45** (2003) 51.

[29]. F. Arena, E. Alongi, P. Famulari, A. Parmaliana, G. Trunfio, *Catal. Lett.* **107** (2006) 39.

[30]. S. Hočevar, J. Batista, J. Levec, *J. Catal.* **184** (1999) 39.

[31]. S. Hočevar, U. Opara Krašovec, B. Orel, A.S. Arico`, H. Kim, *Appl. Catal. B* **28** (2000) 113.

[32]. S.T. Hussain, A. Sayari, F. Larachi, *J.Catal.* **201** (2001) 153

[33]. M. Abecassis-Wolfovich, M.V. Landau, A. Brenner, M. Herskowitz, *Ind. Eng. Chem. Res.* **43** (2004) 5089.

[34]. M. Abecassis-Wolfovich, R. Jothiramalingam, M.V. Landau, M. Herrskowitz, B. Viswanathan, *Appl. Catal. B* **59** (2005) 91.

[35]. F. Arena, J. Negro, G. Trunfio, A. Parmaliana, *Ind. Eng. Chem. Res.* **46** (2007) 6724.

[36]. F. Arena, A. Parmaliana, G. Trunfio, *Sci. Tec. Catal.* **172** (2007) 489.

[37]. A.F.J Santiago, J.F. Sousa, R.C. Guedes, C.E.M. Jerônimo, M. Benachour, *J. Hazard. Mat. B* **38** (2006) 325

[38]. A. Santos, P. Yustos, A. Quintanilla, S. Rodriguez, F. Garcia-Ochoa, *Appl. Catal. B* **39** (2002) 97.

[39]. A. Santos, P. Yustos, A. Quintanilla, F. Garcia-Ochoa, *Appl. Catal. B* **53** (2004) 181.
[40]. A. Santos, P. Yustos, A. Quintanilla, F. Garcia-Ochoa, *Chem. Eng. Sci.* **60** (2005) 4866.
[41]. A. Santos, P. Yustos, A. Quintanilla, G. Ruiz, F. Garcia-Ochoa, *Appl. Catal. B* **61** (2005) 323.
[42]. S. Imamura, *Ind. Eng. Chem. Res.* **38** (1999) 1743.
[43]. F. Arena, G. Trunfio, J. Negro, L. Spadaro, *Appl. Catal. B* **85** (2008) 40.
[44]. F. Arena, G. Trunfio, J. Negro, B. Fazio, L. Spadaro, *Chem. Mater.* **19** (2007) 2269.
[45]. F. Arena, G. Trunfio, J. Negro, L. Spadaro, *Mater. Res. Bull.* **43** (2008) 539.
[46]. F. Arena, G. Trunfio, J. Negro, L. Spadaro, *Appl. Catal. B* **59** (2008).
[47]. F. Arena, G. Trunfio, B. Fazio, J. Negro, L. Spadaro, *J. Phys. Chem. C* accepted for publication.
[48]. J. Prasad, J. Tardio, D.B. Akolekar, S.K. Bhargava, S.C. Grocott, *Ind. Eng. Chem. Res.* **43** (2004) 6363.
[49]. S.-K. Kim, S.-K. Ihm, *Top. Catal.* **33** (2005) 171.
[50]. Q. Wu, X. Hu, Po-l. Yue, *Chem. Eng. Sci.* **58** (2003) 923.
[51]. A. Sadana, J. R. Katzer, *Ind. Eng. Chem. Fundam.* **13 (2)** (1974) 127.
[52]. Y. Harada, A. Nakashiba, H. Matuura, T. Okina, H. Fujitani, K. Yamasaki, Y. Doi, S. Yurugi, *Process for treating wastewater by wet oxidation. Eur. Patent No. 224905,* (1987).
[53]. H.T. Gomes, J.L. Figueiredo, J.L. Faria, P. Serp, P. Kalck, P. *J. Mol. Catal. A:Chem.* **47** (2002) 182.
[54]. A. Fortuny, J. Font, A. Fabregat, *Appl. Catal. B* (1998).
[55]. L. Oliviero, J. Barbier, D, Duprez, A. Guerrero-Ruiz, B. BAchiller-Baeza, I. Rodriguez-Ramos, *Appl. Catal. B* **25** (2000) 267.
[56]. S-K Kim, S-K Ihm, *Ind. Eng. Chem. Res.* **41** (2002) 1967.
[57]. J. Barbier, F. Delano, F. Jabouille, D. Duprez, G. Blanchard, P. Isnard, *J. Catal.* **177** (1998) 378.
[58]. S. Duprez, F. Delano, J. Barbier, P. Isnard, G. Blanchard, *Catal. Today* **29** (1996) 317.
[59]. J. Barbier Jr., L. Oliviero, B. Renard, D. Duprez, *Catal. Today* **75** (2002) 29.
[60]. R. Ukropec, B. F. M. Kuster, J. C. Schoten, R. A. van Santen, *Appl. Catal. B* **23** (1999) 45.
[61]. H. Takayama, Q. Jiang-Yan, K. Inazu, K. Aika, *Chem. Letters* (1999) 377.
[62]. W. An, Q. Zhang, Y. Ma, K. T. Chuang, *Catal. Today* **64** (2001) 289.
[63]. Q. Zhang, K.T. Chuang, *Appl. Cat. B* **17** (1998) 321.
[64]. Q. Zhang, K.T. Chuang, *Environ. Sci. Technol.* **33** (1999) 3641.
[65]. A. Pintar, M. Besson, P. Gazellot, *Appl. Cat. B* **30** (2001) 123.
[66]. A. Pintar, M. Besson, P. Gazellot, *Appl. Cat. B* **31** (2001) 275.
[67]. J. Qin, Q. Zhang, K. T. Chuang, *Appl. Cat. B* **29** (2001) 115.
[68]. G. Baldi, S. Goto, C. K. Chow, J. M. Smith, *Ind. Eng. Chem. Proc. Des. Dev.* **13** (1974) 447.
[69]. S. Goto, J. M. Smith, *AIChE J.* **21** (1974) 714.
[70]. C. de Leitenbourg, D. Goi, A. Primavera, A. trovarelli, G. Dolcetti, *Appl. Cat. B* **11** (1996) L29.
[71]. S. Christoskova, M. Stoyanova, *Wat. Res.* **35** (2001) 2073.
[72]. A. Pintar, J. Levec, *J. Catal. 135* **1992** 345.
[73]. A. Alvarez, P. M. McLurgh, D.P. Plucinski, *Ind. Eng. Chem. Res.* **41 (9)** (2002) 2153.
[74]. A. Fortuny, C. Bengoa, J. Font, F. Castells, A. Fabregat, *Catal. Today* **53 (1)** (1999) 107.
[75]. A. Alejandre, F. Medina, A. Fortuny, P Salagre, J.E. Sueiras, *Appl. Catal., B* **16 (1)** (1998) 53
[76]. S. Imamura, I. Fukuda, S. Ishida, *Ind. Eng. Chem. Res.* **27 (4)** (1988) 718.

[77]. S. Imamura, A. Doi, S. Ishida, *Ind. Eng. Chem. Res. Prod. Res. Dev.* **24 (1)** (1985) 75.

[78]. S. Imamura, M. Nakamura, N. Kawabata, J. Yoshida, S. Ishida, *Ind. Eng. Chem. Res. Prod. Res. Dev.* **25 (1)** (1986) *24*.

[79]. D. Mantzavinos, R. Hellenbrand, A.G. Livingston, I.S. Metcalfe, *Appl. Catal., B* **7 (3-4)** (1996) 379.

[80]. D. Day, R.R. Hudgins, P.L. Silveston, *Can. J. Chem. Eng.* **51 (6)** (1973) 733.

[81]. F.J. Rivas, S.T. Kolaczkowski, F.J. Beltram, D.B. McLough, *Chem. Eng. Sci.*, **53** (1998) 2575.

[82]. H.R. Devlin, I.J. Harris, *Ind. Eng. Chem. Foundam.* **23** (1984) 387.

[83]. A. Eftaxias, J. Font, A. Fortuny, J. Giralt, A. Fabregat, F. Stüber, *Appl. Catal. B* **33** (2001) 175.

[84]. I. Iliuta, F Larachi, *Chem. Eng. Process.* **40** (2001) 175.

Chapter II

CWAO of phenol with Cu-based catalyst

II.1. Preparation

Many works appeared in literature attribute to Cu-based catalyst good activity in the Catalytic Wet Oxydation of phenol and various attempts were carried out in order to shed lights into reaction mechanism and catalyst activity and stability [1-25].

A CuCeO$_x$ catalyst was prepared by co-precipitating the Cu(NO$_3$)$_2$ and (NH$_4$)$_2$Ce(NO$_3$)$_6$ precursors dissolved in a bi-distilled water solution keeping constant the pH at a value of ca. 5.5 by adding a 0.2M solution of NaCO$_3$ for a Cu loading of 3.6wt.%, confirmed by Atomic Adsorption measurements [14,15]. After precipitation, the catalyst was filtered, washed, dried at 100°C all night and further calcined at 500°C for 6h. An aliquot of the calcined sample was pre-treated in a H$_2$ flow at 300 °C (1 h) to attain a full reduction of the active phase [14,15]. The catalyst was tested in the CWAO of phenol in the range 130–170°C using a 0.25 L PTF-lined autoclave equipped with a magnetically driven turbine impeller (~1000 rpm), keeping constant the pressure (P$_{O2}$; 7atm) by feeding pure oxygen at the rate of 0.2Lmin^{-1}. The initial phenol concentration (C$_0$) was fixed at 1000±50 ppm (1000ppm) varying the catalyst load between 1 and 3 in terms of catalyst-to phenol mass ratio (R) [14,15].

II.2. Performance

Experimental activity data are shown in Figure 1 in terms of phenol and TOC conversion (A) and pH and concentration of leached out Cu ions (B) against reaction time.

A rise of reaction temperature enables a regular increase of the CWAO activity evidenced by the minor time required for a complete (90–100%) conversion of the substrate from ca. 6h at 130°C to 0.5h at 170°C.

The mineralization efficiency, directly related to the TOC decrease, attains a final value of ca. 60% at any temperature, concomitantly with the full substrate conversion (Figure 1A). Moreover, irrespective of temperature, both phenol and TOC conversion depict a peculiar 'S-shaped' trend, diagnostic of a kinetic regime depending on the conversion extent [6–9,14,15].
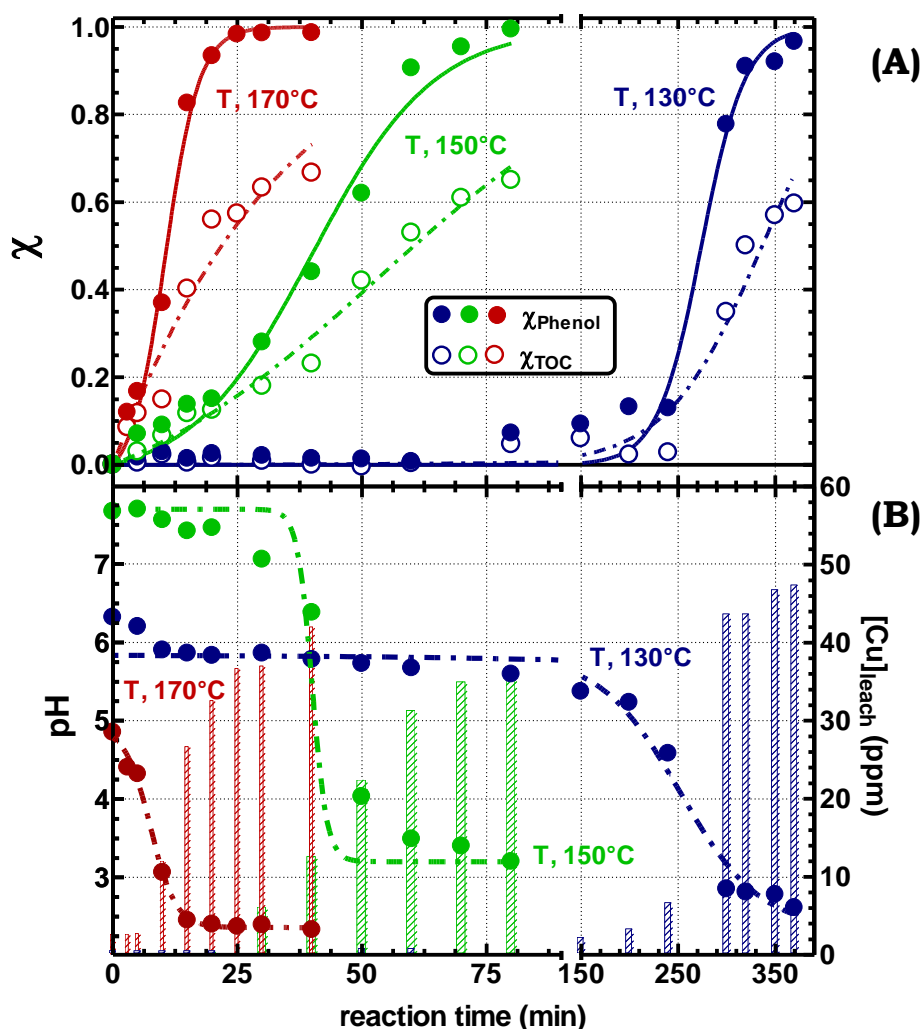
Figure 1. Effect of the reaction temperature on the CWAO of phenol on CuCeO$_x$ catalyst (P$_{O2}$, 7 atm; R, 1). (A) Phenol and TOC conversion vs. reaction time; (B) pH and [Cu]$_{leach}$ *vs.* reaction time.

As a rule, after an 'induction time' inversely correlated to the temperature, a fast kinetic regime leads to a sharp rise of phenol and TOC conversion. At the same time, the pH of the reacting solution (Figure 1B) falls from the initial neutral value [6,7] to acidic range, tending smoothly to final values of ca. 2–3 [14,15]. Closely mirroring the conversion curves (Figure 1A), this trend reflects the formation of light acidic intermediates (e.g., oxalic, formic, acetic acid. etc.) more refractory to total oxidation [1,6–12,14–19]. Then, the pH decrease favors the copper dissolution from the catalytic system (Figure 1B) speeding up, in turn, the reaction kinetics and establishing a

parallel homogeneous reaction mechanism [6,10,11,14-15]. This is documented by simultaneous variations of the derivative curves shown in Figure 2A, which monitor the changes in reaction and leaching rate with time [14-15].
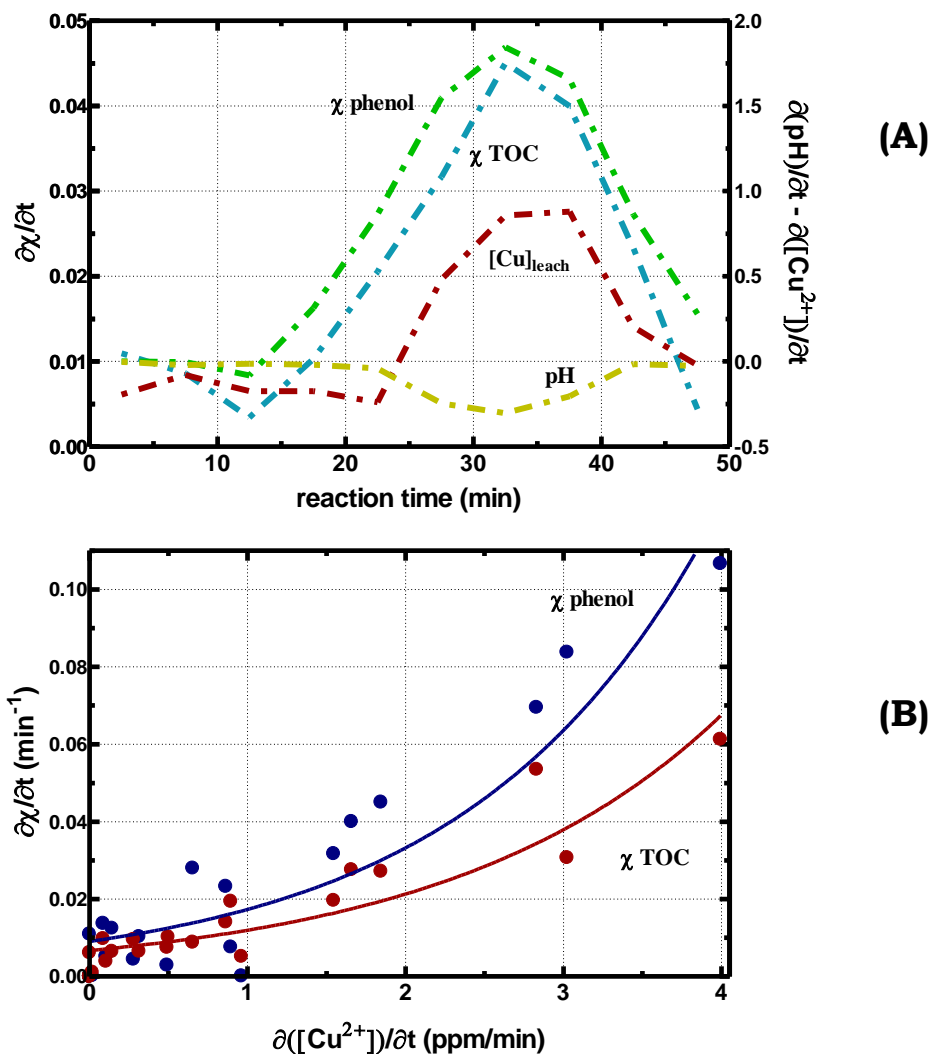
Figure 2. CWAO of phenol on $CuCeO_x$ catalyst (T, 150°C; P_{O2}, 7 atm; R, 1). (A) Rates of phenol and TOC conversion, of pH variations and Cu leaching vs. reaction time. (B) Rates of phenol and TOC conversion vs. rate of Cu leaching.

Actually, these findings entail a close relationship amongst chemical composition of the reacting medium, rate of Cu leaching and reaction kinetics [6–11,14–19], as evidenced by exponential-like relationships between derivative conversion of phenol and TOC and the rate of Cu leaching shown in Figure 2B. Anyway, final $[Cu]_{leach}$ values of 35–45 ppm (Figure 1B) signal a quasi-quantitative loss of the active phase at the end of any runs [14-15].

The above activity data were then analyzed according to the autocatalytic kinetic model proposed in literature [6,9] in order to obtain kinetic constants of phenol and TOC conversion at different T (Table 1). This let us to state the consistency of the apparent activation energy data relative to the autocatalytic kinetic model proposed in literature [6,9]. The kinetic constants of phenol and TOC conversion obtained at different T are summarized in Table 1 and confirm the above mentioned consistency [6–8,10,20].

Table 1. CWAO of phenol (R, 1). Values of the kinetic constants of phenol and TOC conversion according to the homogeneous autocatalytic reaction mechanism proposed on references [6] and [9].

T (°C)	P (atm)	K_{phenol} $(Ls^{-1}mol^{-1})$	k_{TOC} $(Ls^{-1}mol^{-1})$
130	10	0.258	015
150	12	1.055	0.71
170	15	2.730	1.93

Accounting for the effect of temperature, such figures result in reliable straight-line Arrhenius plots (Figure 3), corresponding to apparent activation energy values equal to 88(±8) and 94(±9) kJ/mol for phenol and TOC conversion, respectively. These results are in good agreement with literature data published on the CWAO of phenol with Cu-based catalysts [6–10,21], accounting for the occurrence of a common heterogeneous–homogeneous reaction path.

Therefore, the experimental results showed by the $CuCeO_x$ system, with the peculiar reaction kinetics and relative induction time can be explained by the slow dissolution of Cu ions into the reacting solution. Interestingly, this phenomenon can be related to the fall in pH due to the initial degradation of

phenol into light organic acids. Then, the dissolved metal generate hydroperoxy radicals by means of a homogeneous reaction mechanism, perhaps mediated by the Cu^{2+}/Cu^+ redox couple [6,10,22].
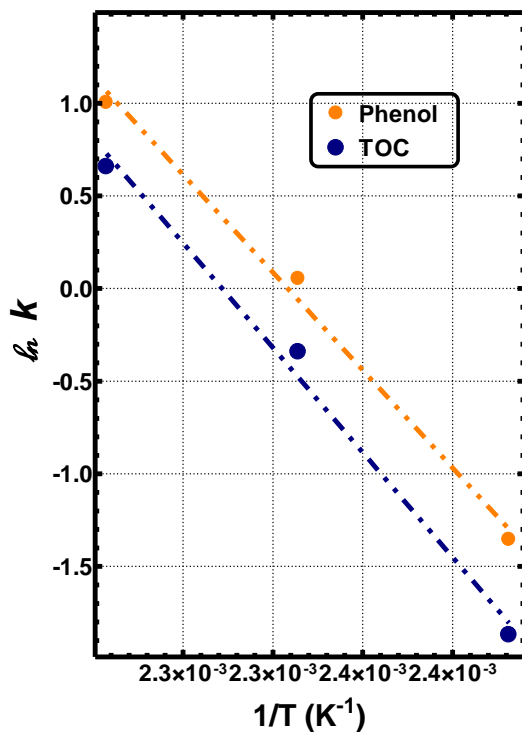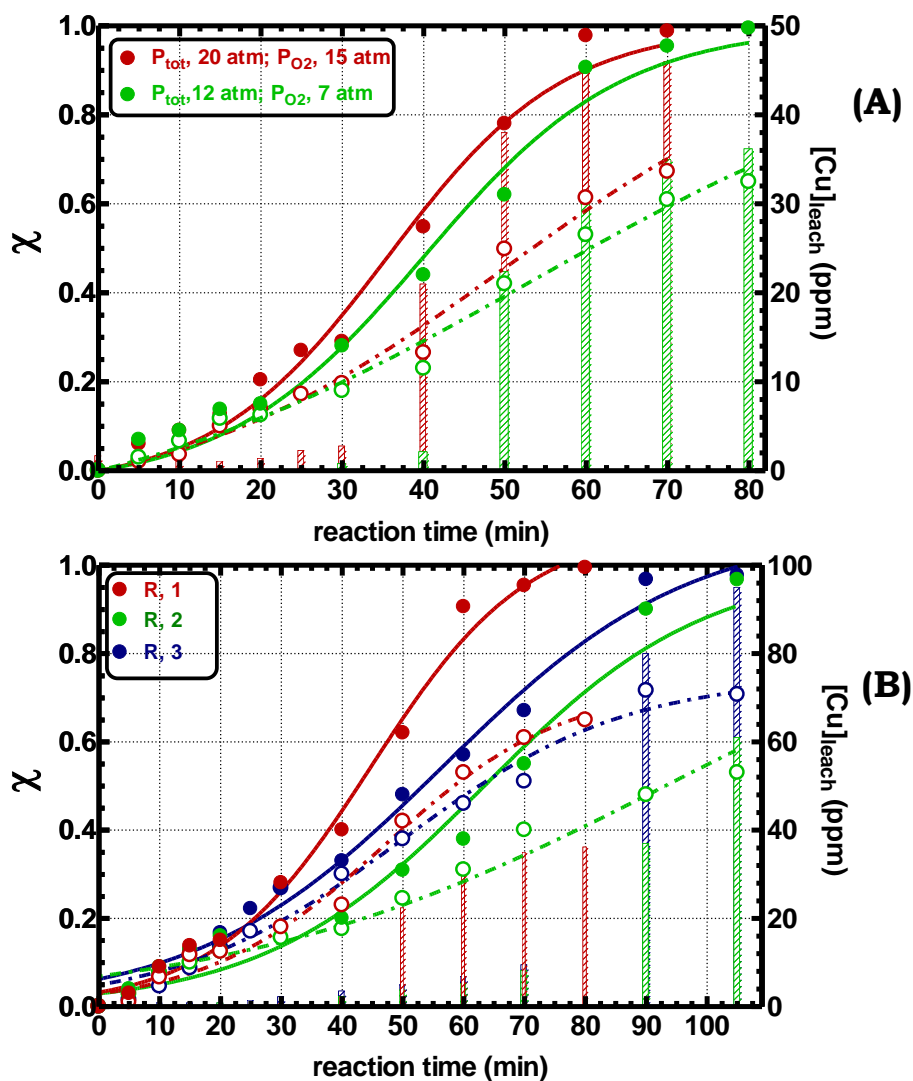

Figure 3. CWAO of phenol on $CuCeO_x$ catalyst (P_{O2}, 7 atm; R, 1). Arrhenius plot of the kinetic constants of phenol and TOC conversion obtained from the autocatalytic kinetic model equation (adapted from references [6] and [9]).

Moreover, the effects of the reaction pressure (A) and catalyst-to phenol mass ratio (B) and catalyst reduction, shown in Figure 4 and 5, respectively, confirm the peculiar reaction path of the Cu-based catalysts in the CWAO of phenol (T,150°C). The negligible influence of the oxygen partial pressure on the rate of phenol and TOC conversion (Figure 4A) essentially denotes the lack of relevant interphase resistances [6–8]. Moreover, according to a (quasi) zero order dependence on oxygen concentration, it rules out the generation of active oxygen species as r.d.s., irrespective of the occurrence of heterogeneous or homogeneous reaction paths [6–8,26].

Also in this case the establishing of a fast kinetic regime parallels the sudden rise in $[Cu]_{leach}$, confirming again that the 'limiting step' lies in the dissolution of the active phase [14,15]. This findings are further confirmed

performing tests with different catalyst-to-substrate mass ratio (R): the reaction rate is slightly faster for a R value of 1 and keeps practically unchanged for Rs equal to 2–3 (Figure 4B). Again, the 'S-shaped' trend of the conversion curves, giving an insignificant role to the solid catalyst, is strongly related to the pH decrease and $[Cu]_{leach}$, still confirming the prevalent contribution of the homogeneous reaction path.

Figure 4. CWAO of phenol on $CuCeO_x$ catalyst (T, 150°C; P_{O2}, 7 atm; R, 1). Influence of pressure (A) and catalyst-to-phenol mass ratio (B) on phenol and TOC conversion and $[Cu]_{leach}$.

The active phase chemical state does not affect the aforesaid CWAO pattern, given the same conversion values, variations in pH and resistance to leaching of the pre-reduced (at 300°C) system similar to those of the calcined catalyst (Figure 5). However, in this case a shorter induction time is observable due to an easier dissolution of the active phase from Cu/CuO particles in comparison to the leaching of Cu^{2+} ions strongly interacting with the support in the calcined system [14,15].
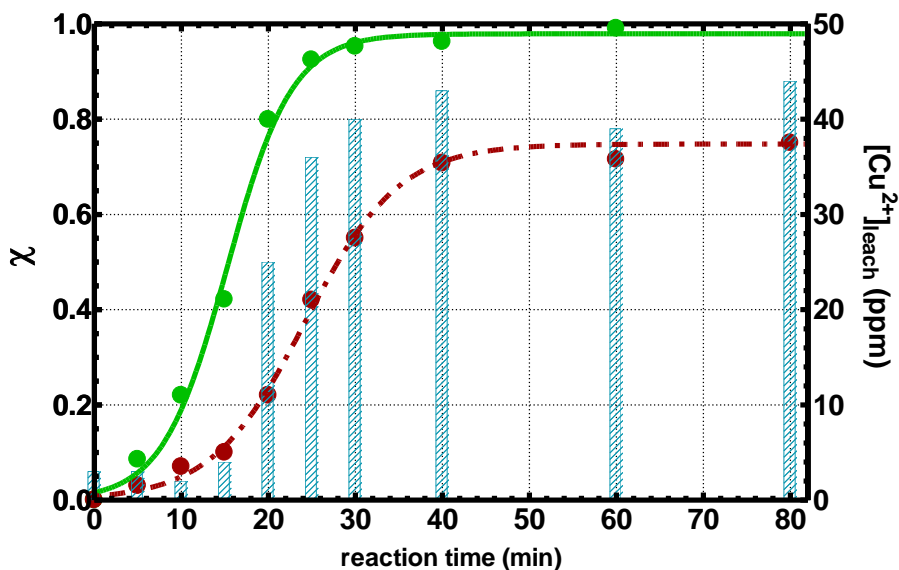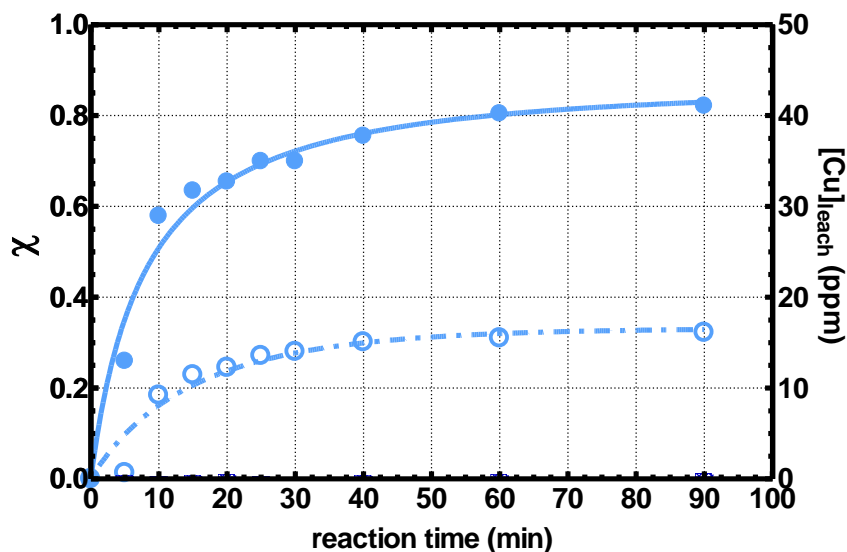

Figure 5. CWAO of phenol on the pre-reduced (300°C) CuCeO$_x$ catalyst (T, 150°C; P$_{O2}$, 12 atm; R, 1). Phenol and TOC conversion and [Cu]$_{leach}$ *vs.* reaction time.

In order to confirm the influence of pH on the reaction mechanism a CWAO of phenol was performed buffering the solution at a mildly basic value by means of a bicarbonate buffered (pH~8) solution. Different phenol and TOC conversion rate, then, confirmed the influence of pH on the CWAO performance of the studied system (Figure 6). In this case, at a first glance, the lack of an 'induction time' denotes some remarkable changes in the main reaction path(s) [11,16–18]. In fact, phenol conversion increases sharply to ca. 60% during the first 10 minutes, and then it rises very smoothly until a value of ca. 85% in the next 80 minutes. Likewise, the TOC conversion rises

progressively to ca. 30% during the first 40 min keeping unchanged until the end of the run.

Interestingly, the halved efficiency in phenol and TOC conversion with respect to those at 'free' pH conditions counterbalance the active phase leaching absence ($[Cu]_{leach}$<1 ppm) detected under such conditions.

**Figure 6.** CWAO of phenol on $CuCeO_x$ catalyst (T, 150°C; P_{O2}, 12 atm; R, 1) in a bicarbonate-buffered (pH~8) reacting solution. Phenol and TOC conversion and $[Cu]_{leach}$ *vs.* reaction time.

According to Santos et al. [16–18], last data entail a reaction mechanism driven by the catalyst surface, generating phenoxy radicals which subsequently react with bicarbonate ions, which act as radical scavengers. Inhibiting the formation of the hydroperoxide radical species, which implies a lower mineralization efficiency, the formation of much lower toxic intermediates would be, thus, the most valuable achievement of Cu-based catalysts in bicarbonate-buffered streams [16–18]. Unfortunately, the scarce efficiency in removing the substrate and the evident production of more refractory intermediates account for a limited activity of the title system when the active phase does not occur.

II.3 Redox behaviour and catalytic mechanism

The CuCeO$_x$ system suitability in driving a redox cycle under CWAO conditions, was evaluated by performing comparative TPR analysis of the catalyst both 'as-prepared' and
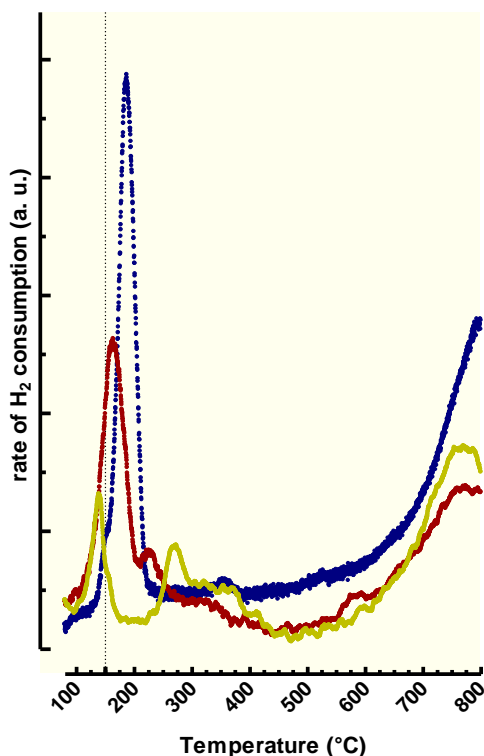
Figure 7. TPR profiles of the 'as-prepared' and gas-phase 'reduced-oxidized' (T, 160°C) CuCeO$_x$ catalyst.

subjected to gas-phase reduction-oxidation treatment. TPR spectra are compared in Figure 7, while the values of reduction maxima and extents of H$_2$ consumption, referred to the reduction of Cu^{2+} (LT) and Ce^{4+} (HT) ions [14-15], respectively, are summarized in Table 1. The TPR profile of the 'as-prepared' system displays a main reduction peak centred at 180°C monitoring the reduction of highly dispersed isolated Cu^{2+} ions in a strong interaction with the support [14-15].

The corresponding supra-stoichiometric H$_2$ consumption (H$_2$/Cu, 1.30) signals the concomitant reduction of surface neighbouring Ce^{4+} ions, evidence of a high active phase dispersion across ceria lattice [14-15]. This characteristic is compulsory for enabling an easy 'electron-transfer' process at the interface between Cu^{2+} ions and the support, which promotes synergistically the redox features of the system [14-15]. A baseline drift at T>500°C, shaping a broad unless resolved peak with maximum at 775°C, signals also an ongoing reduction of the bulk ceria matrix.

Table 2. TPR data of the CuCeO$_x$ catalyst 'as-prepared' and reduced-oxidized at 160°C.
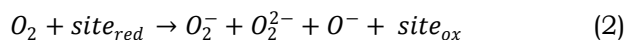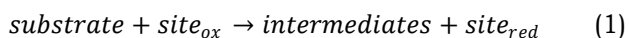
Catalyst	T$_{M1}$ (°C)	T$_{M2}$ (°C)	T$_{M3}$ (°C)	H$_2$ consumption (LT) H$_2$/Cu	(HT) H$_2$/Ce
'As-prepared'	180	–	775	1.30	0.14
'Reduced-oxidized'[a]	163	225	775	1.07	0.09
'Reduced-oxidized'[b]	140	273	768	0.31	0.09

[a]Reduced and oxidized at 160°C under continuous O$_2$ flow for 30 min.
[b]Reduced and oxidized at 160°C by O$_2$-pulses injection.

Furthermore, showing a considerable decrease of the active phase peak area, the TPR profiles of the catalyst subjected to gas-phase reduction/oxidation treatment at 160°C (Figure 7) indicate that the active phase cannot undergo a fully reversible redox cycle under reaction conditions (Table 2). As the straight reduction of Cu^{2+} ions to metal Cu [14-15], a completely reversible redox cycle would be in fact hindered by the formation of 'nascent' metal clusters which modify irreversibly structure, morphology and solid-state interactions of the catalytic system [15].

Catalytic oxidation would entail an incipient reduction of active site(s) for generation of active oxygen species (e.g., peroxy, hydroperoxy, etc.), prompting a surface-assisted reaction path [1,6,7,26,27]. The preliminary (partial) catalyst reduction by the substrate generates activated oxygen species yielding, in turn, a cyclic re-oxidation according to the general scheme [27]:

$$substrate + site_{ox} \rightarrow intermediates + site_{red} \qquad (1)$$

$$O_2 + site_{red} \rightarrow O_2^- + O_2^{2-} + O^- + site_{ox} \qquad (2)$$

On account of this, it is likely that Cu^{2+} ions of the heterogeneous system could undergo the substrate reduction generating electrophilic, strongly oxidising, oxygen species, which then attack the C–C bond degrading the phenol to light intermediates and, at the end, to CO$_2$ [1,2,6–8,14-15,27]. In turn, the incipient formation of light acidic intermediates enables the dissolution of Cu^{2+} ions from the catalyst, enhancing the reaction rate, but leading to the definitive loss of the active phase [14-15]. Then, also on the base of TPR evidences, the CuCeO$_x$ system likely undergoes the reduction step under reaction conditions (reaction 1) without restoring, however, the initial

state (reaction 2), essential for a full reversibility of the surface-assisted reaction redox cycle. Therefore, these data signal that under 'free' pH conditions the stability of Cu-based catalysts could be seriously perturbed even in the absence of leaching phenomena of the active phase [14–19].

On the other hand, hindering any copper leaching in bicarbonate-buffered solutions, basic pH values drive a prevailingly heterogeneous reaction path [15–19]. However, both the deprotonation equilibrium of the substrate and the presence of huge amounts of HCO_3^- ions can concur to deeply affect the CWAO mechanism.
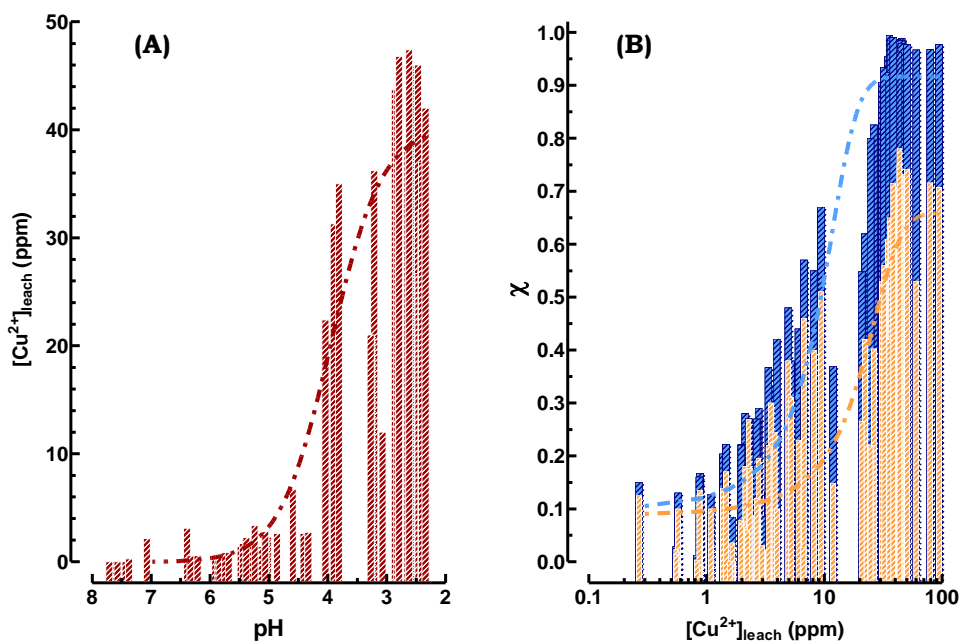
Figure 8. Summary of CWAO activity data under 'free' pH conditions: (A) [Cu]leach *vs.* pH and (B) phenol and TOC conversion *vs.* [Cu]leach.

Even in the case of the pre-reduced catalyst (Figure 5), a preliminary oxidation/dissolution of surface Cu^0 sites does not alter the fundamental features of the above reaction mechanisms. Irrespective of experimental conditions, catalyst formulation and treatments, general relationships among pH, rate of Cu leaching and phenol conversion can be depicted, as shown in Figure 8. Namely, Figure 8A indicates in a window of pH comprised between

4.5 and 4.0 the critical value for an effective dissolution of the active phase, prompting an homogeneous catalytic reaction path. This implies a marked enhancement of kinetics of phenol and TOC conversion (Figure 8B), confirming the peculiar CWAO mechanism of Cu-based systems under 'free' pH conditions [6–8,10,11,14–19].

II.4 Indications

The evidences come out from experimental data of the CWAO of phenol in a wide range of experimental conditions, employing the CuCeO$_x$ system proves that its acceptable activity is due to the active phase leaching into the reacting solution. Due to the presence into the reacting medium of low molecular weight carboxylic acids, byproducts of the incipient degradation of phenol under the CWAO conditions, it determines the definitive catalytic activity loss under "free pH" conditions.

On the other hand, buffering the solution by means of a bicarbonate buffer, thus avoiding the active phase leaching, determines a sensible activity decrease in the abatement of substrate and, more important, of TOC, leading to the presence into the reacting solution of some more refractory, even if less toxic species. Furthermore, TPR evidences confirm that the system is not stable, not presenting the ability to restore its initial reducing features, which represent a fundamental feature of an optimum oxidative catalyst. Moreover, the lack of redox cycles restoring ability represents another important evidence of catalyst deactivation.

Finally, this basic evidences indicate that the Cu-based system does not present the optimal characteristics for speeding up the catalytic wet oxidation of phenol and other organic compounds. In fact, the industrial scale-up of the process would entail the presence of an extra reactor devoted to the separation of the dissoluted copper ions, source of pollution in treated water.

II.5. References

[1].   S. Imamura, *Ind. Eng. Chem. Res.* **38** (1999) 1743.
[2].   F. Luck, *Catal. Today* **53** (1999) 81.
[3].   S. K. Bhargava, J. Tardio, J. Prasad, K. Foger, D.B. Akolekar, S.C. Grocott, *Ind. Eng. Chem. Res.* **45** (2006) 1221.
[4].   A. Cybulski, *Ind. Eng. Chem. Res.* **46** (2007) 4007.
[5].   F. Larachi, *Top. Catal.* **33** (2005) 109.
[6].   A. Pintar, J. Levec, *Chem. Eng. Sci.* **47** (1992) 2395.
[7].   A. Pintar, J. Levec, *Ind. Eng. Chem. Res.* **33** (1994) 3070.
[8].   J. Levec, A. Pintar, *Catal. Today* **24** (1995) 51.
[9].   S. Hoĉevar, J. Batista, J. Levec, *J. Catal.* **184** (1999) 39.
[10]. C. Miro´, A. Alejandre, A. Fortuny, C. Bengoa, J. Font, A. Fabregat, *Water Res.* **33** (1999) 1005.
[11]. A. Santos, E. Barroso, F. Garcia-Ochoa, *Catal. Today* **48** (1999) 109.
[12]. S. Hoĉevar, U. Opara Krašovec, B. Orel, A.S. Aricò, H. Kim, *Appl. Catal. B* **28** (2000) 113.
[13]. Q. Wu, X. Hu, P.L. Yue, X.S. Zhao, G.Q. Lu, *Appl. Catal. B* **32** (2001) 151.
[14]. F. Arena, R. Giovenco, T. Torre, A. Venuto, A. Parmaliana, *Appl. Catal. B* **45** (2003) 51.
[15]. F. Arena, E. Alongi, P. Famulari, A. Parmaliana, G. Trunfio, *Catal. Lett.* **107** (2006) 39.
[16]. A. Santos, P. Yustos, A. Quintanilla, S. Rodriguez, F. Garcia-Ochoa, *Appl. Catal. B* **39** (2002) 97.
[17]. A. Santos, P. Yustos, A. Quintanilla, F. Garcia-Ochoa, *Appl. Catal. B* **53** (2004) 181.
[18]. A. Santos, P. Yustos, A. Quintanilla, F. Garcia-Ochoa, *Chem. Eng. Sci.* **60** (2005) 4866.
[19]. A. Santos, P. Yustos, A. Quintanilla, G. Ruiz, F. Garcia-Ochoa, Appl. Catal. B **61** (2005) 323.
[20]. A. Eftaxias, J. Font, A. Fortuny, A. Fabregat, F. Stüber, *Comp. Chem. Eng.* **26** (2002) 1725.
[21]. A. Fortuny, C. Ferrer, C. Bengoa, J. Font, A. Fabregat, *Catal. Today* **24** (1995) 79.
[22]. A. Fortuny, C. Bengoa, J. Font, F. Castells, A. Fabregat, *Catal. Today* **53** (1999) 107.
[23]. X. Zhang, P.E. Savage, *Catal. Today* **40** (1998) 333.
[24]. A. Eftaxias, *PhD Thesys* Universitat Rovira i Virgili, Tarragona, Spain, December 2002
[25]. A. Eftaxias, J. Font, A. Fortuny, J. Giralt, A. Fabregat, F. Stüber, *Appl. Catal. B* **33** (2001) 175
[26]. Yu.I. Matatov-Meytal and M. Sheintuch, *Ind. Eng. Chem. Res.* **37** (1998) 309.
[27]. A. Bielansky, J. Haber, in *Oxygen in Catalysis* Marcel Dekker,Inc., New York, (1991).

Chapter III

Reactor corrosion during the CWAO of phenol

III.1. Homogeneous and heterogeneous catalysis of the CWAO of phenol

Preliminary analysis of previous blank tests (BT) data appeared in literature and relative to the wet air oxidation of phenol discloses an unexpected degree of uncertainty, as can be found out from Figure 1. At a glance, there is a substantial lack of reproducibility which can not be directly related to the effects of temperature (Figure 1A) on the extent and rate of substrate and TOC conversion [1-5]. Moreover, such unpredictability cannot be ascribed either to mass-transfer efficiency effects,
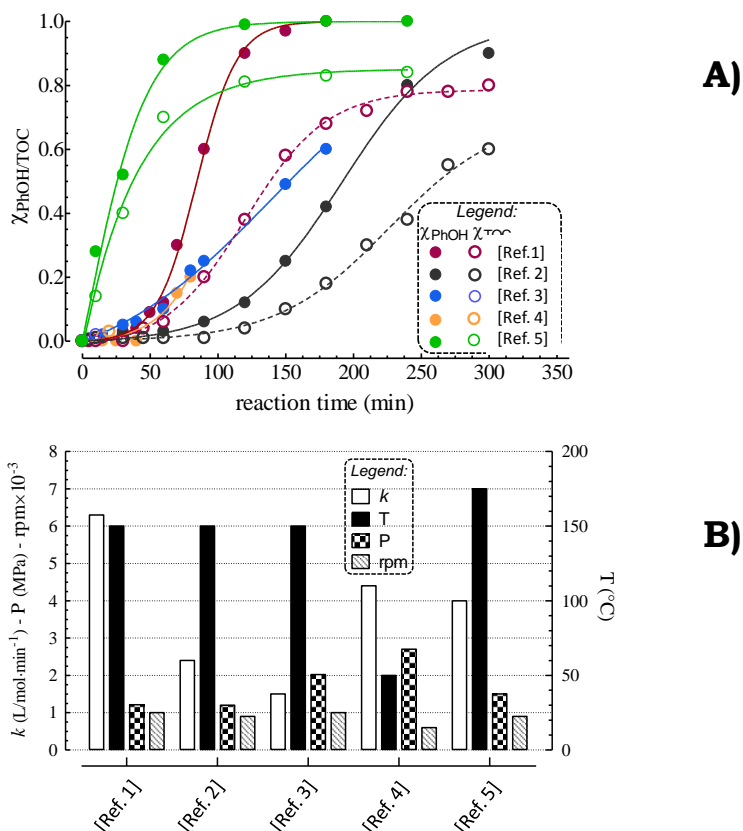
Figure 1. Literature "blank test" data in the wet air oxidation of phenol *(adapted from references [1-5])*. A) Phenol and TOC conversion *vs.* reaction time. B) Kinetic constant of the *homogeneous autocatalytic free-radical* reaction mechanism of phenol conversion.

since the lack of any correlation among the kinetic constant of the *homogeneous autocatalytic reaction* model [1-5], pressure and stirring speed (Figure 1B). It must be stated that those data were obtained using stainless-steel (SS) reactors, which seems to be the sole characteristic similar for all data analyzed [1-5].
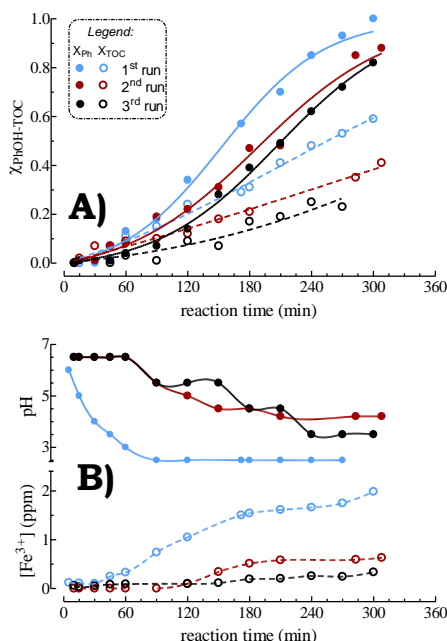
Figure 2. Blank test (BT) data in the wet air oxidation of phenol at 150°C. A) Phenol and TOC conversion *vs.* reaction time; B) pH and $[Fe^{3+}]$ *vs.* reaction time.

In order to shed lights into this strange unpredictability, a series of attempts was carried out to well reproduce the kinetics of phenol wet air oxidation previously obtained in an Inconel reactor [2], as shown on Figure 2. Although an almost complete (80-100%) final removal of phenol, different kinetic trends and a TOC conversion spanning between 30 and 60% are recorded during 5h of reaction time (Figure 2A). More interestingly, a drop in pH to values ranging between 2.5 and 4.0 coupled with a growing concentration of Fe^{3+} ions (Figure 2B) into the reacting solution was observed. Both phenomena parallel a TOC conversion higher than ca. 20%.

Not surprisingly, these findings could surmise an important role of the "foreign" Fe^{3+} species on the main reaction path, recalling the trends of oxidation promoted by Cu^{2+} ions [1,2,6-14]. Moreover, it was demonstrated that iron species are able to speed up the reaction rate and were employed both as homogeneous and as active phase in heterogeneous catalysts in many scientific works [15-20].

Since the lack of contamination of the initial solution, the presence of such species can be related to reactor-shield corrosion phenomena. High temperature and pressure and the presence of organic acids when phenol starts to be degraded cause an incipient corrosion of metallic surfaces, with the consequent leaching of Fe ions, as indicated by brown rust-stains on the top surfaces of the PTF vessel. Besides, evaporation (not avoidable at this high temperatures, even if under the water boiling point) and high stirring speed (required to avoid mass transfer limitations) could allow the wetting of some inner parts of the SS reactor-shield beneath PTF connectors and fittings [21]. Keeping in mind these evidences the PTF-connections and fittings were insulated by PTF-tape, to avoid any contact of the inner metal surfaces with the reacting solution.

With this change in reactor configuration, further homogeneous blank tests resulted reproducible in terms of extent and trend of phenol and TOC conversion, product selectivity and pH, while the concentration of Fe^{3+} was always below the AAS detection limit (<0.1 ppm). In particular, the phenol conversion keeps low (10-15%) during the first two hours of reaction time, rising abruptly in the 3rd hour and then progressively slows until an almost complete removal of the substrate in the subsequent 2 hours (Figure 2). With a much slower rate the TOC conversion gets a final value of ca. 20% (Figure 3). Final gravimetric measurements conducted after 6h (not reported in the Figure) indicate a CO_2 selectivity of only 8% of the theoretic value, in apparent discrepancy with the TOC abatement. The peculiar *sigmoidal* curves of the conversion trends were then modeled with the proposed mathematic equation adapted to a typical homogeneous *autocatalytic free radical* path [2-6,22,23].

In order to ascertain the active role of Fe^{3+} ions in the catalytic wet oxidation of phenol, tests in presence of $FeBr_3$ salt, put in an amount such as the homogeneous Fe^{3+} species vary in the range 0.5-10 ppm, were conducted.
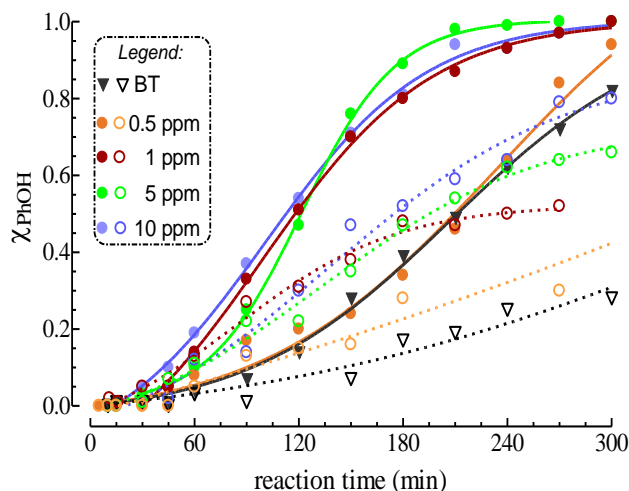
Figure 3. Homogeneous wet air oxidation of phenol at 150°C. Phenol and TOC conversion in absence (BT) and in the presence of the [Fe^{3+}] catalyst at different concentration.

Relative test data shown in Figure 3 indicate a significant promoting effect of that species which is explicated only for an ion concentration higher than 0.5 ppm. In fact, for lower concentration both phenol and TOC conversion proceeds like in BT, while a higher catalyst load causes the disappearance of the initial induction time promoting a complete removal of phenol in 3h. Meanwhile, a TOC conversion of ca. 50% increases slightly in the subsequent two hours until ca. 55 and 70% for Fe^{3+} concentration of 1 and 10 ppm, respectively. Therefore, such data signal a very low catalyst-to-substrate molar ratio (10^3) able to promote the CWAO of phenol.

Also in these tests the measured CO_2 selectivity resulted lower than TOC conversion by ca. 30%, while a final pH of ca. 3.5 matches the residual concentration of light organic acids. Then, experimental data confirm that the Fe^{3+} catalyst promotes the same *free-radical* reaction mechanism of the non-catalytic wet air oxidation [2,6,22,23], that is at the origin of the discrepancy between CO_2 selectivity and TOC conversion

74

values. In fact, the unselective pattern of the homogeneous radical oxidation path allows the formation of a range of C-intermediates, including volatile aldehydes, which at 150°C are stripped away by the oxygen flow with a consequent TOC loss. HPLC and TOC analyses of the "CO_2-trap" solution, not reported here and performed only for qualitative information, confirmed the presence of this organic compounds, mostly acroleyn and, to lower extent, of formaldehyde and acetaldehyde, in the outlet reaction stream.

Therefore, the efficiency of Fe^{3+} in the CWAO of phenol, at concentration as low as $\approx 10^{-7}$ mol/L, substantiates an indirect "active" contribution of the reaction system, likely at the origin of the low predictability and reproducibility of BT data (see Figures 1 and 2).

At variance, the composite MnO_x-CeO_2 system, representing a reference material as active heterogeneous catalyst [22-29], exhibits a superior CWAO efficiency denoted by the absence of any induction time and a complete elimination of both phenol and TOC after ca. 15 minutes of reaction time, as can be seen from Figure 4A. However, at the same reaction conditions, a slight, though continuous, rise of TOC mirrors a growing concentration of C2 acids responsible of the progressive pH decrease (Figure 4B). The pH value of 4.5 gives evidence of a considerably poorer production of acidic intermediate than homogeneous reactions, while a constant rate of CO_2 production (≈ 200 $\mu mol \cdot g_{cat}^{-1} \cdot h^{-1}$) ensures a cumulative mineralization selectivity of ca. 50% at the end of run (Figure 4A). With regard to the active phase leaching, despite of the acidic pH, a negligible ion concentration ($[Mn^{2+}] < 1$ ppm) rules out any significant contribution of the homogeneous catalytic path on the CWAO activity pattern of the $MnCeO_x$ system [27].

Besides, Figure 5 demonstrate the scarce activity of and Mn ions as homogeneous catalyst in that reaction: the acidic initial pH, given by the metal presence in the solution, instantly increase in concomitance with the injection of phenol in the reaction solution, making the Mn^{2+} ions

precipitating as MnO_2.
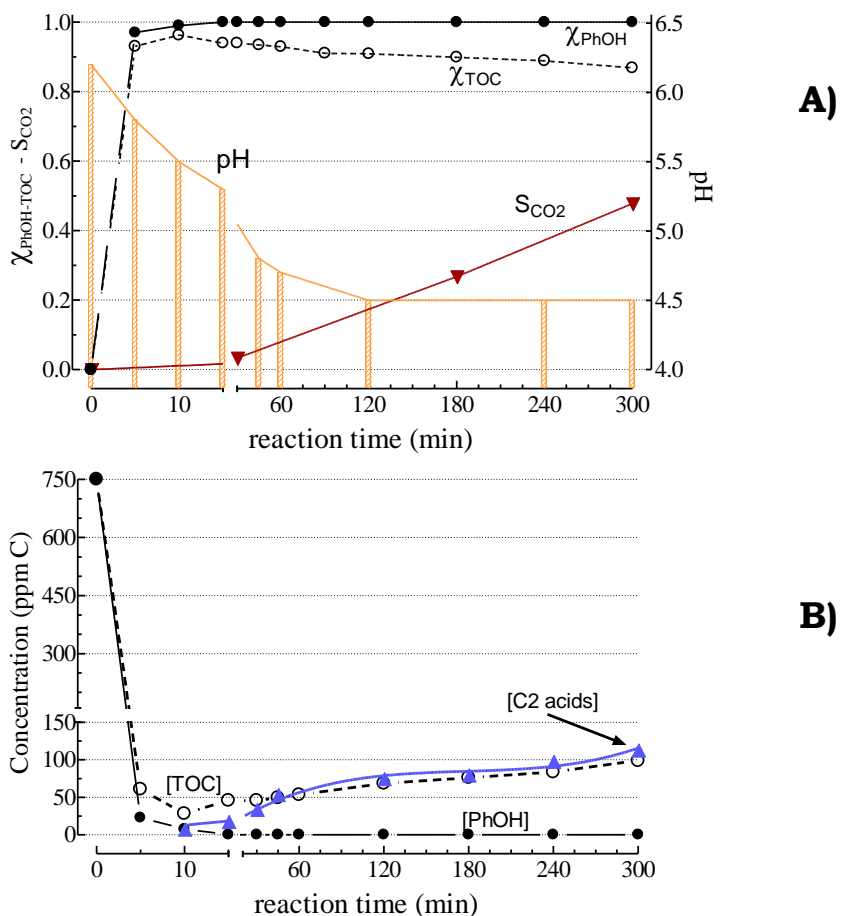
Figure 4. Catalytic wet air oxidation of phenol at 150°C using the heterogeneous $MnCeO_x$ system (R, 5). A) Phenol and TOC conversion, pH and CO_2 selectivity *vs.* reaction time; B) Concentration of phenol, TOC and C2 organic acids *vs.* reaction time.

Therefore, apart from the production of some common intermediates, experimental data disclose that the heterogeneous catalyst drives a different and cleaner reaction mechanism enabling a superior CWAO

efficiency in terms of TOC abatement and mineralization selectivity [27].
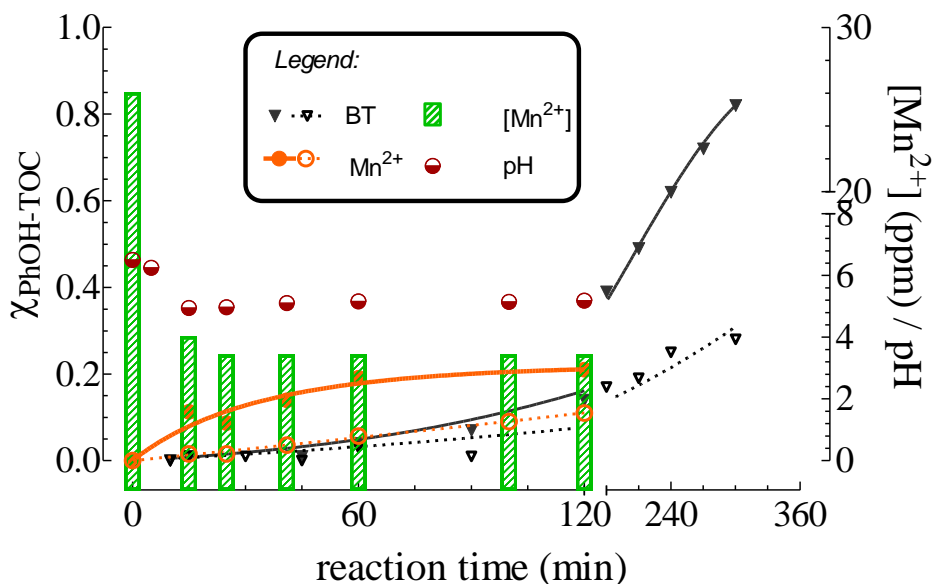
Figure 5. Homogeneous wet air oxidation of phenol at 150°C. Phenol and TOC conversion in the presence of 30ppm Mn^{2+} catalyst.

III.2. Mechanistic evidences

Further clues into the chemistry of the wet air oxidation of phenol are evident from Figure 6, comparing the HPLC chromatograms after 2h of reaction time of WAO performed in absence of any catalyst and in presence both of homogenous ([Cu^{2+}] and [Fe^{3+}], 5 ppm) and of the heterogeneous $MnCeO_x$ system. Several common intermediates (i.e., hydrobenzoquinone, catechol, benzoquinone, maleic acids, acroleyn and C1-C2 acids), confirm the progress of both non-catalytic and catalytic homogeneous wet air oxidation *via* the same unselective reaction mechanism [1-3,6]. On the other hand, the heterogeneous $MnCeO_x$ system drives a very "clean" CWAO path, allowing only trace amounts of oxygenated aromatics (≈2 ppm) and light organic acids (≈50 ppm C) to be detected after 2h of reaction time [27].

The cleaner reaction path is visibly confirmed by the quasi-undetectable brown color given by benzoquinone, which represents one of the first intermediates of the phenol degradation, in contrast with strongly colored solution of homogeneous catalysed tests. The progressive rise in TOC caused by a progressive release, from the catalyst surface, of light and more refractory to oxydation carboxylic acids, as already seen in Figure 4, confirms yet a scarce, if any, CWAO functionality of the $MnCeO_x$ system towards such refractory intermediates [22-29].

Further, a representative conversion-selectivity pattern of a homogeneous CWAO test ($[Fe^{3+}]$, 5 ppm) displays the typical trends of consecutive reactions (Figure 7). In particular, it is evident that at the beginning of the reaction the conversion of the substrate into oxygenated aromatic compounds like hydroquinone, catechol and benzoquinone takes palce. Then, those molecules are subsequently oxidized to a mixture of C4, C3 and C2 intermediates, the latter undergoing a slow mineralization to CO_2.
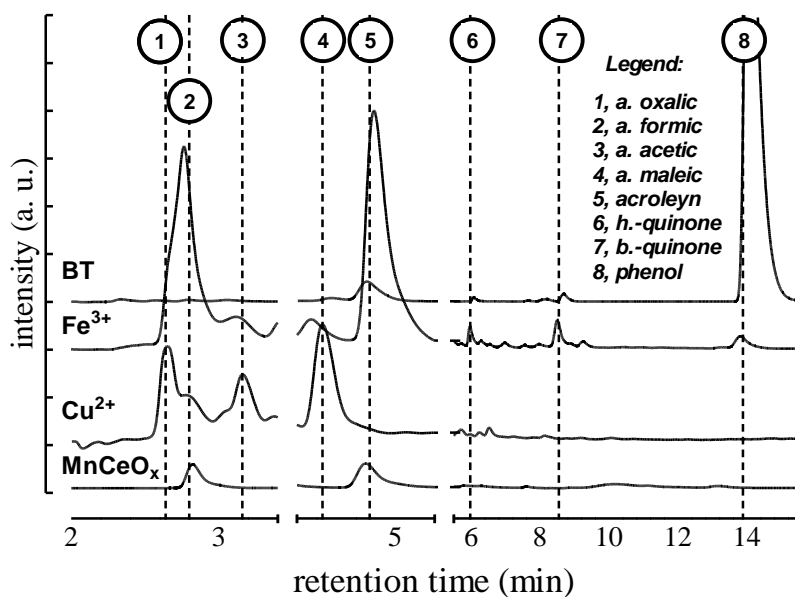
Figure 6. Wet air oxidation of phenol at 150°C. HPLC chromatograms after 2h of

reaction time of the BT and in the presence of homogeneous Cu^{2+} and Fe^{3+} (5 ppm) and heterogeneous $MnCeO_x$ catalysts.
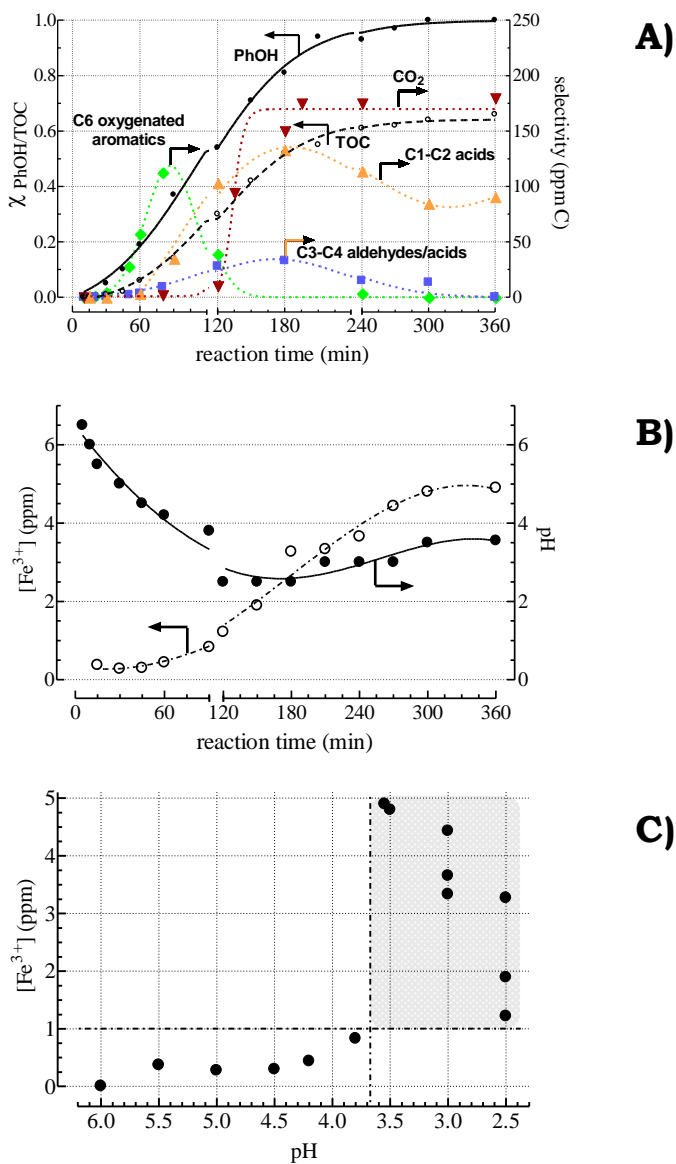
Figure 7. Homogeneous ($[Fe^{3+}]$, 5 ppm) catalytic wet air oxidation of phenol at 150°C. A) Conversion-selectivity pattern. B) pH and $[Fe^{3+}]$ *vs.* reaction time. C) $[Fe^{3+}]$ *vs.* pH correlation.

Thus, the first oxidative radical oxygen species attack results in a quick insertion of a radical OH groups into the aromatic-ring of phenol (producing catechol and hydroquinone) followed by the further water elimination (benzoquinone). The subsequent oxidative attack causes the rupture of the aromatic ring producing a mixture of C2, C3 and C4 aldehydes and acids, probed by the presence in the solution of maleic acid, acroleyn and acetic, oxalic and formic acid.

Although a parallel-consecutive total oxidation path accounts for a mineralization of ca. 175 ppm C after 3h, the plateau in TOC conversion and CO_2 selectivity curves, in concomitance with the highest concentration of C2 acids (Figure 7A), substantiate the high resistance to total oxidation of the latter intermediates [1-6,10-12,22-26].

The final cumulative CO_2 production, corresponding to a theoretic C-mineralization of ca. 25%, sensibly mismatches the much higher (60%) TOC conversion, because of the stripping of volatile compounds produced all the reaction time long, mostly phenol, benzoquinone (denoted by a pale yellow colour of the $Ba(OH)_2$ trap-solution) and aldehydes. This gap gets a maximum (30-35%) in 2h, keeping unchanged thereafter and owing to the overwhelming production of polar carboxylic acids (Figure 7A).

Furthermore, a rising trend of $[Fe^{3+}]$ opposite to the pH decay (Figure 7B), and leading to a final concentration equal to the initial catalyst load (5 ppm), explains the slight effect of the ion concentration on the CWAO efficiency (Figure 3). This depends upon the aqueous chemistry of Fe^{3+} ions as the very low solubility of $Fe(OH)_3$ implies a quantitative precipitation of the catalytic species at the beginning of the reaction test, which keeps the Fe^{3+} concentration below 1 ppm (Figure 7C). The decrease of pH below a "limit" value of ca. 3.7 yields an ongoing solubilization of the iron hydroxide (Figure 7C), allowing a rise of $[Fe^{3+}]$ over the lower concentration limit (≥ 1 ppm) for homogeneous catalysis (Figure 3). Indeed, such pH and $[Fe^{3+}]$ values correspond to a K_{ps} in the order of 10^{-36}, that is in a satisfactory agreement with that of $Fe(OH)_3$ (i.e., $K_{ps} \approx 10^{-38}$ at r.t.). The interaction of Fe^{3+}

ions with organic moieties, then, generates reduced Fe(II) ions acting as "electron-donor" species promoting the activation of molecular oxygen to electrophyilic O-radical species.

Then, the detection of some common intermediates, the intrinsic reactivity of leached out transition metal ions and a low functionality of solid catalysts, somewhat inhibiting radical reactions [3-5], are likely at the origin of the misleading assumption of a unique *homogeneous radical path* accounting for the CWAO pattern of both homogeneous and heterogeneous systems [1,2,6,9-12].

Whereas, the heterogeneous $MnCeO_x$ system drives a typically surface L-H reaction mechanism allowing a very fast adsorption of the substrate. This results in the concomitant abatement of phenol and TOC (Figure 4), which can be modeled with a pseudo-first order kinetic law [27-28]. Then, adsorbed phenol reacts with the surface catalyst oxygen undergoing a slow surface oxidation to CO_2 (Figure 4A), this constituting the *rate limiting step* (*r.l.s.*) of the mineralization process [27,28,30,31]. A strong irreversible adsorption of phenol at the catalyst surface favors indeed the oxidative attack by huge amount of *electrophylic* oxygen species markedly promoting the total oxidation path though, because of their poor chemical affinity for the catalyst surface, a slight release of C2 acidic intermediates parallels a constant combustion rate of adsorbed C-species (Figure 4) [27,28,30,31]. However, competitive side reactions of adsorbed phenol, such as degradation and polymerization, generally results in the accumulation of poorly reactive carbonaceous deposits, causing catalyst deactivation by *fouling* [22-31].

Then, an accurate C-mass balance (>95%) based on the cumulative amount of CO_2 formed (Figure 4A), the residual TOC in the solution (Figure 4B) and the weight-loss recorded by TGA-DSC analysis of the "used" catalyst (Figure 8) indicates the occurrence of a typical L-H heterogeneous reaction pathway [27,28,30,31]. On this account, textural and redox properties determine the activity-selectivity-stability pattern of the

heterogeneous $MnCeO_x$ catalyst reflecting on the overall efficiency of the CWAO process [24-31]. Namely, the efficiency of water decontamination depends on the catalyst adsorption capacity, basically relying on textural and surface chemical properties of the catalyst. On the other hand, dispersion and redox properties of the active phase control the oxidation of adsorbed C-species, determining both the selectivity pattern and stability against *fouling-poisoning* phenomena [22-31].
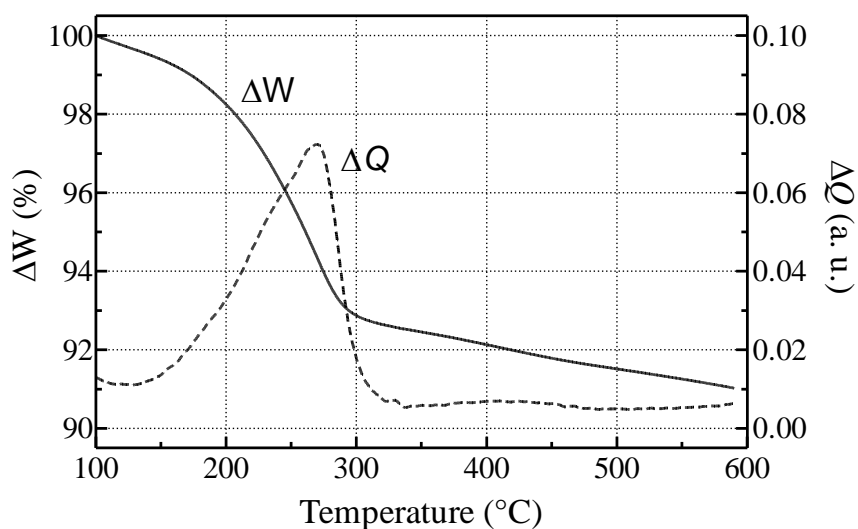
Figure 8. TGA-DSC profile of the "used" $MnCeO_x$ catalyst (see Figure 4).

III.3 Indications

The poor correspondence of blank test results reported in literature, not directly depending on the main reaction conditions, and the scarce reproducibility of tests in absence of any catalyst are in a straight line correlation with the Fe^{3+} ions leaching, further to reactor-shield corrosion phenomena. This strongly suggests to deeply insulate the reactor wall and all of its connections, in order to prevent any possible metal dissolution

into the reacting solution, which would affect the catalytic experimental results, even if present in trace amount.

Homogeneous catalysts drive an "unselective" *homogeneous free-radical* reaction path similar, but much faster, to that of oxidation conducted in absence of catalyst, producing huge amount of acidic intermediates more refractory to the further mineralization. Those compounds, besides affecting the CO_2 selectivity, make the reacting solution more aggressive through the reactor components, severely shortening the apparatus lifetime, so increasing process operative costs. Moreover, the presence of volatile byproducts, as aldeydes, increases the unreproducibility of the system because of the stripping of such products by the oxygen flow.

On the other hand, the heterogeneous $MnCeO_x$ catalyst allows a faster and cleaner reaction path promoting the quicker adsorption of the substrate on the catalyst surface, which abate the pollutant concentration into the reacting solution. The subsequent oxidation by means of the surface catalyst oxygen lead to the desired mineralization, without any detectable active phase leaching. Unfortunately, the last reaction proceed with a much slower rate representing, thus, the reaction rate determining step of the overall reaction. This let the adsorbed carbonaceous species to polymerize on the catalyst surface, so leading to the classic phenomenon of fouling which then deactivate the system. On the other hand, adsorbed species can desorbe from catalytic system before total oxidation as acidic compounds, so decreasing the mineralization selectivity. All this disadvantages, anyway, indicate the way to improve the activity, selectivity and stability of the $MnCeO_x$ system by strengthening its textural and redox properties.

Finally, while the heterogeneous system drives a clean and simple reaction path from phenol directly to CO_2, except of undesirable byproducts, homogeneous systems is most complicated, giving rise to even refractory intermediates, as shown by the following scheme:
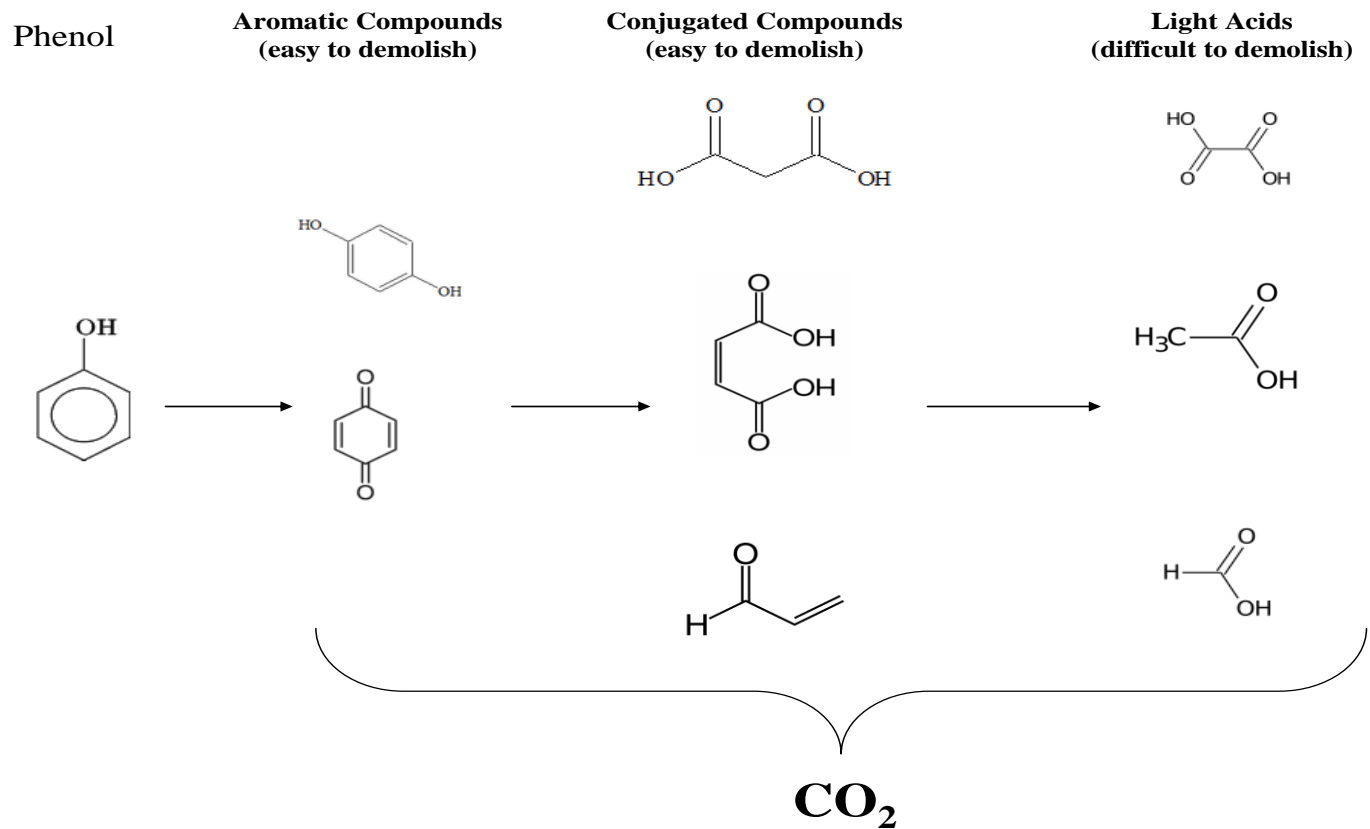
Scheme 1. Schematic reaction pathway of the homogeneous CWAO of phenol

.

II.4. References

[1]   S. Hočevar, J. Batista, J. Levec, *J. Catal.* **184** (1999) 39.
[2]   F. Arena, R. Giovenco, T. Torre, A. Venuto, A. Parmaliana, *Appl. Catal. B* **45** (2003) 51.
[3]   S.-K. Kim, S.-K. Ihm, *Top. Catal.* **33** (2005) 171.
[4]   Q. Wu, X. Hu, P.-L. Yue, *Chem. Eng. Sci.* **58** (2003) 923.
[5]   S. Hamoudi, F. Larachi, A. Sayari, *J. Catal.* **177** (1998) 247.
[6]   F. Arena, E. Alongi, P. Famulari, A. Parmaliana, G. Trunfio, *Catal. Lett.* **107** (2006) 39.
[7]   G. Busca, S. Berardinelli, C. Resini, L. Arrighi, *J. Hazard. Mater.* **160** (2008) 265.
[8]   F. Luck, *Catal. Today* **53** (1999) 81.
[9]   J. Levec, A. Pintar, *Catal. Today* **24** (1995) 51.
[10]   A. Santos, P. Yustos, A. Quintanilla, S. Rodriguez, F. Garcia-Ochoa, *Appl. Catal. B* **39** (2002) 97.
[11]   A. Santos, P. Yustos, A. Quintanilla, F. Garcia-Ochoa, *Appl. Catal. B* **53** (2004) 181.
[12]   A. Santos, P. Yustos, A. Quintanilla, G. Ruiz, F. Garcia-Ochoa, Appl. Catal. B **61** (2005) 323.
[13]   A. Fortuny, C. Ferrer, C. Bengoa, J. Font, A. Fabregat, *Catal. Today* **24** (1995) 79.
[14]   A. Fortuny, C. Bengoa, J. Font, F. Castells, A. Fabregat, *Catal. Today* **53** (1999) 107.
[15]   J. Prasad, J. Tardio, D.B. Akolekar, S.K. Bhargava, S.C. Grocott, *Ind. Eng. Chem. Res.* **43** (2004) 6363.
[16]   J. Guo, M. Al-Dahhan *Appl. Catal.* A **299** (2006) 175.
[17]   A. Quintanilla, J.A. Casas, J.A. Zazo, A.F. Mohedano, J.J. Rodriiguez *Appl. Catal. B* **62** (2006) 115.
[18]   A. Xu, M. Yang, R. Qiao, H. Du, C. Sun, *J. Hazard. Mater.* **147** (2007) 449.
[19]   A. Quintanilla, J.A. Casas, J.J. Rodriguez, M.T. Kreutzer, F. Kapteijn, J.A. Moulijn, *Int. J. Chem. React. Eng.* **5** (2007) 1.
[20]   R.J.G. Lopes, A.M.T. Silva, R.M. Quinta-Ferreira, *Appl. Catal. B* **73** (2007) 193.
[21]   P. Kritzer, *J. of Supercritical Fluids,* **29** (2004) 1.
[22]   S. Imamura, *Ind. Eng. Chem. Res,.* **38** (1999) 1743.
[23]   Yu.I. Matatov-Meytal, M. Sheintuch, *Ind. Eng. Chem. Res.* **37** (1998) 309.
[24]   F. Larachi, *Top. Catal.* **33** (2005) 109.
[25]   S.K. Bhargava, J. Tardio, J. Prasad, K. Foger, D.B. Akolekar, S.C. Grocott, *Ind. Eng. Chem. Res.* **45** (2006) 1221.
[26]   S.T. Hussain, A. Sayari, F. Larachi, *J.Catal.* **201** (2001) 153
[27]   F. Arena, J. Negro, G. Trunfio, A. Parmaliana, *Ind. Eng. Chem. Res.* **46** (2007) 6724.
[28]   F. Arena, G. Trunfio, J. Negro, L. Spadaro, *Appl. Catal. B* **85** (2008) 40.
[29]   A. Cybulski, *Ind. Eng. Chem. Res.* **46** (2007) 4007.
[30]   M. Abecassis-Wolfovich, M.V. Landau, A. Brenner, M. Herskowitz, *Ind. Eng. Chem. Res.* **43** (2004) 5089.
[31]   M. Abecassis-Wolfovich, R. Jothiramalingam, M.V. Landau, M. Herrskowitz, B. Viswanathan, *Appl. Catal. B* **59** (2005) 91.

Chapter IV

Methodology and Apparatus

IV.1. **Materials**

After the preliminary employment of Cu-based catalysts, our attention was focused on the $MnCeO_x$ system, which is expected to represent the sole reliable alternative to nobel metal catalysts in the catalytic wet air oxidation of pollutant organic substrates present in wastewater streams. In fact, their cheaper costs are coupled with high activity in the title reaction, not presenting the important drawback of active phase leaching which allowed us to set away the $CuCeO_x$ system [1-8]. Unfortunately, also this Mn-based catalysts presents several disadvantages like deactivation by fouling [9-18], and the aim of this work is to improve their catalytic characteriscs for an economical industrial approach of the CWAO process.

IV.2. Catalyst preparation

IV.2.1. Classic co-precipitated catalysts

MnCeO_x catalysts with Mn_{at}/Ce_{at} equal to 0.75 (A) and 1.0 (B) were prepared by the conventional co-precipitation method [9,11,13-15], by adding a 10 wt% Na_2CO_3 solution to $Mn(NO_3)_2$-$Ce(NO_3)_3$ or $MnCl_2$-$CeCl_3$ precursors couple, dissolved in distilled water (pH$\cong$4.0) [14-15]. After filtration and washing, all the samples were dried at 373K all night and further calcined in air at temperature ranging from 673K to 1273K for 6h. An aliquot of the dried samples was doped with K (4 wt%) by the incipient wetness method using an appropriate KNO_3 aqueous solution [13]. Thereafter, the doped samples were dried at 373K and calcined at 673K, as above specified. A list a samples, along with their main characteristics is reported in Table 1.

Table 1. List of co-precipitated catalysts.

Catalyst	Mn$_{at}$:Ce$_{at}$	[Mn][a] (wt%)	[K] (wt%)	T$_{calc}$ (K)	SA$_{BET}$ (m^2/g)	CeO$_2$ size [b] (nm)
M3C4-P4	3:4	15.7	-	673	69	5
M3C4-P6	3:4	15.7	-	873	50	10
M3C4-P8	3:4	15.7	-	1073	25	27
M3C4-P10	3:4	15.7	-	1273	16	32
KM3C4-P4	3:4	15.1	4	673	30	5
M1C1-P4	1:1	20.9	-	673	99	3
KM1C1-P4	1:1	20.1	4	673	61	6

[a] from XRF elemental analysis. [b] from the Scherrer equation applied to the <111> reflex of the cerianite.

IV.2.2. Redox-precipitated catalysts

A series of *MnCeO$_x$ catalysts* in the Mn$_{at}$/Ce$_{at}$ range of 0.33-3.00 was prepared by means of the novel "*redox-precipitation*" route [19-22], according to the following procedure. An amount of the KMnO$_4$ precursor, in 10% stoichiometric excess, was dissolved into 0.3 L of deionized water (pH≈8.5) and titrated at 333K under vigorous stirring with a solution (pH≈3) of the Ce(NO$_3$)$_3$ and Mn(NO$_3$)$_2$ precursors, keeping constant the pH at a value of 8.2 (±0.3) by the addition of a 0.2M KOH solution. After titration, the solid was digested for 30 min at 333K and then filtered, washed with hot distilled water and dried at 373K (16h). Dried samples were further calcined at 673K (6h). A list a samples, along with their main characteristics is reported in Table 2.

Table 2. List of "redox-precipitated" catalysts.

Catalyst	Mn/Ce [a]		[Mn]	[K]	SA	PV	APD [b]	Mn/Ce [c]
	Des.	Exp.	(wt%)	(wt%)	(m^2/g)	(cm^3/g)	(nm)	
M1C3-R4	0.33	0.34	9.3	0.1	168	0.28	5.1	0.58
M1C2-R4	0.50	0.47	12.3	0.3	161	0.42	7.6	n.d.
M3C4-R4	0.75	0.71	16.7	0.7	169	0.47	7.2	1.00
M1C1-R4	1.00	0.95	20.5	0.8	154	0.49	11.7	1.33
M1C1-R	*1.00*	*0.95*	*20.5*	*0.8*	*213*	*0.53*	*76*	*1.33*
M3C2-R4	1.50	1.44	26.6	3.3	157	0.45	14.3	1.80
M2C1-R4	2.00	2.12	32.7	4.1	140	0.50	16.7	2.69
M3C1-R4	3.00	2.76	36.8	5.4	114	0.46	18.3	3.42

a) Mn/Ce atomic ratio from design and XRF measurements, respectively; b) average pore diameter; c) surface Mn/Ce atomic ratio from XPS measurements.

In order to evaluate the influence of synthesis parameter on the catalyst structure, the concentration of the del $KMnO_4$ precursor was varied in the range 5-20 g/L, keeping constant the titration speed (ca. 1L/h). Another series of catalysts was prepared using different bases to keep constant the pH (LiOH, NH_3OH), in order to monitor the influence of the reaction medium on the catalyst morphology, too.

Table 3. Influence of synthesis parameters on the textural properties of M1C1-R4 system.

Catalyst	Base	Mn/Ce [b]	[K]	T$_{calc}$	SA	PV	APD [c]
			(wt%)	(K)	(m^2/g)	(cm^3/g)	(nm)
M1C1-R4	KOH	0.95	0.8	673	154	0.49	12
M1C1-R4[a]	KOH	0.97	0.8	673	171	0.43	11
M1C1-R4N	NH$_4$OH	0.94	0.1	673	166	0.43	6
M1C1-R4L	LiOH	0.98	0.7	673	163	0.45	9
M1C1-R4C	CsOH	0.98	0.5	673	127	0.45	112

Moreover, another series of catalysts was prepared varying the calcination temperature of the representative M1C1-R sample, in order to take into account also the effect of this important parameter on the catalyst features. On Table 3 is reported the list of samples so obtained.

Table 4. Influence of the calcinations temperature on the textural properties of M1C1-R system.

Sample	[Mn]	[K/Mn]	Tcalc	SA$_{BET}$	PV	APD
	%		K	(m^2/g)	(cm^3/g)	(Å)
M1C1-R1	20.5	0.149		216	0.61	84
M1C1-R2	20.5	0.149	**473**	205	0.74	130
M1C1-R5	20.5	0.149	**773**	107	0.59	165
M1C1-R6	20.5	0.149	**873**	90	0.47	197

IV.2.3. Model compound

The CWAO was performed using phenol purchased by Sigma-Aldrich (99+% purity) as model compound. Phenolic solutions were prepared so that injecting 8ml into the reactor vessel the 0.15L of reacting solution resulted as 1000ppm.

IV.3. Catalyst characterization

All samples synthesized both with the classic co-precipitation route and the novel redox-precipitation one were characterized in order to confirm the designed chemical composition and to shed lights into their surface, textural and redox features and, along with results from CWAO of phenol testing, to determine the basic requirements for further improvements.

IV.3.1 Atomic Adsorption Spectroscopy

The manganese loading in each sample was confirmed measuring its concentration by means of an Atomic Adsorption spectrometer *Analyst 200, Perkin Elmer.* An aliquot of the sample was dissolved in a strong fluoridic water solution under ultrasound and vigorous stirring in a concentration ranging between 1 and 5ppm, so to stay within the proportionality range of the instrument. The concentration was evaluated by comparing the absorbance values (λ=279.5nm) with a standard solution of manganese nitrate taken as reference. The AAS technique was used also to evaluate the amount of leaching during the CWAO tests.

IV.3.2. X-ray Fluorescence spectrometry

The manganese loading, along with cerium and potassium (or litium or cesium in catalysts prepared using different bases as pH controller), was also evaluated by means of an *Explorer X-ray Fluorescence spectrometer (BRUKER AXS)* on solid samples. The instrument was previously calibrated in the Energy range of 0.11-0.60 keV, corresponding to wavelength comprised between 11.3 and 0.02, respectively.

IV.3.3. N₂ phisisorption

Surface area (SA$_{BET}$) values and *pore size distribution (PSD)* were obtained from the nitrogen absorption isotherm at 77K using an *ASAP 2010* (*Micromeritics Instruments*) previously outgasing the samples at 100 or 150°C, depending on the calcinations treatment at which the sample was previously treated, untill reaching a residual pressure lower than 0.01 atm. The isotherms were elaborated in the p/p^0 range of 0-0.2, according to the B.E.T. method for the determination of the N₂ amount adsorbed on the "monolayer" (V$_m$) for surface area determination. From the same isotherm curves the pore size distributions were obtained, using the Horvath-Kavazoe and BJH methods for micro and meso-pore evaluation, respectively.

IV.3.4. *X-ray* Diffraction (XRD)

X-ray Diffraction (XRD) analysis of powdered samples were performed by a *Philips X-Pert* diffractometer operating with a Ni *β*-filtered Cu K$_\alpha$ radiation at 40 kV and 30 mA. The average particle size of the ceria matrix was calculated using the Sherrer's equation:

$$d = \frac{K \cdot \lambda}{B \cdot \cos\left(2\theta/2\right)}$$

where K is a constant equal to 1.00, λ=1.5406 Å, B is the width of the main peack of the diffractogram and the relative position of the maximum. Peaks were then identified on the base of the JCPDS database for reference compounds.

IV.3.5. *X-ray* Photoelectron Spectroscopy (XPS)

X-ray Photoelectron Spectroscopy (XPS) data were obtained by a *Physical Electronics GMBH PHI 5800-01* spectrometer, using a monochromatized Al-*Kα* radiation at power beam of 350 W and pass energy of 60 eV. The BE regions

investigated were 635-680 eV (Mn_{2p}), 280-300 eV (C_{1s}), 525-540 eV (O_{1s}) and 870-935 eV (Ce_{3d}). The BE scale was calibrated on the C_{1s} line (284.8 eV) of *adventitious* carbon.

IV.3.6. Transmission Electron Microscopy (HRTEM)

Morphology and structural characteristics of various samples were evaluated at microscopoic level with an electronic *PHILIPS CM12* Microscope (point-to-point resolution, 3Å). Samples were prepared by ultrasonically dispersing the powder in isopropanol and then depositing them over a thin carbon film supported on a standard copper grid.

IV.3.7. Scanning Electron Microscopy (SEM)

Scanning Electron Microscopy (SEM) analysis was carried out using a *PHILIPS XL 20* microscope with an accelerating voltage of 20 kV after gold sputtering of samples.

IV.3.8. Temperature programmed reduction (TPR)

Redox properties of catalysts, with or without pre-treatment at 400°C with oxygen (0.5h), were evaluated by performing Temperature Programmed Reductions (TPR) in the range 493-1073K in a linear quartz micro-reactor (i.d., 4 mm). An amount of ca. 30mg of sample, positioned in the middle of the reactor between two layers of quartz wool, let to respect the P parameter under such reducing conditions:

$$P= (β·S·n)/(F·C)$$

where $β$ is the heating rate (12°C·min^{-1}), S the fraction of reducible species present in the catalyst, n the stoichiometry of hydrogen consumption, F the reducing flux (60 *stp* mL min^{-1}) and C the fraction of H_2 in the reducing flux (6% H_2/Ar mixture). The hydrogen consumption was monitored by a TCD

connected to a PC for data storage and processing after quantitative calibration of peaks' area by the comparison with the reduction peak of a CuO known amount reduced under the same conditions. A scheme of the apparatus is reported in Figure 1.
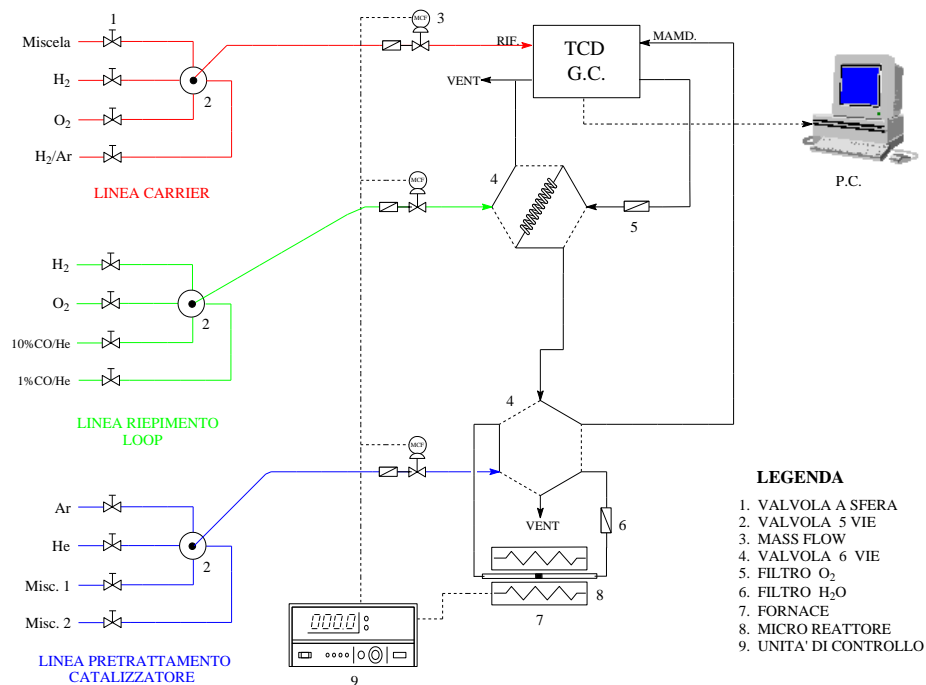
Figure 1. Scheme of the apparatus for the TPR characterization.

IV.3.9. *Thermogravimetric (TG-DSC)* analysis

Thermogravimetric (TG-DSC) analysis of the "used" samples, recovered at the end of some relevat CWAO of phenol was performed in static air atmosphere, using a *Netzsch Simultaneous Thermal Analysis Instrument STA 409C.* Measures were performed burning the carbonaceous deposits of ca. 5mg of used sample with a heating rate of 10K/min in the range 30-600°C.

IV.3.10. Temperature programmed reduction (TPO)

"Used" catalyst, recovered at the end of some representative CWAO of phenol, and "fresh" one impregnated with 5% wt of phenol, were oxidized in oxygen atmosphere under programmed temperature in the same microapparatus described in section IV.3.8. and schematized in Figure 1. Analysis were conducted in the range 20-600K with a 10% O_2/He mixture at the rate of 30 STP mL/min empoying ca. 30mg of sample. The outlet stream was analized by means of quadrupole mass spectrometer (*Thermolab, Fisons Instruments*) operating in the MIM (Multiple Ion Monitoring) with a ionization tension of 70V signal acquisition relative to the m/z ratio of:

$$4 \text{ (He)}, 17 \text{ (OH)}, 28 \text{ (CO)}, 44 \text{ (CO}_2\text{) and } 94 \text{ (C}_6\text{H}_5\text{OH)}$$

was made using the SEM (Secondary Electron Multiplier) operating with a tension of 1500V.

IV.3.11. Micro-Raman spectroscopy

Micro-Raman spectra were taken at room temperature in back-scattering geometry, using a He-Ne laser excitation source (λ, 632.8 nm) focused onto the sample with a microscope (50×). An incident power of 0.5 mW was used in order to avoid thermal laser-induced effects. The signal was collected by the microscope, dispersed by a HR460 monochromator (*Horiba-Jobin Yvon*) and detected by a charge-coupled device array sensor (77K) with a resolution of ca. 3 cm^{-1}.

IV.4. Catalyst testing

The catalytic wet air oxidation of phenol is the nuclei of the present work and particular attention was focused in the testing apparatus analytical instruments. In particular, following the indication of previous tests conducted in order to reproduce blank tests reported in literature, a complete insulation of the inner parts of the reactor vessel, included all connections which could be in contact with the strong corrosive reacting solution, was done to perform the oxidation in an optimal condition [8,23].

IV.4.1. Reactor vessel

The CWAO of phenol was performed in a semi-batch mode, loading 1000÷5000 ppm of catalyst in a 0.25 L PTF-lined autoclave made of AISI 316 (T_{max}, 220°C; P_{max}, 50 atm; V_{max}, 0.250 L) equipped with a magnetically driven turbine impeller (≈2,000 rpm), totally covered of Teflon, included all connections, schematized in Figure 2. Pressure was kept constant by continuously feeding pure oxygen at 10÷15 atm by means of a "back-pressure" (*DRÄGER TESCOM*) at the rate of 200 stp mL·min^{-1}, measured by an electronic Mass Flow Controller (*Brooks Instruments, DDE Smart Series 2000*). As temperature stabilized at 373÷423K, the reaction was started injecting 1,000÷5000±50 ppm (1 g/L) of phenol in order to obtain a catalyst-to-phenol mass ratio (R) ranging from 1 to 5 [7,8,14,15,19-22].

The following scheme summarize the reaction conditions:

- *Volume, 150 mL;*
- *Starting pH, 6-7 (water solution of phenol);*
- *$T_{reaz.}$; 100÷160±2 °C;*
- *P_{tot}, 10±15 atm) - P_{O2}, 9 atm;*
- *Stirring speed, 2000 rpm;*
- *O_2 Flux, 0.2 stp L/min;*
- *[PhOH], 1÷5± 0.03 g/L;*
- *w_{cat}/w_{Ph}, ratio, 5;*
- *Particle catalyst diameter < 20 μm.*
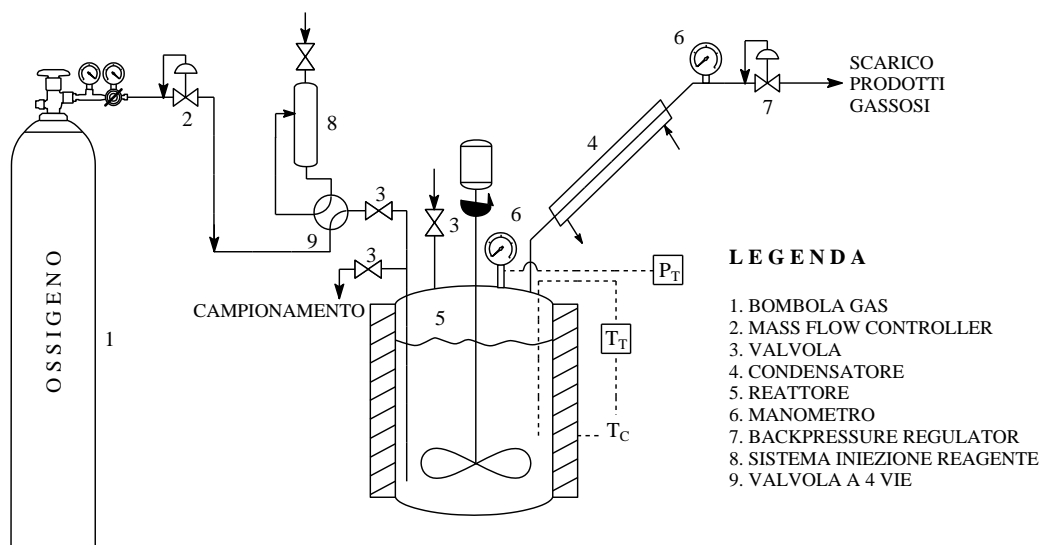
Figure 2. Scheme of the *semi-batch* reactor employed for the CWAO of phenol.

Products were analyzed periodically withdrawing ca. 0.2ml of liquid from the reactor to evaluate: (i) the pH, (ii) the $Mn^{2+}/Cu^{2+}/Fe^{3+}$ ions concentration. Results were then analyzed in terms of conversion against reaction time following the equation [7,8,14,15,19-22]:

$$\chi_{Phenol/TOC} = 1 - \frac{C}{C_0}$$

Where X is the conversion, C and C_0 represent phenol and TOC concentration, respectively, at time t and t_0, respectively.

Under such conditions, intraparticle mass-transfer resistances were negligible, according to the Weisz-Prater criterion [14]:

$$\frac{r_{app}\rho_p(d_p/2)^2}{D_{eff}C_{eff,S}} \cong (0.3 - 0.9) * 10^{-4} \quad (\ll 0.15)$$

Where r_{app} is the apparent velocity ρ_p is the density, d_p is the catalyst particle diameter, D_{eff} is the phenol diffusivity and C_{eff}, is the concentration of phenol.

IV.4.2. Quantitative determination of phenol (HPLC)

Phenol and byproducts concentration were determined by means of a high performance liquid chromatography (HPLC) system (*Dionex Pump Series P680*) furnished of a manual injector (*mod. rheodyne*), a Phenomenex Gemini 5μ C6-Phenyl 110A column for the separation and identification of products and a UV-Vis detector (Dionex UV-Vis detector UVD 170S/340S) operating at a wavelength of 210÷220÷230nm, depending on the by-products. The instrument operative control, data acquisition and elaboration was made by a particular operational software (*Chromeleon Chromatografy Management System*). As eluent was employed a mix of 97% of a buffered fosphoric aqueous solution (pH~2.5) and 3% of pure methanol at the flow rate of 0.8÷2ml/min. Chromatogram peaks were calibrated by building the calibration curve with different solutions of the pure products at known concentration.

IV.4.3. Quantitative determination of TOC

The TOC present in the solution was determined using a combustion/nondispersive infrared gas analyzer (SHIMAZU Mod. 5000A) [22]. Organic compounds are burnt at high temperature (ca. 1373K) and the quantitative CO_2 formed is detected by means of a NDIR (non-dispersive infrared gas analyzer) detector. Calibration curves were previously done in order to obtain quantitative results.

IV.4.4. CO_2 Gravimetric determination

Finally, the CO_2 production was monitored by bubbling the gas purge into a saturated $Ba(OH)_2$ solution and, after filtration and drying, weighing the $BaCO_3$

produced. Selectivity to mineralization was then evaluated referring the CO_2 formed to the theoretical amount of carbon dioxide produced if all the phenol was converted to carbon dioxide [14]:

$$S_{CO2} = \frac{\frac{X}{197}}{\left(\frac{PhOH_i}{94} * 6\right)}$$

where X is the amount of $BaCO_3$ produced, 197 its molecular weight, $PhOH_i$ the amount of phenol loaded, 94 its molecular weight and 6 the CO_2 molecular number of produced per phenol molecule destroyed.

IV.5. References

[1]. S. Hoĉevar, J. Batista, J. Levec, *J. Catal.* **184** (1999) 39.

[2]. S. Hoĉevar, U. Opara Kraŝovec, B. Orel, A.S. Aricò, H. Kim, *Appl. Catal. B* **28** (2000) 113.

[3]. A.Santos, P. Yustos, A. Quintanilla, S. Rodriguez, F. Garcia-Ochoa, *Appl. Catal. B* **39** (2002) 97.

[4]. A. Santos, P. Yustos, A. Quintanilla, F. Garcia-Ochoa, *Appl. Catal. B* **53** (2004) 181.

[5]. A. Santos, P. Yustos, A. Quintanilla, F. Garcia-Ochoa, *Chem. Eng. Sci.* **60** (2005) 4866.

[6]. A. Santos, P. Yustos, A. Quintanilla, G. Ruiz, F. Garcia-Ochoa, *Appl. Catal. B* **61** (2005) 323.

[7]. F. Arena, R. Giovenco, T. Torre, A. Venuto, A. Parmaliana, *Appl. Catal. B* **45** (2003) 51.

[8]. F. Arena, E. Alongi, P. Famulari, A. Parmaliana, G. Trunfio, *Catal. Lett.* **107** (2006) 39.

[9]. S. Imamura, *Ind. Eng. Chem. Res,.* **38** (1999) 1743.

[10]. Yu.I. Matatov-Meytal, M. Sheintuch, *Ind. Eng. Chem. Res.* **37** (1998) 309.

[11]. F. Larachi, *Top. Catal.* **33** (2005) 109.

[12]. S.K. Bhargava, J. Tardio, J. Prasad, K. Foger, D.B. Akolekar, S.C. Grocott, *Ind. Eng. Chem. Res.* **45** (2006) 1221.

[13]. S.T. Hussain, A. Sayari, F. Larachi, *J.Catal.* **201** (2001) 153

[14]. F. Arena, J. Negro, G. Trunfio, A. Parmaliana, *Ind. Eng. Chem. Res.* **46** (2007) 6724.

[15]. F. Arena, G. Trunfio, J. Negro, L. Spadaro, *Appl. Catal. B* **85** (2008) 40.

[16]. A. Cybulski, *Ind. Eng. Chem. Res.* **46**, (2007) 4007.

[17]. M. Abecassis-Wolfovich, M.V. Landau, A. Brenner, M. Herskowitz, *Ind. Eng. Chem. Res.* **43** (2004) 5089.

[18]. M. Abecassis-Wolfovich, R. Jothiramalingam, M.V. Landau, M. Herrskowitz, B. Viswanathan, *Appl. Catal. B* **59** (2005) 91.

[19]. F. Arena, G. Trunfio, J. Negro, B. Fazio, L. Spadaro, *Chem. Mater.* **19** (2007) 2269.

[20]. F. Arena, G. Trunfio, J. Negro, L. Spadaro, *Mater. Res. Bull.* **43** (2008) 539.

[21]. F. Arena, G. Trunfio, J. Negro, L. Spadaro, *Appl. Catal. B* **59** (2008)

[22]. F. Arena, G. Trunfio, B. Fazio, J. Negro, L. Spadaro, *J. Phys. Chem. C* (2009) accepted for publication

[23]. P. Kritzer, *J. of Supercritical Fluids,* **29** (2004) 1.

Chapter V

Classic Co-precipitated MnCeO$_x$ catalysts for the CWAO of phenol

V.1. Preparation

Depending the Cu-based catalyst activity mostly on the leaching of the active phase which drives an effective, but homogeneous, reaction path, so leading to a fast deactivation [1-8], Mn-based systems represent to date the most promising alternative to noble metal systems, as they can join high activity and selectivity with an excellent resistance to leaching [9-29]. Their catalytic improvement is, thus, fundamental to abate the operative costs for an economical application of the CWAO at industrial scale [11-17].

In this context, a series of *MnCeO$_x$ catalyst* with Mn$_{at}$/Ce$_{at}$ equal to 0.75 (M3C4-P) and 1.0 (M1C1-P) were prepared and tested to determine the basic requirements for the ideal CWAO catalyst. For this purpose the conventional co-precipitation method was employed, so to have a useful indication of the main characteristic required for the development of the suitable CWAO catalyst. With this in mind, samples were prepared by adding a 10 wt% Na$_2$CO$_3$ solution to Mn(NO$_3$)$_2$-Ce(NO$_3$)$_3$ or MnCl$_2$-CeCl$_3$ precursors couple, dissolved in distilled water (pH$\cong$4.0) [17-22]. After filtration and washing, samples were dried at 373K (16h) and further calcined in air at temperature ranging from 673K to 1273K (6h). An aliquot of the dried samples was doped with K (4 wt%) by the incipient wetness method using a KNO$_3$ aqueous solution. Thereafter, the doped samples were dried at 373K and calcined at 673K, as above specified. Co-precipitated samples obtained with this procedure are summarized in Table 1 in section IV.2.1. Catalysts were tested in the CWAO of phenol, at T=100°C and keeping constant P$_{O2}$ (9 atm), using the 0.25 L PTF-lined autoclave described in section IV.4.1. and schematized on the same section in Figure 2. The initial phenol concentration was set at 1,000 ($\pm$100) ppm and the catalyst load at 5,000 ppm.

V.2. Catalyst performance

Calcination treatment being required for co-precipitated systems, at least at 400°C, due to the imperative need to remove undesired substances both in the bulk and in the catalyst surface, such as, in our case, nitrates or chlorides

coming from precursors, the effects of the calcination temperature on the activity of the system are reported in Figure 1. Experimental data in the CWAO of phenol at 373K and 1.0MPa are evaluated in terms of phenol and TOC conversion *vs.* reaction time for catalyst testing lasting 2 hours. It is immediately evident that the calcination treatment strongly controls the CWAO performance of the $MnCeO_x$ system with Mn/Ce atomic ratio of 0.75, being strongly depressed for temperatures in excess of 873K. Indeed, the M3C4-P4 and M3C4-P6 samples feature a similar catalytic activity leading to a ca. 90% phenol conversion in 2h of reaction time, while the TOC removal attains a final degree of 50-60%. Instead, the sample calcined at 1073K is less reactive as, in the same time (2h), it ensures phenol and TOC conversions of ca. 70 and 30% respectively. Yet, the M3C4-P10 sample, with phenol and TOC conversion of only 30 and 10%, features the poorest and insignificant CWAO performance. This evidences lead to the decision of continuing tests with catalysts calcined at a temperature of 400°C [17].
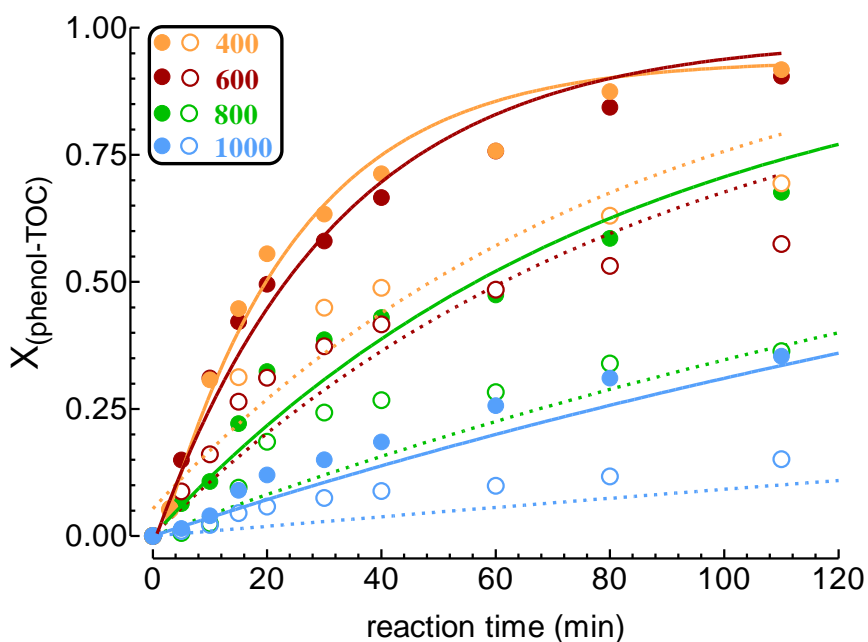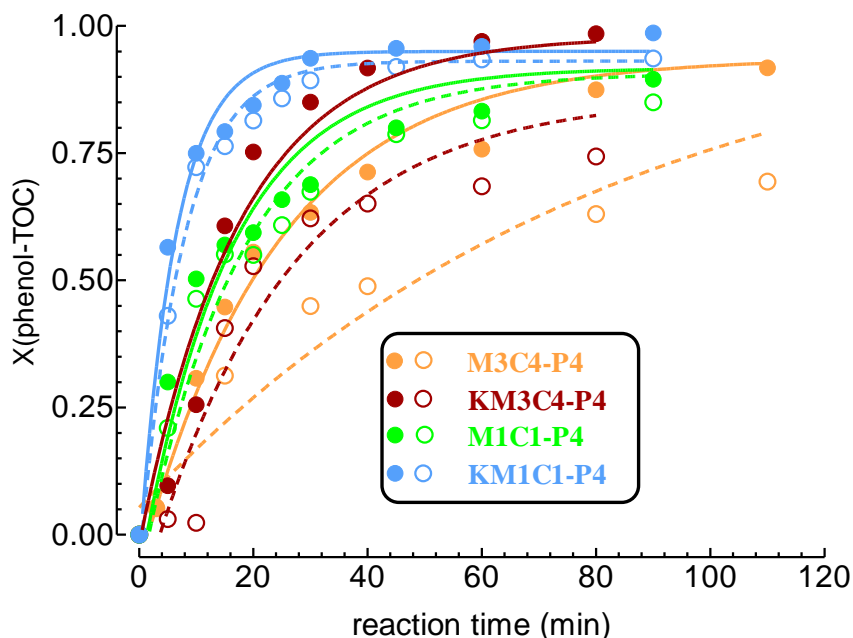

Figure 1. CWAO of phenol on coprecipitated catalysts (T_R, 373K; P_R, 1.0MPa; w_{cat}/w_{phen}, 5). Effect of calcination temperature on the activity of M3C4-Py catalysts.

Then, keeping a calcination temperature of 673K, an increase in the Mn loading (Mn_{at}/Ce_{at}, 1.0) visibly improves the CWAO activity of the $MnCeO_x$ system [11-14,18], allowing a comparable conversion of the substrate (>90%) and, mostly, a much deeper (ca. 85%) TOC removal, in a shorter (90 min) reaction time (Figure 2).

In Figure 2 the effect of potassium (4 wt%) addition in both catalysts is also showed. It can be seen that it promotes the CWAO pattern of the M3C4-P4 catalyst, speeding up the rate of phenol conversion in a time (80 min) even shorter than that of the M1C1-P4 sample, though the final degree of TOC removal is slightly lower (ca. 75%). This findings result in well agreement with literature data [20-23], which state that the K-promoted system (Mn/Ce, 1) exhibits a higher CWAO activity, resulting in the elimination of more than 90% of both phenol and TOC after just 30-40 min, so making the system sensibly attractive for the CWAO of organic pollutants.

Figure 2. CWAO of phenol on co-precipitated catalysts (T_R, 373K; P_R, 1.0MPa; w_{cat}/w_{phen}, 5). Effect the Mn loading and K addition on the activity of MxCy-P4 catalysts calcined at 673K.

Notably, in spite of a pH decrease to final values of ca. 4.5, evidently caused by an ongoing formation of light carboxylic acid intermediates, like oxalic, acetic, formic acids [12,30,31], all the catalysts result rather stable against leaching, with final concentration value of Mn ions in the reacting solution in the order of undetectable or, at least, few ppm (2-5) [14-23], corresponding to less than 1% of the total Mn load [17]. That is an important evidence in comparison with the Cu-based catalysts, which were set away because of the active phase leaching [7,8].

As evident from Figure 1 and 2, all the activity data follow, with satisfactory accuracy, 1st-order reaction kinetics:

$$\frac{dC_X}{dt} = k_X \cdot C_X \cdot [Cat]$$

then, a quantitative comparison of the reactivity of the various catalysts can be made on the basis of the kinetic constants of phenol (k_{phen}) and TOC (k_{TOC}) conversion. The relative kinetic constants values, expressed *per* weight ($L \cdot g_{cat}^{-1} \cdot h^{-1}$) and catalyst surface area ($L \cdot m_{cat}^{-2} \cdot h^{-1}$) units are compared in Table 1, along with the percentage weight loss recorded by TG-DSC analyses of the various "used" samples.

Table 1. Kinetic constants of phenol and TOC removal and weight loss of the "spent" catalyst samples.

Catalyst	k_{Phen}		k_{TOC}		ΔW
	$(L \cdot g_{cat}^{-1} \cdot h^{-1})$	$(L \cdot m_{cat}^{-2} \cdot h^{-1})$	$(L \cdot g_{cat}^{-1} \cdot h^{-1})$	$(L \cdot m_{cat}^{-2} \cdot h^{-1})$	(%)
M3C4-P4	3.9E-01	5.7E-03	1.8E-01	2.6E-03	17
M3C4-P6	3.5E-01	7.0E-03	1.4E-01	2.7E-03	15
M3C4-P8	1.3E-01	5.4E-03	3.6E-02	1.4E-03	13
M3C4-P10	4.5E-02	2.8E-03	1.2E-02	7.3E-04	7
KM3C4-P4	6.5E-01	2.2E-02	3.0E-01	9.9E-03	17
M1C1-P4	5.6E-01	5.6E-03	4.9E-01	4.9E-03	18
KM1C1-P4	1.5E+00	2.5E-02	1.2E+00	2.0E-02	19

For the sake of comparison, it must be evidenced that such figures well compare with k_{phen} values ($0.46 \div 1.2$ L·g_{cat}^{-1}·h^{-1}) quoted by Abecassis-Wolfovich *et al.* for similar co-precipitated $MnCeO_x$ systems [15,16]. The analysis of intrinsic kinetic constants reported in Table 1 confirm the following reactivity scale:

$$KM1C1\text{-}P4 > KM3C4\text{-}P4 \approx M1C1\text{-}P4 \, »$$
$$M3C4\text{-}P4 \approx M3C4\text{-}P6 > M3C4\text{-}P8 > M3C4\text{-}P10,$$

Moreover, the above results can be further related to the surface area exposure (Table 1). Indeed, the surface specific constants signal that the intrinsic activity of the M3C4-Py sample calcined at different temperatures and M1C1-P4 sample is comparable on a surface area basis in contrast whith the M3C4-P10 system which shows a lower surface activity, mostly for TOC removal, probably due the sensible particles crystallization. On the contrary, due to the decrease in surface area (Table 1) because of the potassium addition, which blokes some pores, the intrinsic activity of K-promoted catalysts is much higher than that of any undoped catalyst [14,20-23].

In addition, TGA-DSC data indicate that the extent of weight loss of the "used" samples is somewhat related to the magnitude of the kinetic constants (Table 1). Notably, weight loss reported for samples calcined at 400°C, which abate all the phenol present into the reacting solution, corresponds to full substrate adsorption (phenol-to-catalyst mass ratio, 1/6) and a negligible conversion to CO_2. On the other hand M3C4-P8 and M3C4-P10 catalysts, characterized by the lowest kinetic constants and, above all, partial substrate conversion values (Figures 1 and 2), feature a weight loss of 13 and 7% respectively, against an average of 15-17% of the other systems [17]. Therefore, as the physical properties of the catalysts rule out the constraints of internal diffusion resistances on reaction kinetics, it can be argued that relative abundance and chemical features of the surface phases/species control the SRA and CAC, previously taken as a measure of the CWAO efficiency of the $MnCeO_x$ system [15,16].

V.3. Catalysts characterization

V.3.1. Structural characterization (XRD)

Then, a systematic investigation of the structural properties of the various systems has been carried out by the XRD technique and relative diffractograms are showed in Figure 3.
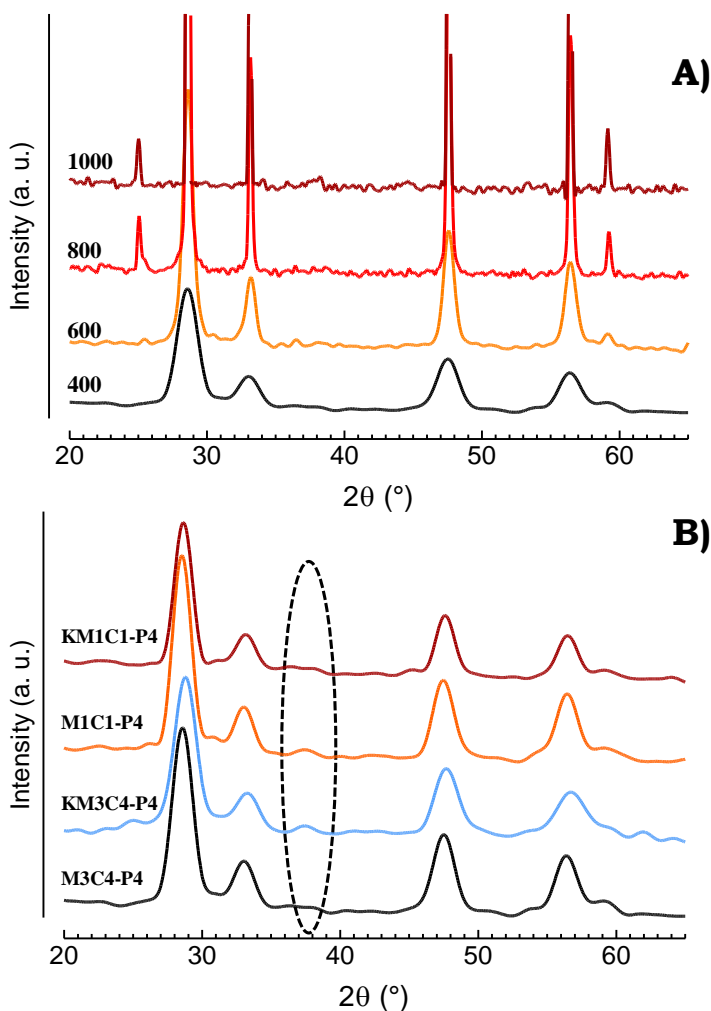
Figure 3. XRD patterns of coprecipitated catalysts. Effect of the calcination temperature on the pattern of M3C4-P4 catalysts (A); effect of Mn loading and K addition on the pattern of catalyst calcined at 673K (B).

The diffractograms of samples calcined at different temperature (Figure 3A) show in any case the main diffraction peaks (28.6, 33.3, 47.5, 56.5, 59.2°) of the *cerianite* with the fluorite-like structure. The sharper and more symmetric shape of such reflexes at higher T_{calc} confirms a growing degree of the crystallinity of ceria, consistent with the surface area decay induced by sintering [32]. Indeed, the fact that the ceria average particle size, calculated applying the Scherrer equation to the main peak positioned at 28.6° and relative to the <111> crystal plane, is inversely related to the SA_{BET}, denotes the main contribution of the ceria support to the surface area exposure [16,32].

The sample calcined at 600°C signals the incipient formation of the Mn_2O_3 species, whose concentration and crystallinity increase as T_{calc} gets higher. Although no great changes are evident in the diffractograms of catalysts with higher Mn loading and/or doped with potassium (Figure 3B), a small reflex at 37.5° denotes an incipient crystallization of manganese oxide (e.g. MnO_2) in the form of *pyrolusite* [33]. Actually, being almost all peaks relative to ceria matrix, it is evident that the catalyst structure is mainly due to CeO_2, which seems to act really as a support for the Mn active phase.

V.3.2. Redox characterization (TPR)

As previously documented, a change in the structural properties generally implies a different surface exposure and dispersion of the active phase, markedly affecting the redox behaviour of MnO_x-based systems [33]. Then, TPR analysis were conducted on all samples and results are shown in Figure 4, while the temperature of onset ($T_{o,red}$) and maximum (T_{Mi}) reduction and hydrogen consumption data are summarized in Table 3. As can be seen, the calcination temperature allowes marked effects on the redox behaviour of the M3C4-Py system, in qualitative and quantitative terms (Figure 4A), as a systematic shift of the onset temperature of reduction with T_{calc} parallels an appreciable decrease in the extent of H_2 consumption between 293 and 750K (LTR). In fact, two-three peaks in the LTR zone monitor the reduction of Mn ions of different structures/phases and/or with a different A.O.N [33,34]. The

M3C4-P4 sample is the only one showing two reduction peaks centred at 608 and 688K, whose area corresponds to a H_2/Mn ratio of 0.76. They should be related to the reduction of poorly crystalline MnO_2 particles well dispersed across the ceria matrix (608K) along with a fraction (ca. 25%) of Mn^{3+} belonging to poorly crystallized Mn_2O_3 clusters, respectively [33,34]. Probably, the superimposition of its main reflex (32.9°) with that at 33.1° of the ceria carrier and a poor crystallinity of Mn_2O_3 clusters render undetectable such species on
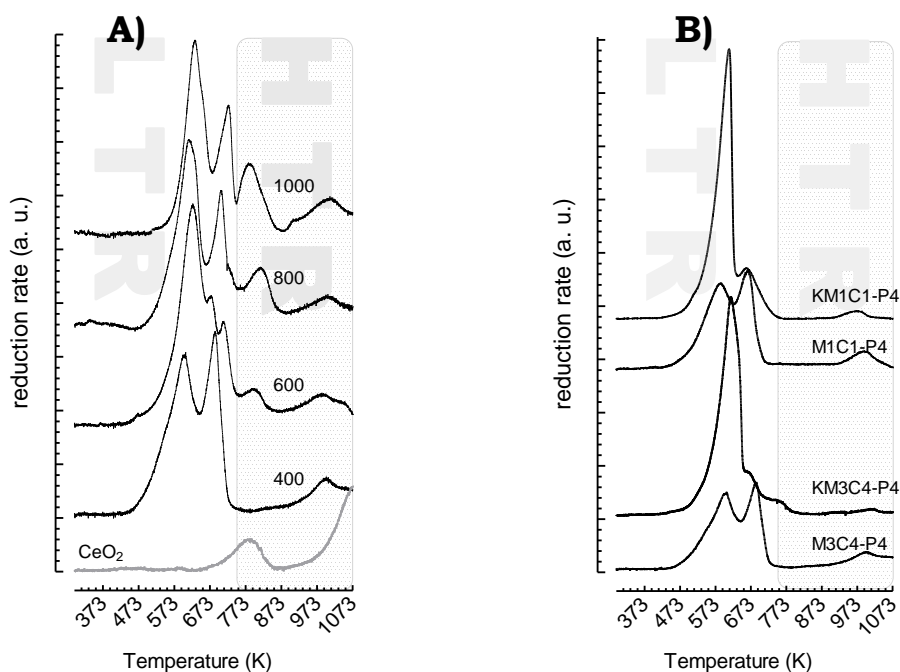
Figure 4. TPR profiles of coprecipitated catalysts. Effect of the calcination temperature on the profile of M3C4-Py catalysts (A); effect of Mn loading and K addition on the profile of catalyst calcined at 673K (B).

the M3C4-P4 sample by XRD analysis (Figure 3A). Rising the calcination temperature to 873K, the main peak keeps an almost unchanged position (625K) while the intensity is visibly larger. Two other small peaks are visible on its decreasing side, while another small, though resolved, component at ca. 793K, is associated with the reduction of surface Ce ions [17,24]. Anyhow, slight changes in the H_2/Mn ratio indicate minor variations in the A.O.N. of

Table 3. TPR data of bare and doped co-precipitated $MnCeO_x$ catalysts.

Catalyst	LTR [a]				HTR [b]	
	$T_{o,red}$ (K)	T_{M1} (K)	T_{M2} (K)	H_2/Mn_{at} (mol/atom)	T_{M3} (K)	H_2/Ce_{at} (mol/atom)
A4	434	608	685	0.76	1000	0.13
A6	448	625	675(710)	0.72	985	0.15
A8	492	613	708	0.64	1000	0.22
A10	509	628	728	0.56	1010	0.26
B4	413	590	663	0.90	1000	0.15
KA4	413	606	-	1.17	990	0.17
KB4	413	623	-	1.06	1010	0.10

[a] in the range 293-750K; [b] in the range 750-1073K.

manganese ions. At higher calcination temperature (1073-1273K), the main peak centred at 613-628K becomes sharper, while the area of the second component (T_{M2}, 708-728K) becomes larger. Overall, a decrease of the H_2/Mn ratio to 0.64 and 0.56 for the catalysts calcined at 800 and 1000°C, respectively, is recorded (Table 3).
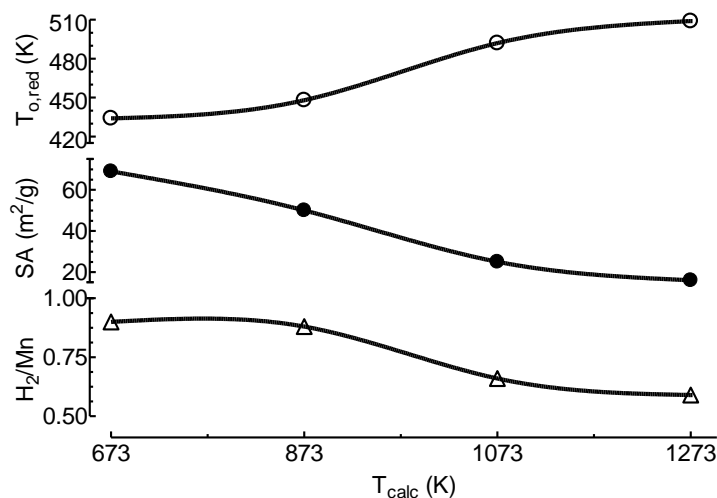
Figure 5. Effect of calcination temperature on the SA_{BET}, onset of reduction temperature ($T_{o,red}$) and extent of hydrogen consumption in the range 293-750K (LTR) (see Table 2).

Consistent with XRD data, indicating an increasing formation of the Mn_2O_3 species, such findings point to a steady decrease in the A.O.N. of manganese from ca. 3.5 to 3.1 as T_{calc} rises from 673 to 1273K. Meanwhile, the peak at

787-813K, due to reduction of surface cerium ions not interacting with Mn ones becomes progressively more evident, because of the rising crystallization and the consequent segregation of MnO_x and CeO_2 phases (Figure 4A) [17].

Therefore, higher surface area and dispersion of the active phase across the ceria support imply higher A.O.N. of the active phase and an enhanced catalyst reducibility, as documented by Figure 5, showing the trends of SA_{BET}, $T_{o,red}$ and H_2/Mn with T_{calc} for the M3C4-Py system.

On the other hand, inspecting the effects of the Mn loading and K-addition on the reduction pattern of the $MnCeO_x$ system (Figure 4B), it can be noticed a substantial analogy of the TPR profile of the M1C1-P4 with that of the M3C4-P4 catalyst, as two main peaks centred at 590 and 663K (LTR) account only for a larger H_2/Mn ratio (0.90). At least, addition of potassium to the M3C4-P4 system causes the disappearance of the component at higher temperature and a marked increase of the intensity of that at low temperature (T_{M1}, 606K) resulting in a much larger (1.17) H_2/Mn ratio [20,21]. As for undoped M3C4-P4 and M1C1-P4 samples, very slight are the differences in the TPR profiles of the KM1C1-P4 sample in comparison to the KM3C4-P4 one, as a main peak centred at 623K accounts for a H_2/Mn ratio equal to 1.06. In both cases A.O.N. formally higher than +4 (e.g., 4.12-4.34) would indicate the transformation of the Mn_2O_3 phase of the bare systems into a more or less crystalline MnO_2 phase (Figure 3B), according to the tendency of alkaline dopants to stabilize higher oxidation states of the interacting oxide species [20-23].

Therefore, both surface area exposure and A.O.N., in turn related to the dispersion of the active phase, are the key issues of the CWAO performance of the $MnCeO_x$ system. Indeed, large total surface area and higher A.O.N. favour the adsorption of the substrate at the catalyst surface and its subsequent degradation by oxidative reactions until the ultimate formation of CO_2. However, very slow kinetics of carbon-gasification, testified by weight loss close to the phenol-to-catalyst mass ratio (Table 1), represent the main drawbacks for their potential application in large-scale continuous processes [11-13].

114

V.3.3. Redox features (TPO)

Considering then that the adsorption of the substrate is the first fundamental step of the CWAO reaction, we attempted to shed lights into the phenol oxidation path by performing some gas-phase temperature programmed oxidation (TPO) tests. In particular, the TPO profiles of phenol (5 wt%) deposited by incipient wetness on a "fresh" KM1C1-P4 sample (Figure 6A)
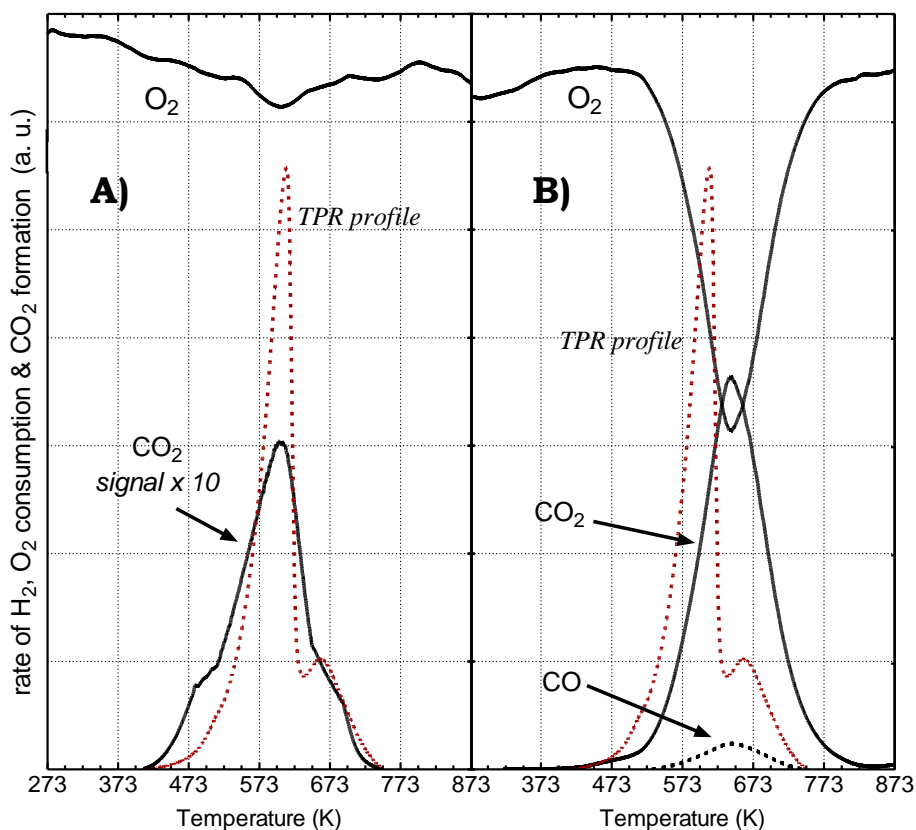
Figure 6. TPO profiles of phenol (5 wt%) adsorbed on the KM1C1-P4 sample (A) and of the "spent" KM1C1-P4 catalyst sample (see Figure 2) (B). For comparison the TPR profile (Figure 4B) of the fresh system is shown.

and that of carbonaceous deposits on the "used" KM1C1-P4 sample (Figure 6B), are compared with the TPR pattern of the "fresh" KM1C1-P4 catalyst in Figure 6 [17,22].

Analogous onset temperatures of reduction, O_2 consumption and CO_2 formation signal a direct correlation between the rate of phenol oxidation and that of catalyst reduction. In other words, these findings indicate that the catalyst *oxygen mobility* and *availability*, mediated by redox cycle(s) involving Mn ions, control the oxidation rate of phenol [17,22]. However, while the rate of phenol oxidation practically parallels that of the catalyst reduction, resulting the highest in concomitance with the maximum reduction rate (Figure 6A), the shift of the maximum of CO_2 formation to higher temperature on the "spent" sample (Figure 6B) matches a partial conversion of the substrate into less reactive intermediates by parallel coupling/polymerization reactions [10-22].

V.4. Reaction path

Thus, the catalytic action of the $MnCeO_x$ system stems from the adsorption (i) and interaction of the substrate with the catalyst oxygen (ii) prompting a reversible redox reaction cycle, "looped" by the gas-phase oxygen replenishing step (v) [17,22]:

$$Ph\text{-}OH + \alpha \leftrightarrows Ph\text{-}OH_{(s)} \qquad \text{i)}$$

$$Ph\text{-}OH_{(s)} + \sigma\text{-}O \rightarrow P_{(s)} + \sigma \qquad \text{ii)}$$

$$P_{(s)} \leftrightarrows P_{(l)} \qquad \text{iii)}$$

$$P_{(s)} + n\,\sigma\text{-}O \rightarrow CO_x \qquad \text{iv)}$$

$$\sigma + O_2 \rightarrow \sigma\text{-}O \qquad \text{v)},$$

where "*P*" is a generic intermediate adsorbed ($P_{(s)}$) or released in the liquid phase ($P_{(l)}$), while "σ-O" and "σ" the oxidised and reduced forms of active Mn sites, respectively. Although the adsorption of the substrate could take place regardless of the surface chemical composition and the state of the active phase, however, TPR data suggest that high kinetics of phenol and TOC removal of the promoted KM3C4-P4 and KM1C1-P4 catalysts (Table 1) could be linked also to the higher A.O.N of manganese and/or an improved surface affinity induced by potassium [20-23]. Anyway, the CWAO reaction of phenol

should proceed *via* a typically heterogeneous *"concerted"* redox reaction path, promoted by an enhanced reducibility of the active phase. Indeed, "Mn←O" *electron-transfer* processes control the formation of very reactive electrophylic oxygen species wich react with phenol, this being the rate determining step (*r.d.s.*) of the CWAO process [17,22].

V.5. Indications

All findings relative to classic co-precipitated catalysts, besides confirming literature data, indicate that structural, morphological and redox properties of the active phase altogether determine the CWAO efficiency of the system. Thus, basic requirements for the design of more efficient CWAO catalysts rely on their textural and redox features enhancement. Improving the redox pattern, by a proper tuning of the structure and dispersion of the active phase, is then a benchmark for enhancing the performance of the $MnCeO_x$ system.

Affecting the dispersion of the active species across the support, the preparation method determines the oxidation state of manganese and the "oxide-support" interaction, evidenced by a synergetic effect of ceria carrier on the redox features of the MnO_x phase. While, favouring the stabilization of higher Mn oxidation states, K doping represents a further option for upgrading their CWAO performance. Moreover, the active phase loading could affect the catalyst efficiency and must be taken into account in the design of new catalysts.

V.6. References

[1]. S. Hoĉevar, J. Batista, J. Levec, *J. Catal.* **184** (1999) 39.

[2]. S. Hoĉevar, U. Opara Kraŝovec, B. Orel, A.S. Aricò, H. Kim, *Appl. Catal. B* **28** (2000) 113.

[3]. A. Santos, P. Yustos, A. Quintanilla, S. Rodriguez, F. Garcia-Ochoa, *Appl. Catal. B* **39** (2002) 97.

[4]. A. Santos, P. Yustos, A. Quintanilla, F. Garcia-Ochoa, *Appl. Catal. B* **53** (2004) 181.

[5]. A. Santos, P. Yustos, A. Quintanilla, F. Garcia-Ochoa, *Chem. Eng. Sci.* **60** (2005) 4866.

[6]. A. Santos, P. Yustos, A. Quintanilla, G. Ruiz, F. Garcia-Ochoa, Appl. Catal. B **61** (2005) 323.

[7]. F. Arena, R. Giovenco, T. Torre, A. Venuto, A. Parmaliana, *Appl. Catal. B* **45** (2003) 51.

[8]. F. Arena, E. Alongi, P. Famulari, A. Parmaliana, G. Trunfio, *Catal. Lett.* **107** (2006) 39.

[9]. S. Imamura, *Ind. Eng. Chem. Res,* **38** (1999) 1743.

[10]. Yu.I. Matatov-Meytal, M. Sheintuch, *Ind. Eng. Chem. Res.* **37** (1998) 309.

[11]. F. Larachi, *Top. Catal.* **33** (2005) 109.

[12]. S.K. Bhargava, J. Tardio, J. Prasad, K. Foger, D.B. Akolekar, S.C. Grocott, *Ind. Eng. Chem. Res.* **45** (2006) 1221

[13]. A. Cybulski, *Ind. Eng. Chem. Res.*, **46**, (2007) 4007.

[14]. S.T. Hussain, A. Sayari, F. Larachi, *J. Catal.* **201** (2001) 153.

[15]. M. Abecassis-Wolfovich, M.V. Landau, A. Brenner, M. Herskowitz, *Ind. Eng. Chem. Res.* **43** (2004) 5089.

[16]. M. Abecassis-Wolfovich, R. Jothiramalingam, M.V. Landau, M. Herrskowitz, B. Viswanathan, *Appl. Catal. B* **59** (2005) 91.

[17]. F. Arena, J. Negro, G. Trunfio, A. Parmaliana, *Ind. Eng. Chem. Res.* **46** (2007) 6724.

[18]. H. Chen, A. Sayari, A. Adnot, F. Larachi, *Appl. Catal. B* **32** (2001) 195.

[19]. S. Hamoudi, F. Larachi, A. Sayari, *J. Catal.* **177 (**1998) 247.

[20]. S.T. Hussain, A. Sayari, F. Larachi, *Appl. Catal. B* **34** (2001) 1.

[21]. S.T. Hussain, A. Sayari, F. Larachi, *J. Catal.* **201** (2001) 153.

[22]. F. Arena, A. Parmaliana, G. Trunfio, *Sci. Tech. Catal.* **172** (2007) 489.

[23]. A.F.J Santiago, J.F. Sousa, R.C. Guedes, C.E.M. Jerônimo, M. Benachour, *J. Hazard. Mat. B* **2006**, *38*, 325.

[24]. S. Imamura, in *Catalysis by Ceria and Related Materials,* (A. Trovarelli, Ed.), Imperial College Press,London, UK, **14** (2002) 431.

[25]. F. Arena, G. Trunfio, J. Negro, L. Spadaro, *Appl. Catal. B* **85** (2008) 40.

[26]. F. Arena, G. Trunfio, J. Negro, B. Fazio, L. Spadaro, *Chem. Mater.* **19** (2007) 2269.

[27]. F. Arena, G. Trunfio, J. Negro, L. Spadaro, *Mater. Res. Bull.* **43** (2008) 539.

[28]. F. Arena, G. Trunfio, J. Negro, L. Spadaro, *Appl. Catal. B* **59** (2008)

[29]. F. Arena, G. Trunfio, B. Fazio, J. Negro, L. Spadaro, *J. Phys. Chem. C* accepted for publication

[30]. H.R. Devlin, I.J. Harris *Ind. Eng. Chem. Foundam.,* **23** (1984) 387.

[31]. F.J. Rivas, S.T. Kolaczkowski, F.J. Beltram, D.B. McLough, *Chem. Eng. Sci.*, **53** (1998) 2575.

[32]. X.-M. Lin, L.-P. Li, G.-S. Li, W.-H. Su, *Mater. Chem. Phys.* **2001**, *69*, 236.

[33]. L.-X. Yang, Y.-J. Zhu, G.-F. Cheng, *Mater. Res. Bull.* **2007**, *42*, 159.

[34]. F. Kaptejin, J.A. Moulijn, S. Matzner, H.P. Boehm, *Carbon* **37** (1999) 1143.

Chapter VI

Novel "redox-precipitated" MnCeO$_x$ catalysts for the CWAO of phenol

VI.1. MnCeO$_x$ development

Findings come out from previous studies reported in literature and the systematic investigation on co-precipitated catalysts presented in the previous section let us to state that, with the appropriate development, Mn-based systems represent to date a reliable alternative to the expansive noble metal catalysts for the catalytic oxidation of phenol and other organic pollutants present in the wastewater streams [1-24].

VI.1.1. MnCeO$_x$ catalyst requirements

Previous studies on the reactivity and reaction mechanism of the catalytic wet air oxidation of phenol with the MnCeO$_x$ system, conducted by many researchers all over the world in recent years, evidenced that, in contrast to the proposed *homogeneous autocatalytic free radical* path [3], triggered by the catalyst surface, the reaction proceed with a typical heterogeneous mechanism. The substrate is rapidly (depending on the reaction temperature) adsorbed on the catalyst surface and then the electrophilic oxygen species attack the various molecule bonds. The subsequent oxidation to CO_2 results to be very slow, representing, thus, the rate determining step (r.d.s.) of the overall reaction. Because of this drawback phenol can polymerize on the surface before being mineralized to carbon dioxide, so leading to the catalyst deactivation by the classic phenomenon of fouling [13]. The reaction mechanism can be synthesized as follows:

$$\text{Ph-OH} + \alpha \leftrightarrows \text{Ph-OH}_{(s)} \qquad \text{(i)}$$

$$\text{Ph-OH}_{(s)} + \sigma\text{-O} \rightarrow P_{(s)} + \sigma \qquad \text{(ii)}$$

$$P_{(s)} \leftrightarrows P_{(l)} \qquad \text{(iii)}$$

$$P_{(s)} + n\,\sigma\text{-O} \rightarrow \text{CO}_x \qquad \text{(iv)}$$

$$\sigma + \text{O}_2 \rightarrow \sigma\text{-O} \qquad \text{(v),}$$

where "*P*" is a generic intermediate adsorbed ($P_{(s)}$) or released in the liquid phase ($P_{(l)}$), while "σ-O" and "σ" the oxidised and reduced forms of active Mn sites, respectively.

These experimental evidences are confirmed by the works of Abecassis-Wolfovich et al. who deduced the fundamental role of catalyst textural and redox features on their mineralization activity (selectivity) [11-12]. They demonstrated that the strong adsorption of carbon deposits implies the progressive deactivation of the studied system, and proposed to regenerate the catalyst in a separate reactor [11-12]. This option would increase the operative costs of the process because of the presence of another unit which must works at temperatures higher than the CWAO reaction in order to burn the carbonaceous species previously adsorbed on the catalyst surface.

In particular, focusing their attention on structural properties of "fresh" and "used" catalysts, they proposed the *Surface Reactive Adsorption* (*SRA*, $g_{phenol\ reag}/g_{phenol\ ads}$) and *Catalyst Adsorption Capacity* (*CAC*, $g_{phenol\ ads}/g_{cat}$) concepts in order to characterize the fundamental requirements for the improvement of the title $MnCeO_x$ system [11-12]. This requirements are high surface area, to speed up the substrate and TOC adsorption, and an easy reducibility of the active phase, crucial for the activation and generation of electrophilic oxygen species ($O^{\bullet}$, O^{2-}, O^{-}, etc.), which then oxidize phenol and its reaction intermediates at the same reaction temperature.

Another important deduction proposed by the same authors is that the Mn_3O_4 crystalline phase represents the one able to conduct the CWAO of phenol, in contrast with the ipothesys previously proposed by Larachi et al. [1,6-10]. In fact, the latter group observed a direct relationship between surface area , dispersion, active phase reducibility and average oxidation state (A.O.N.) of the Mn ions [6-8]. Then, the stabilization of high A.O.N numbers is the major key for improving the activity and stability of the system against the fouling by carbonaceous deposits. They proposed, thus, the doping with potassium (founding in 4 wt% the optimum amount) in order to stabilize the higher A.O.N. of the system [9].

Finally, besides some disagreement by various authors on the interpretation of activity data and on structure-reactivity relationships, it is evident from literature analysis that the optimization of $MnCeO_x$ catalysts for the CWAO of phenol and other refractory substrates lies on the improvement of structural, textural and redox features [1-14]. The maximization of this peculiar characteristics would be crucial for lowering the reaction temperature of the process, so rendering possible its feasibility at industrial scale in the very next future [2,3,21].

The improvement of this characteristics lies on the preparation method, given the need to mix at an atomic scale the Mn and Ce oxides for a maximum dispersion and a high synergistic effect of ceria on the oxidant activity of the active phase [4,25]. In fact, the major limitation of the conventional coprecipitation technique, which is the most common used in the preparation of such catalysts, consists in a scarce active phase dispersion and in a poor surface area exposure, due to the different solubility of precursors, reflected in the diverse kinetic precipitation of various cations. As a rule, this implies the formation of more or less homogeneous mix of "monocomponent" precipitate particles which is really difficult to control. Evidently, this drawback can be easily ascribable to the operator ability more than to the method principles, leading to a strong irreproducibility of results between various laboratories or, at least, in the same production [26].

Thus, the exploitation of new synthesis route is compulsory in order to obtain a selective cogeneration of mixed oxides in consequence of "specific" and "controlled" interaction between the appropriate precursors of manganese and cerium, used in the appropriate concentration.
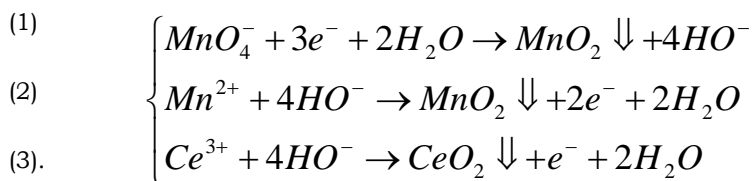
VI.1.2. The "redox-precipitation" route

In this context, preliminary qualitative tests let us to ascertain that the precipitation of Ce^{3+} and Ce^{4+} cations at a concentration of 10^{-3} M as oxides/hidroxides takes place at different pH (8.4 and 3.1, respectively) [27]. These concentrations correspond to K_{ps} equal to $1.6 \cdot 10^{-20}$ e $2.5 \cdot 10^{-47}$ for

$Ce(OH)_3$ e $Ce(OH)_4$, respectively, while, in accordance with literature data the $Mn(OH)_2$ species have got a K_{ps} equal to $1.5 \cdot 10^{-13}$.

Then, for the new synthesis route a redox reaction between Ce^{3+} and Mn^{2+} precursors is compulsory in order to obtain the simultaneous generation of MnO_2 and CeO_2 species. More important, because of the necessity of electronic exchange between oxidant and reductant species, the two precursors have to come up against, so generating intimately and contemporaneously the two oxides and ensuring the precipitation at an "atomic" level [16,17].

For this purpose a water solution of the $KMnO_4$ precursor ($\approx 10g/L$) has been titrated a constant pH (8.0 ± 0.3) with a solution of ions in order to generate the following reactions:

$$
\begin{cases}
(1) & MnO_4^- + 3e^- + 2H_2O \rightarrow MnO_2 \Downarrow + 4HO^- \\
(2) & Mn^{2+} + 4HO^- \rightarrow MnO_2 \Downarrow + 2e^- + 2H_2O \\
(3). & Ce^{3+} + 4HO^- \rightarrow CeO_2 \Downarrow + e^- + 2H_2O
\end{cases}
$$

Considering the concentration of the MnO_4^-, Mn^{2+}, Ce^{3+}, Ce^{4+} and OH^- species and the K_{ps} corresponding values, previously determined, and applying the Nerst equation for the obtainment of a catalyst with a ratio equal to 1 , the redox potential for the above mentioned reaction results as

$$E = E^0 + \frac{R \cdot T}{n \cdot F} \ln \frac{[Ox]}{[Rid]}$$

$$E_1 = 0.595 + \frac{333 \cdot 8.21 \cdot 2.302}{3 \cdot 96500} \log \frac{5.5 \cdot 10^{-2}}{1} = 0.595 + 0.021 \times (-1.26) = 0.57V$$

$$E_2 = 1.224 + \frac{333 \cdot 8.21 \cdot 2.302}{2 \cdot 96500} \log \frac{[10^{-6}] \cdot [10^{-8}]^4}{1.5 \cdot 10^{-13}} = 1.224 + 0.033 \times (-25.2) = 0.39V$$

$$E_3 = 1.610 + \frac{333 \cdot 8.21 \cdot 2.302}{1 \cdot 96500} \log \frac{2.5 \cdot 10^{-47}}{[10^{-6}]^4} \cdot \frac{[10^{-6}]^3}{1.6 \cdot 10^{-20}} = 1.610 + 0.065 \times (-20.8) = 0.255V$$

Confirming that the redox reaction of ions by means of the MnO_4^- precursor is possible tank to the *"concentration"* effect [27]. Anyway, so to favor the kinetic, the synthesis has been conducted at 60°C under vigorous stirring and with a 10% excess of $KMnO_4$ reductant in order to accomplish the entire reduction of Ce^{3+} and Mn^{2+} ions present into the solution.

Favoring the formation of highly dispersed mixed oxides with the consequent strong interaction between support and active phase for a synergistic electronic donor effect of ceria, this novel synthesis route would meet the above mentioned requisites for an optimum oxidative catalyst.

With a lower limit in terms of Mn_{at}/Ce_{at} ratio of 0.33 (e.g., $mol_{Mn^{II}}=0$), the atomic composition of the "redox-precipitated" catalyst is easily determined during the project design by dosing the precursors' concentration on the base of quantitative relationships which come out from the following equation scheme:

$$
\begin{cases}
3mol_{Mn^{VII}} = 2mol_{Mn^{II}} + mol_{Ce^{III}} & \text{(a)} \\[2mm]
\dfrac{mol_{Mn^{VII}} + mol_{Mn^{II}}}{mol_{Ce^{III}}} = \left(\dfrac{Mn_{at}}{Ce_{at}}\right)_{design} & \text{(b)} \\[2mm]
mol_{Mn^{VII}} + mol_{Mn^{II}} + mol_{Ce^{III}} = 1 & \text{(c),}
\end{cases}
$$

which are referred to the electronic balance (a), mass balance (b) and to the designed Mn/Ce atomic ratio, respectively [16,17].

A scheme of the co-generation of the oxides with both the novel "redox-precipitation" and co-precipitation routes is proposed in Figure 1 which well explain the limitation of the former one on the formation of molecularly dispersed oxides.

The list of samples prepared with the two procedures is showed in Tables 2,3 and 4 in section IV.2.2.
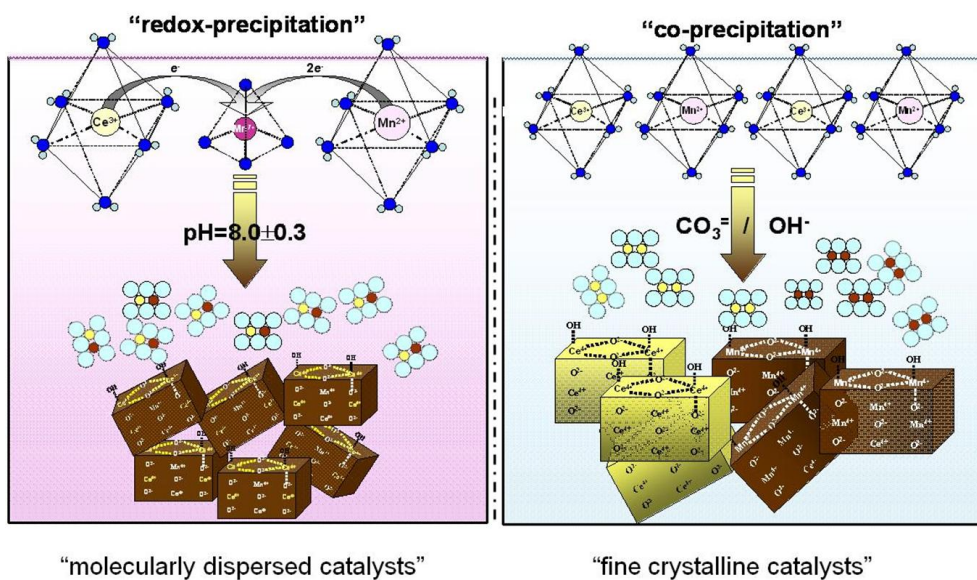
Figure 1. Scheme of the MnOx and CeOx oxides formation during the novel "redox-precipitatio" and the classic co-precipitation route.

IV.2. Preliminary comparison between novel and classic MnCeOₓ catalysts

A preliminary, though fundamental, indication of the effectiveness of the new preparation method is represented by the surface area values of both dried and calcined samples with an increase of ca.50% with respect to the better co-precipitated calcined system [13]. In effect, no comparison is possible between dried samples, due to the necessity of taking away from the catalyst the precipitant ions or the precursor counterions generated during the precipitation with the classic coprecipitation method, while the new one directly produces the two oxides [13,16,17].
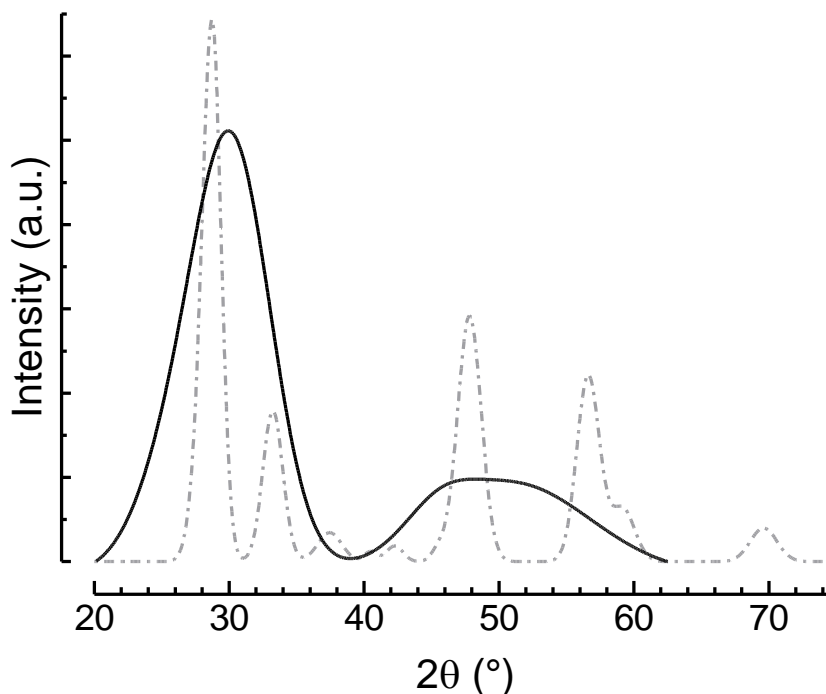
Figure 2. XRD pattern of redox (back and continuous line) and co-precipitated (grey and dotted line) catalysts.

The strong increase in surface area exposure parallels substantial differences in the structural properties, as probed by the comparison of XRD patterns of the M1C1-P4 and M1C1-R4 catalysts in Figure 2 The diffractogram of the redox-precipitated sample shows two unusually broad, "hill-shaped"

127

reflexes spanned in the ranges 20-38° and 40-60°, respectively, with the former much more intense than the latter one [13].

Although the larger development of total surface area, such peculiar pattern, typical of amorphous materials, cannot be only related to the different solid texture, being rather the consequence of an extremely homogeneous dispersion of MnO_x-CeO_2 species hindering any "long-range" crystalline order. On the other hand, as evidenced in section V.3., the XRD pattern (showed with grey line in Figure 2) of the M1C1-P4 presents the well defined peaks of cerianite, accounting for a crystalline arrangement of the system [28].

Markedly different textural features (see Table 1, 2, 3, 4 in section IV.2.1 and IV.2.2) confirm the diverse genesis of the solid formation in "redox-precipitation" and "co-precipitation" routes. Namely, the high surface area (154 m^2/g) and PV (0.49 cm^3/g) of the M1C1-R4 sample are evidently the result of the formation of *molecularly* mixed MnO_x and CeO_2 units which aggregate into very small particles further to the peculiar interaction of precursors, implying preferentially the generation of novel solid nuclei rather than an uncontrolled growth of existing ones [16,17], as schematized in Figure 1. This is a strong improvement in the preparation method with respect to the poor efficiency of the conventional co-precipitation method in enabling the mixing of the oxide components at an "atomic level". This is further confirmed by negligible variations of the <111> *d*-spacing for the M1C1-P4, which allows for an easier growth of CeO_x and MnO_x precipitate particles. The much larger ceria particle size (54Å) of the latter sample reflects the lower catalyst surface area and pore volume [13].

This findings are supported by a comparison of HRTEM images relative to the same catalysts, presented in Figure 3. The co-precipitated sample (Figure 3B) appears as an intricated array of randomly and "stepped" oriented particles (5-10 nm), characterized by the presence of ordered fringes with an estimated interatomic distance of 3.2Å, typical of crystalline ceria [13,16]. On the other hand, the "redox-precipitated" system looks much more uniform, the fringes of the crystalline ceria particles being much less evident (Figure 3A) [13,16]. Taking into account the irregular shape, a rough size in the order of

few nanometers (3-5 nm), can be estimated. Thus, direct observations support the XRD evidence of a prevalently amorphous character of the redox system [13,16,17]. The "molecular mix" of the MnO_x and CeO_2 species results thus in a very homogeneous dispersion of the active phase, affecting in a significant way the reduction pattern of the $MnCeO_x$ system.
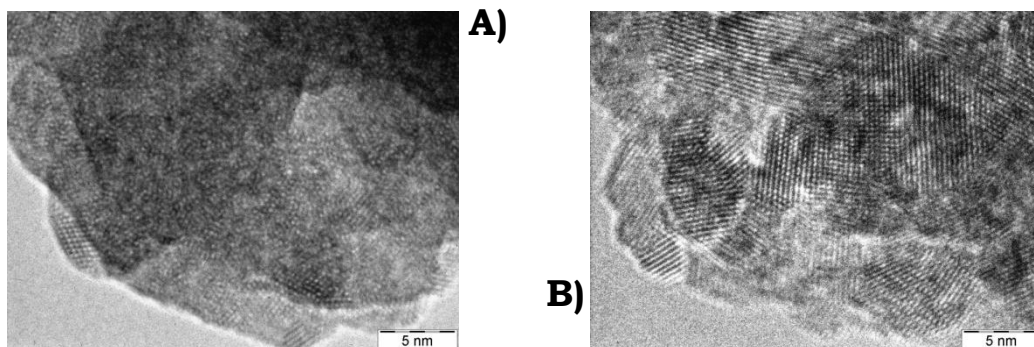
Figure 3. HRTEM images (x920,000) of the redox (A) and co-precipitated catalysts (B).

Indeed, the TPR profile of the redox sample (Figure 4) consists of a "narrower" band of hydrogen consumption, considerably shifted to lower temperature ($T_{o,red}$, 293K), where a resolved maximum at 583K with a shoulder at ca. 543K is observable. The former peak is related to the reduction of poorly crystalline MnO_2 particles, while that at lower temperature monitors the presence of "isolated" Mn^{4+} ions "embedded" into the defective positions of the ceria lattice. Their reduction is promoted by a high degree of coordinative unsaturation and, perhaps, by neighbouring Ce ions.[15,16] In addition, a resolved component centered at 422K monitors the reduction of very reactive oxygen species stabilized on "isolated" Mn^{4+} ions [16,17]. Overall, this reduction pattern accounts then for a larger amount of hydrogen consumption, resulting in a H_2/Mn ratio (1.06) larger than one. Though a simultaneous partial reduction of surface Ce^{4+} ions could balance the reduction of lower Mn-oxides, these findings are consistent with higher dispersion and A.O.N. of the active phase, greatly improving the *oxygen capacity* and *mobility* in the range 293-523K. Then, the redox sample misses the component at ca. 673K relative to reduction of Mn_2O_3 species, while, in the spectrum of the co-precipitated

system, the peaks at 420 and at 543K of "isolated" Mn^{4+} ions are nearly absent, as a much lower dispersion of the active phase [16,17].
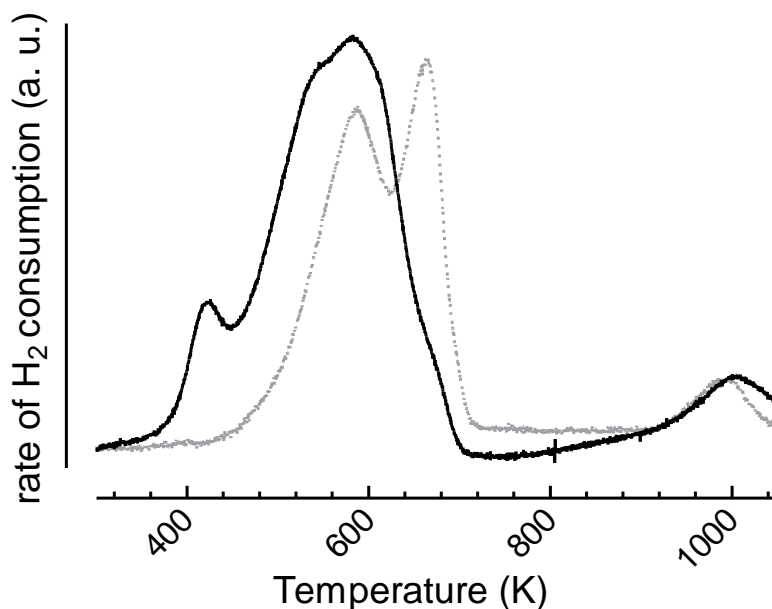

Figure 4. TPR profiles of redox (back and continuous line) and co-precipitated (grey and dotted line) catalysts.

Then, comparing the CWAO activity data of the co-precipitated and bare and K-doped catalysts with that of the "redox-precipitated" system (Figure 4), a noticeable upgrading of the CWAO performance induced by the new preparation method is evident. In particular, the M1C1-R4 system features a much superior activity in comparison to bare and K-promoted co-precipitated samples, resulting in a complete phenol and TOC removal in less than 15 minutes. In the same time the K-doped co-precipitated catalyst attains a phenol conversion of only ca. 50% along with an extent of TOC removal lower than 30%, while a complete phenol disappearance is recorded only after 1h in concomitance with a degree of TOC conversion of ca. 80% [13].

Such data clearly account for much higher 1st-order kinetic constant values of both phenol and TOC conversion. Namely, with the remarkable values of 2.6 $L \cdot g_{cat}^{-1} \cdot h^{-1}$ and 2.1 $L \cdot g_{cat}^{-1} \cdot h^{-1}$ for k_{phen} and k_{TOC}, respectively, these are

more than fivefold greater than those of the co-precipitated sample (k_{phen}, 0.56 $L \cdot g_{cat}^{-1} \cdot h^{-1}$; k_{TOC}, 0.49 $L \cdot g_{cat}^{-1} \cdot h^{-1}$) and almost twice as much (k_{phen}, 1.5 $L \cdot g_{cat}^{-1} \cdot h^{-1}$; k_{TOC}, 1.2 $L \cdot g_{cat}^{-1} \cdot h^{-1}$) those of the more active K doped one (see Table 1 in section V.2.) [13].
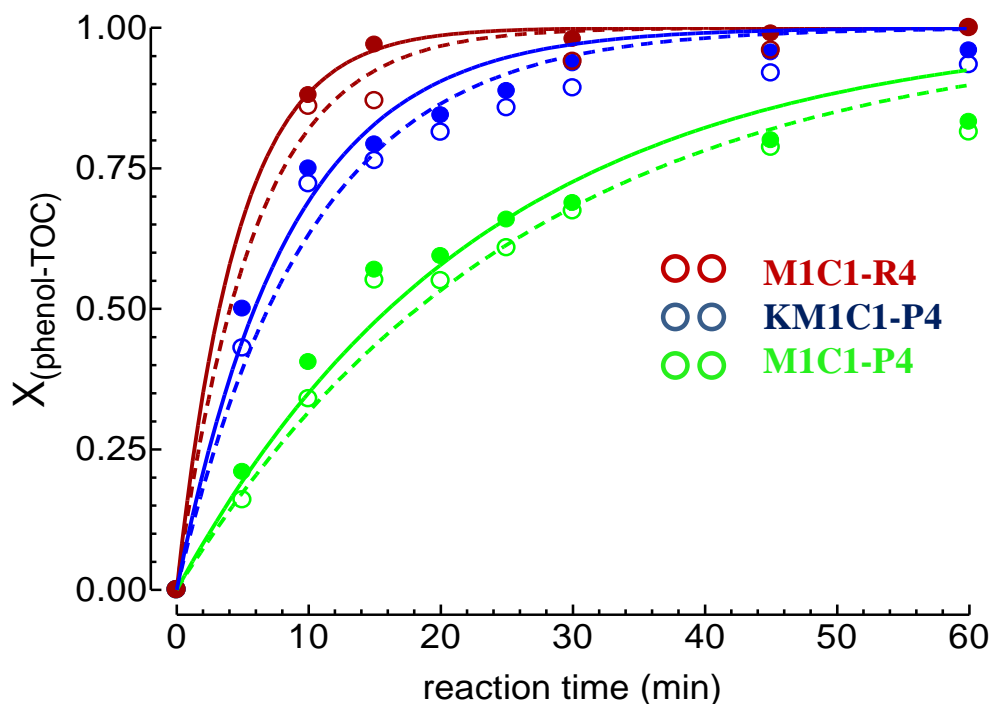
Figure 5. CWAO of phenol on the "redox-predipitated" and bare and K-doped C4 catalysts (T_R, 373K; P_R, 1.0MPa; w_{cat}/w_{phen}, 5).

Finally, TG-DSC characterization data of the "used" M1C1-P4 and M1C1-R4 catalysts, recovered after the testing in CWAO of phenol are shown in Figure 6. Although a comparable weight loss (20-21%) indicate no dramatic improvements of the mineralization activity under CWAO conditions, the rate of CO_2 formation in the gas-phase is considerably higher on the "redox-precipitated" catalyst, the maximum falling at a temperature ($\cong$523K) appreciably lower than that ($\cong$563K) of the co-precipitated sample. This allows for a

considerable narrowing of the temperature range for the complete oxidation of C-containing species on the former system. In agreement with the improved redox behaviour (Figure 4), therefore, the major oxygen mobility of the M1C1-R4 system in the range 293-523K results in a comparatively superior oxidation strenght than the counterpart M1C1-P4 sample, leading to a deeper oxidative degradation of the substrate under CWAO conditions. This is confirmed by the cumulative amount of CO_2 formed during the CWAO run, which resulted ca. three times higher for the "redox-precipitated" sample than for the coprecipitated one, accounting for total (CO_2) selectivity values of ca. 1.5 and 0.5%, respectively.
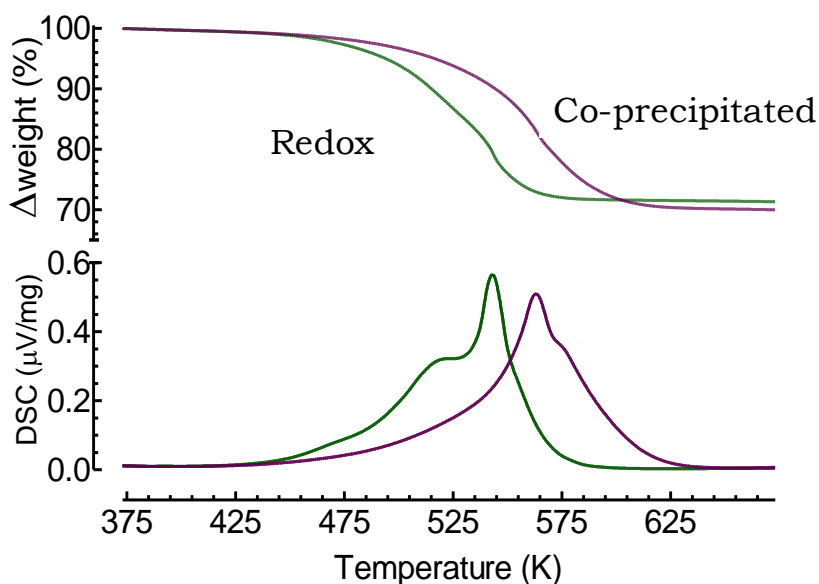
Figure 6. TG-DSC analysis of the "spent" redox-and co-precipitated catalysts, recovered after the CWAO of phenol (see Figure 5).

In conclusion, it can be stated that, in spite of the drop in pH to 4.0-4.2, the extent of the Mn leaching for the C4 system at the end of the run was negligible, confirming thus the high resistance to leaching of the $MnCeO_x$ catalyst irrespective of the preparation method [6-9,13].

All this findings let us to state that the new synthesis route designed for obtaining appropriate catalysts for an efficient abatement of substrate in the

CWAO of phenol meet the fundamental requirements previously indicated by systematic studies with classic samples [13].

In particular, The new redox-precipitation route allows to obtain highly dispersed $MnCeO_x$ systems with much improved physico-chemical properties in comparison to conventional "co-precipitated" systems and exhibits a superior performance in the CWAO of phenol under "mild" reaction conditions both in terms of activity and CO_2 selectivity. With this in mind a further systematic investigation of the new system with respect to Mn loading, synthesis parameter and calcinations treatment will provide the ideal design for this kind of catalysts.

VI.3. Redox-precipitated catalysts characterization

VI.3.1. Surface Area

The easy application of the new system can be assessed preparing various samples with different Mn/Ce ratio or using bases different from KOH, as pH controller. The lists of the samples used in this work, along with their main characteristics, are reported in Table 2, 3 and 4 of section IV.2.2. Surface area values with no tremendous variation implies the occurrence of the same precursors' molecular mixing allowing the possibility to change the active phase load with no particular interference on the surface texture, which is claimed to be one of the crucial characteristics of the title system [13]. As expected, the calcination treatment, allowing the stabilization of particles, lower the SA_{BET}, though maintaining high values also at high T_{Calc}, in comparison to those reported for the $MnCeO_x$ systems obtained by the classic coprecipitation routes [1,6-11].
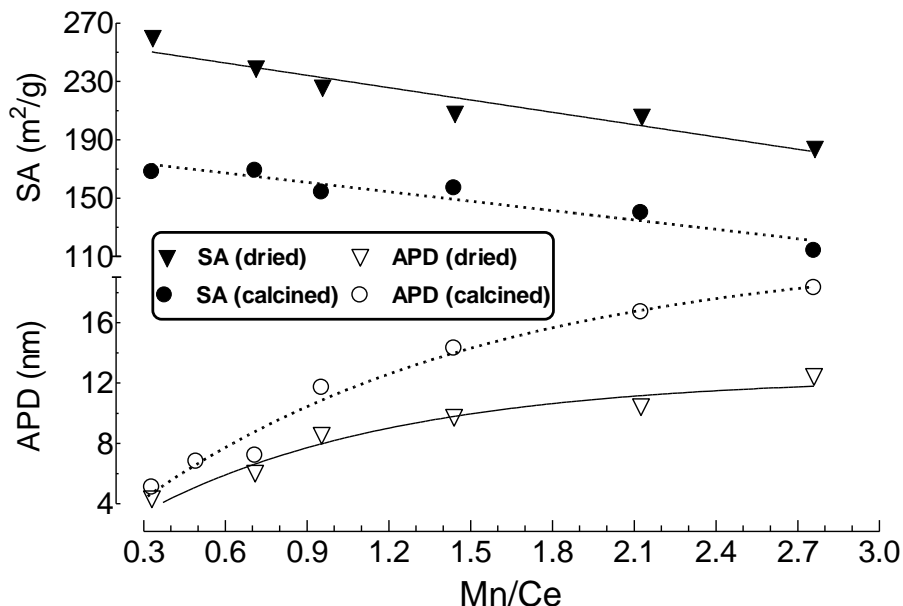
Figure 7. Influence of the Mn/Ce atomic ratio on surface area (SA) and average pore diameter (APD) of dried and calcined "redox-precipitated" catalysts.

Although the potential of the redox-precipitation route in forwarding a fairly reproducible catalyst architecture,[23,24] the regular variations in surface area of dried (270-190 m^2/g) and calcined (170-120 m^2/g) catalysts confirm the occurrence of a *composition-effect* on the morphology of redox-precipitated samples [15]. Figure 7 shows indeed that these correspond in both cases to a linear decrease in SA with the Mn/Ce ratio, accompanied by a progressive growth in average pore diameter (APD). Considering the "soft" thermal treatment of the dried samples, this negative influence of the MnO_x loading on the textural features of the redox-precipitated system confirms that it is a true consequence of the particle "sticking" and progressive closure of tinier pores produced by the MnO_x phase [29].

This is evident from the pores size distributions (PSD) of the dried (Figure 8A) and calcined (Figure 8B) catalysts in Figure 8, disclosing a strong influence of the preparation method on the porous structure of the M1C1 system (Figure 8B), but much slighter effects of the calcination treatment on the PSD of the redox-precipitated one. Apart from a minor contribution (10-20%) of micropores, the PSD's of the dried and calcined catalysts display a narrow *Gaussian*-like shape, whose center shifts from 4-5 to 10-11 nm rising the Mn/Ce ratio from 1/3 to 2/1. Such a composition-effect also account for different PSD of the M3C1-R (Figure 8A) and M3C1-R4 (Figure 8B) samples, induced by a concomitant broadening and upward shift that displaces the descending branch of the Gaussian curve out of the mesopore range [19].

Further, in spite of a regular decrease in SA ($\approx$30%) caused by surface dehydroxylation [16], slight changes in PSD and pore volume (PV, 0.5-0.6 cm^3/g) indicate that the calcination treatment does not influence the original morphology of the redox-precipitated system [16-18]. This is a valuable consequence of the straight formation of oxide phases in the redox-precipitation route and the consequent lack of phase-transformation and decomposition processes in the calcination stage [6,25].

At variance, the lower SA and PV and the featureless PSD (Fig. 8B) of the M1C1-P4 sample reflect the low control of the co-precipitation technique on:
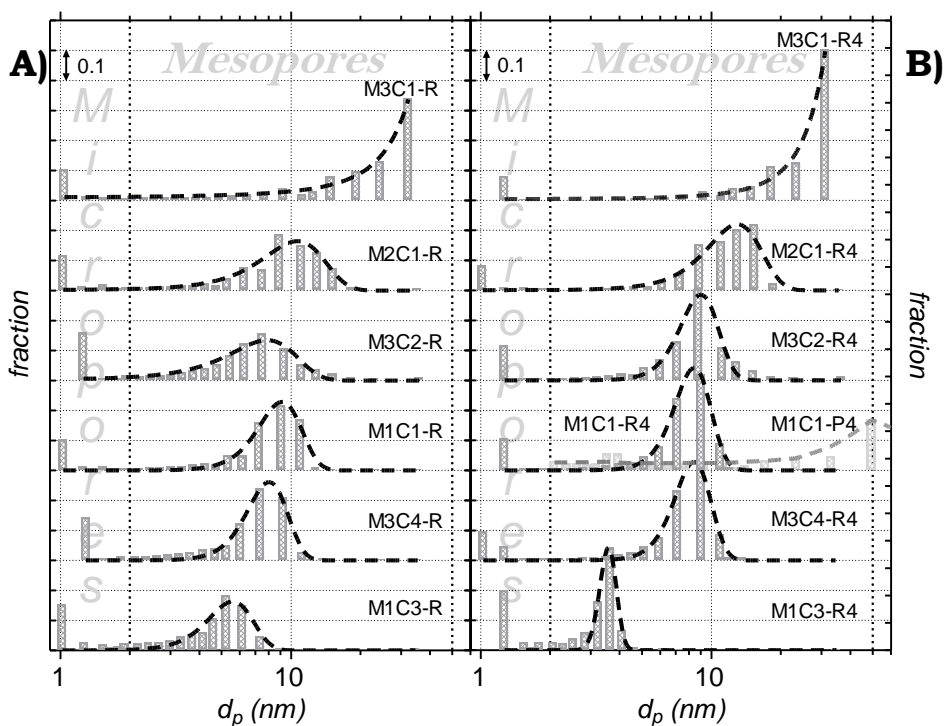
Figure 8. Pore size distribution of the dried (A) and calcined (B) "redox-precipitated" catalysts.

i. composition and precursor (Ce^{4+}/Ce^{3+}, nitrates, chlorides) effects;

ii. nucleation/growth processes during co-precipitation;

iii. precursor-decomposition and phase-reconstruction processes in the calcination stage [1,6,11-15,30-34].

iv.

Finally, the effect of the calcination treatment on the M1C1-R system has been evaluated, comparing the SA, PV and APD in the range 373-873K (Figure 9A) and the relative PSD (Figure 9B). As expected, a rise of the calcination temperature causes a noticeable decrease in SA from 215 (M1C1-R) to 90 m²/g (M1C1-R6), while minor changes in PV value account for a growth of the APD almost specular to SA decay. Moreover, the calcination temperature does not influence the aforesaid shape of the PSD, apart from an upward shift and

broadening recorded for the sample calcined at 873K, in agreement with the growth of the APD due to the closer packing induced by higher calcination temperatures [19].
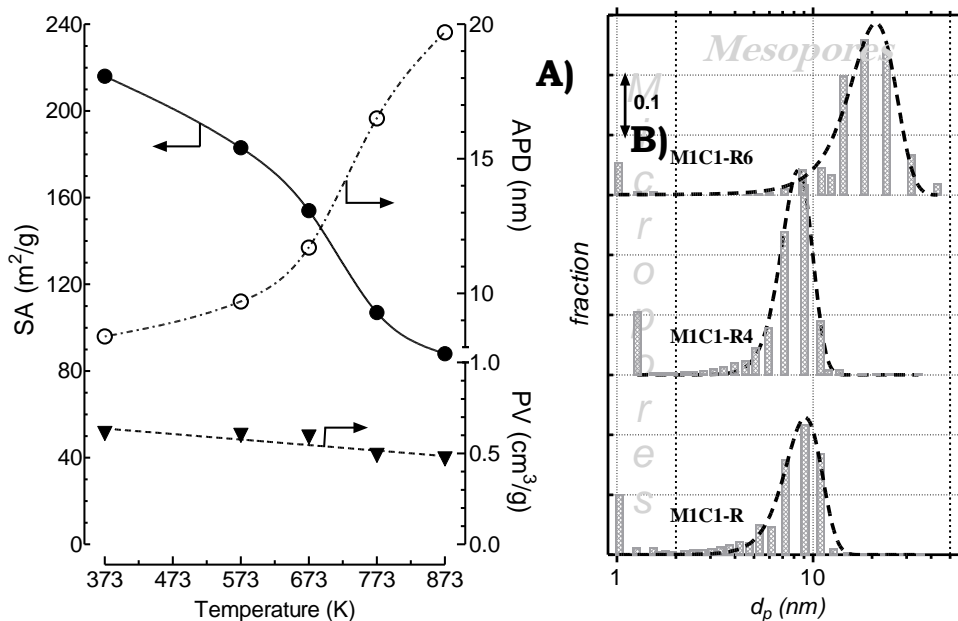
Figure 9. A) Effect of the calcination temperature on surface area (SA), average pore diameter (APD) and pore volume of the M1C1-R catalyst; B) Effect of the calcination temperature on the pore size distribution (PSD) of the M1C1-R catalyst.

VI.3.2. Surface morphology

The marked influence of the preparation method on the textural features of the $MnCeO_x$ system actually reflect a strongly different catalyst morphology that was probed by TEM and SEM observations of representative M1C1-R4 and M1C1-P4 samples (Figure 10). The former consists of spherical particles agglomerates of regular size, comprised between 10 and 20 nm (Figure 10A), giving

137
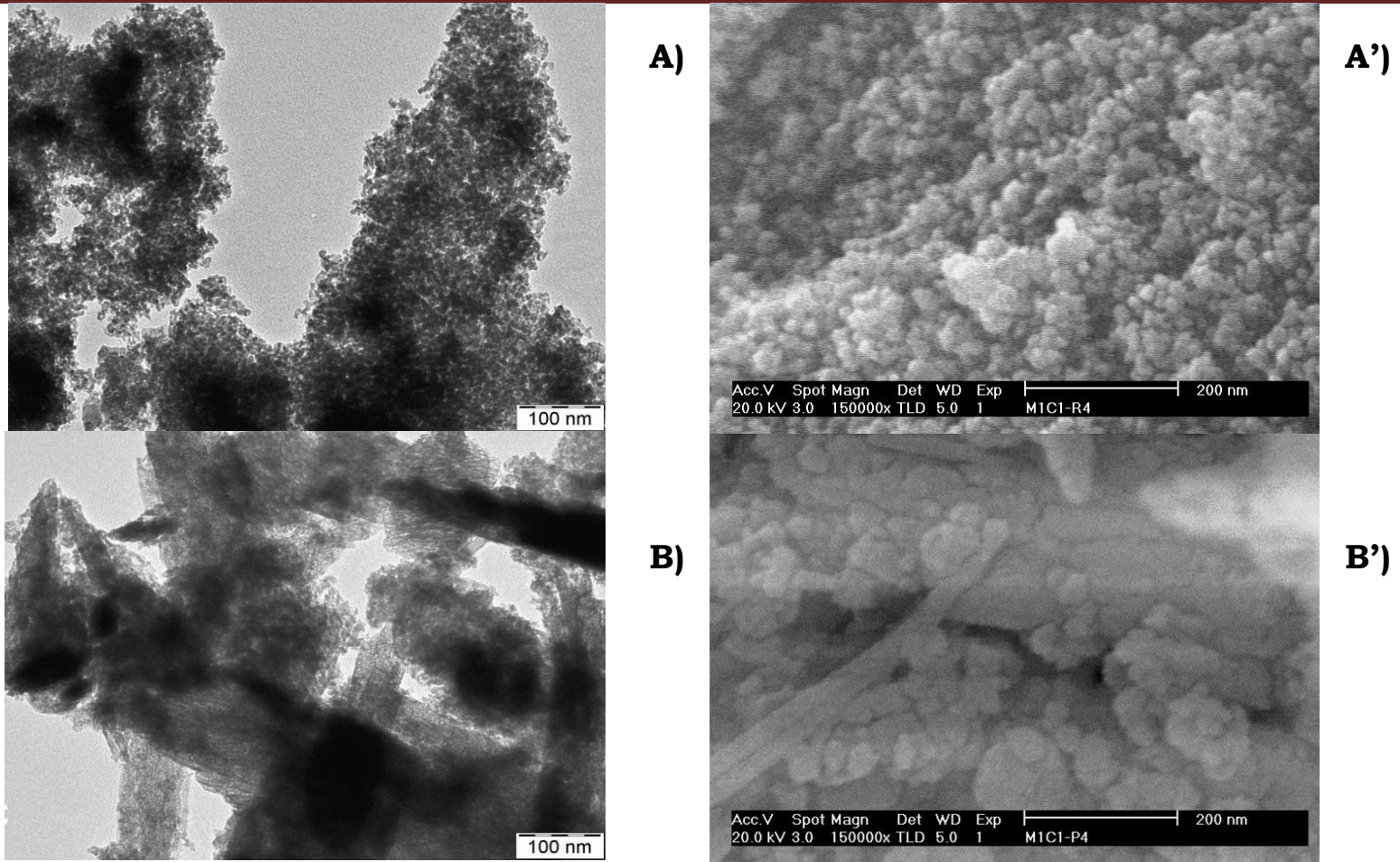
Figure 10. TEM (A, B, ×200,000) and SEM (A', B', ×150,000) micrographs of the M1C1-R4 (A) and M1C1-P4 (B) catalysts.

a sponge-like structure with a rather uniformly sized porous network (Figure 10A') that well accounts for the relative narrow PSD (Figure 8B). On the other hand, the co-precipitated catalyst shows bulky and stepped aggregates of size from ten to hundreds nanometers (Figure 10B), forming a very irregular porous network (Figure 10B'), in agreement with the "flat" PSD of the M1C1-P4 sample (Figure 8B) [19].

VI.3.3. Chemical composition (XRF)

As can be seen from Table 2, 3 and 4 of section IV.2.2, the chemical composition determined by the XRF analyses of each sample confirm the simple applicability of the method in the design of this kind of mixed oxides, even changing the reaction conditions, ensuring fast and reproducible catalyst preparation. Anyway, a particular evidence of XRF analysis is the presence of potassium on the samples' chemical composition.


Within the chart:
$$y = 0{,}068x - 0{,}018$$
$$R^2 = 0{,}972$$

Y-axis: K_{at}

X-axis: Mn/Ce
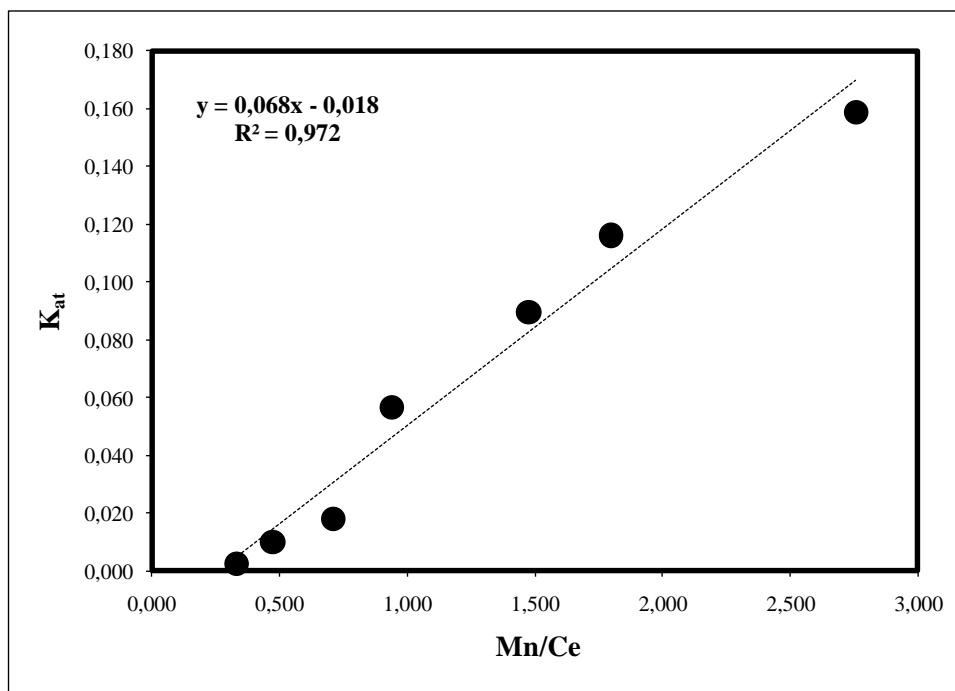
Figure 11. Relationship between Mn loading and K in the "redox-precipiataed catalysts.

Its regular increasing with Mn loading (Figure 11) cannot be related to the $KMnO_4$ precursor, being the potassium nearly absent when bases different from KOH are utilized. In fact, in the concentration of K^+ (or Li^+, Cs^+, NH_4^+), in the aqueous solution medium is about ten-fold greater than that due to the permanganate, allowing its preferential uptake on the catalyst. In fact, this is confirmed by the sample prepared using CsOH which shows a high content of Cesium and a low content of potassium. On the other hand, the parallel increase with Mn loading denotes the particular affinity of manganese, instead of cerium atoms, for the cation.

VI.3.4. Structure (XRD)

X-ray diffraction in the range 20-80° give information on the structure and on the cristalline phases of the systems. In Figure 12 the diffractograms of dried samples with different Mn loading are compared, revealing a very amorphous structure with no diffraction peaks, which are typical of crystalline phases.
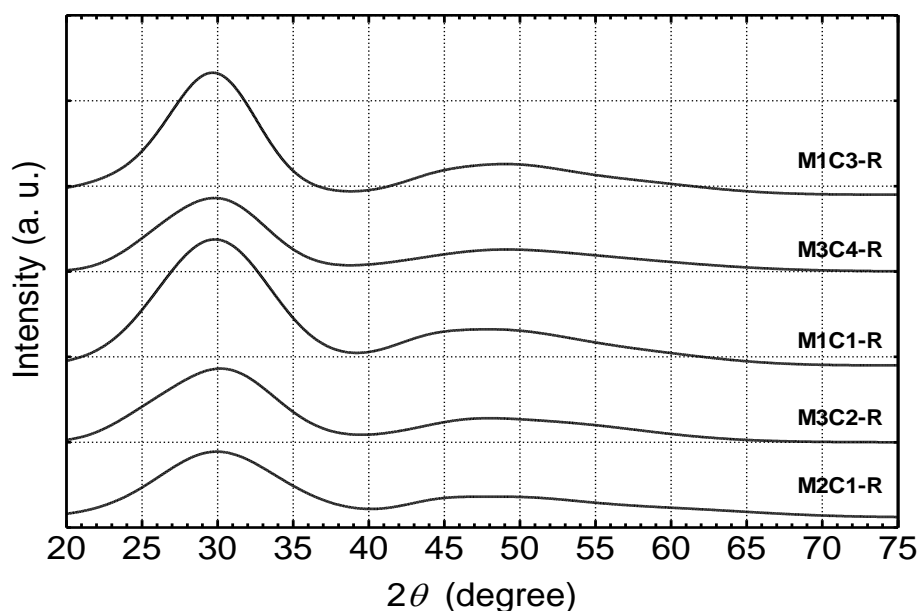
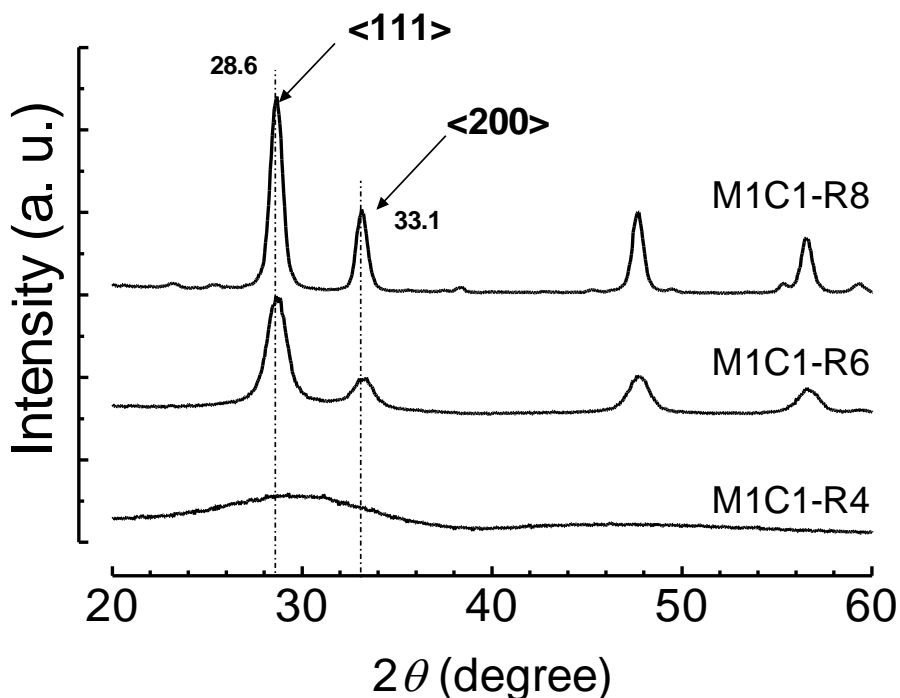**Figure 12.** XRD patterns of the dried redox precipitated MnCeOx catalysts.

This implies that the novel synthesis route lead to the formation of solids missing "long range" order, irrespective of the chemical composition [13,15].

Anyway, this structural "disorder" is not ascribable to the absence of calcinations treatment. In fact, though sample treated for 6 hours at 400°C present a lower surface exposure, due to a partial particles re-arrangement and dehydroxilation, the diffractograms of those catalysts look practically similar to previous ones (Figure 13).
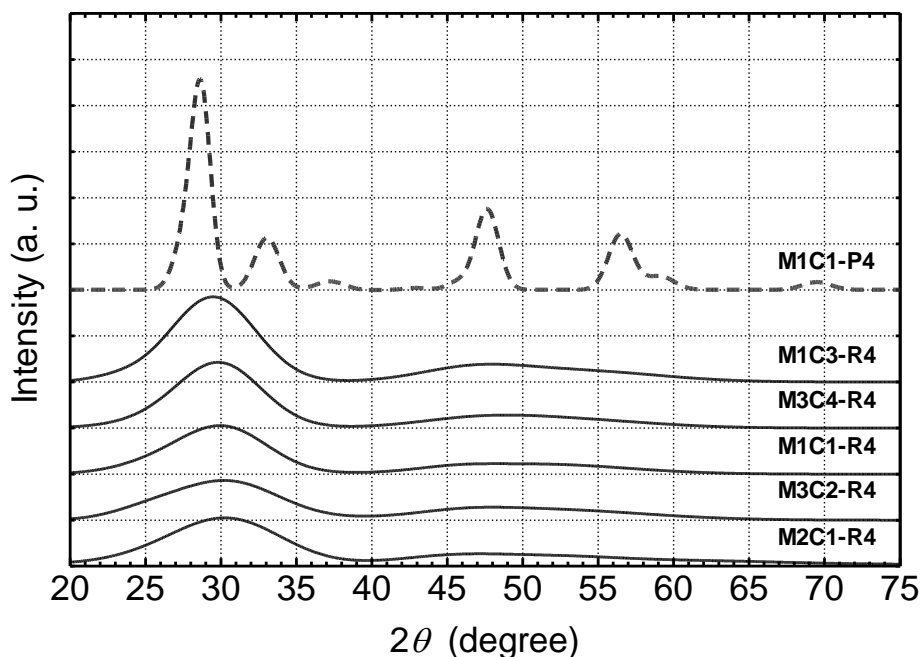
Figure 13. XRD patterns of the redox precipitated MnCeOx catalysts calcined at 400°C. For reference the M1C1-P4 sample is reported (grey and dotted line).

In this case the intensity of the broad peaks gets lower with the increase of Mn loading, suggesting that they are prevalently related to ceria. On this account, XRD analyses were conducted also on samples calcined at 600°C and 800°C and their diffractograms are reported in Figure 14. For the M1C1-R6 sample the reflex of cerianite with the fluorite structure [6-10,25,30,31,35-38]
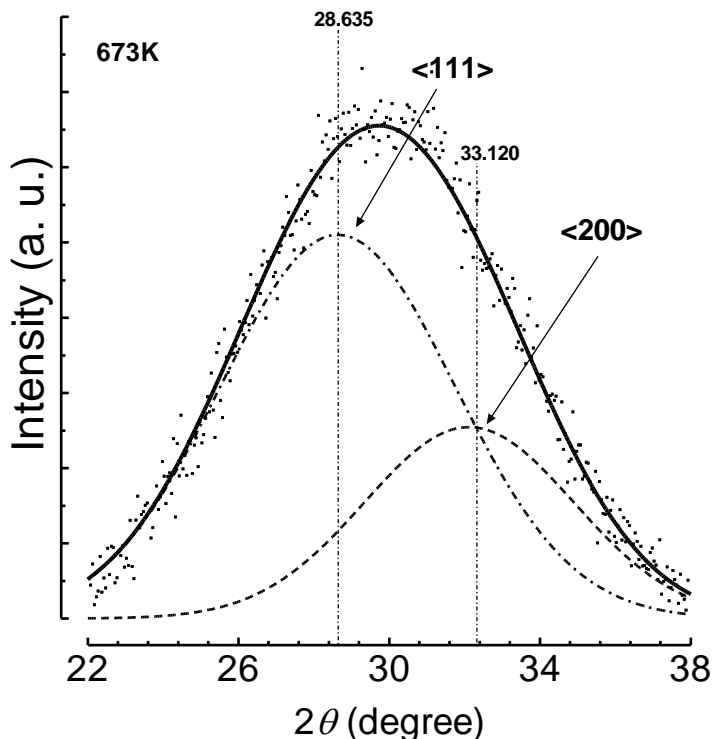
Figure 14. XRD patterns of the redox precipitated MnCeOx catalysts calcined at 400, 600 and 800°C.

and the absence of manganese related phases confirm that signals in the range 20-40° and 40-60° are ascribable to ceria. In particular, the first peak is due to the superimposition of very broad peaks at 28.6 and 33.1° relatives to <111> and <200> cerianite plans, respectively, as can be demonstrated by the deconvolution of that peak (Figure 15).

Applying the Scherrer equation to the <111> peak, even if it must be stated that it is taken as an estimation, the average particle size of ceria was calculated to be equal to 1.2nm. It must be evidenced that similar diffractograms are reported in literature for extremely disperse ceria system whose ceria average particle size was estimated in the order of 1-2nm [39]

Therefore, the diffractograms of "redox-precipitated" catalysts monitor a high spatial anisotropy, resulting from "sticking" of MnO_x and CeO_2 species at


Figure 15. XRD patterns of the redox precipitated M1C1-R4 catalyst in the 2θ range 20-40°. Deconvolution with Gaussian curves relative to the <111> e <200>plans of the cerianite structure.

a (quasi)molecular level, whereas the inadequacy of the conventional coprecipitation route in getting an effective mixing of the oxide components is confirmed by different XRD patterns, denoting the presence of crystalline phases in the M1C1-P4 sample (Figure 1B). Finally, XRD patterns prove that the novel synthesis procedure lead to very high dispersion of the active phase due to the molecular contact of the Mn and Ce oxides given by the redox reactions between the precursors [13,15,16].

VI.3.5. Structure (Raman)

The above morphological features arise from a very different structural pattern according also to micro-Raman measurements (Figure 16) coupled

with the above showed HRTEM images (Figure 3) of the representative M1C1-R4 and of the M1C1-P4 samples. The Raman pattern of the former system displays indeed a featureless signal in the whole spectral range that is diagnostic of the substantial lack of whatever "long-range" crystalline order (Figure 16). The relative HRTEM picture (Figure 3A) shows then a prevalently "amorphous" background embedding few nanosized (≈5 nm) crystalline nuclei with fringes of ca. 0.31 nm d-spacing, typical of the <111> planes of cerianite [19,40].
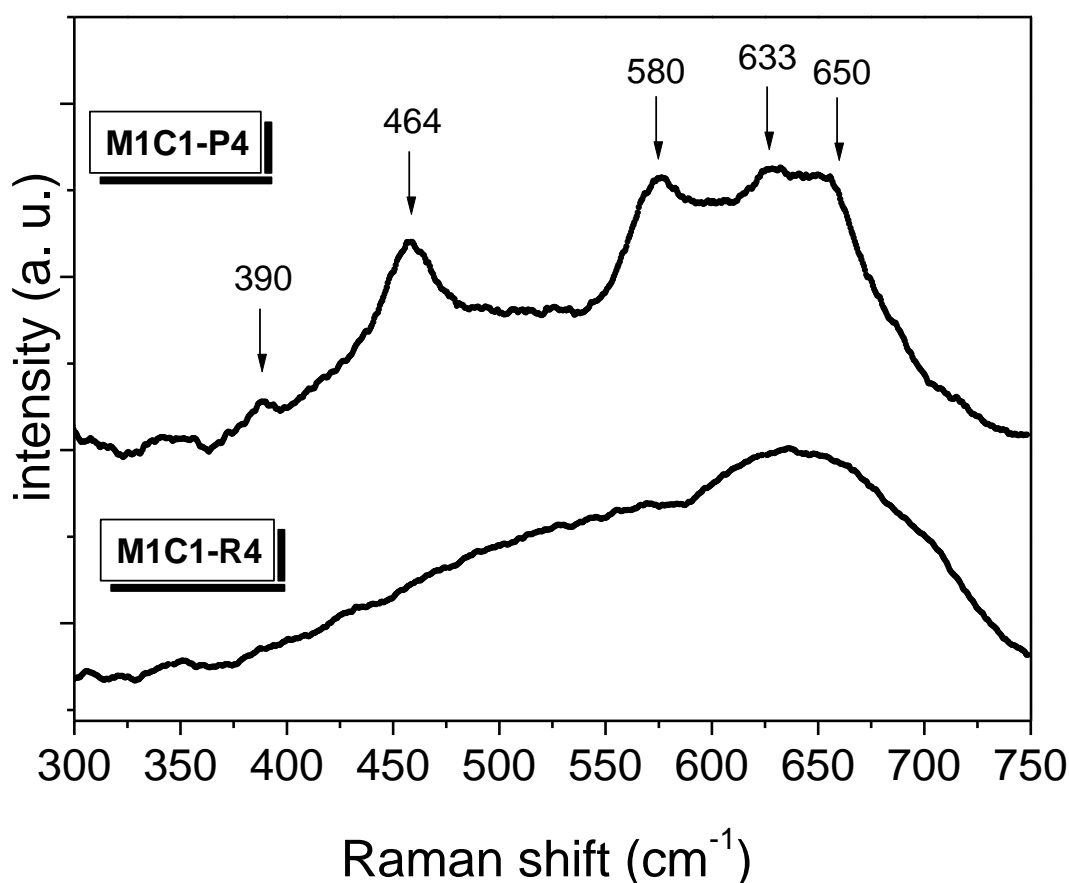
**Figure 16.** Micro-Raman spectra of the M1C1-R4 and M1C1-P4 catalysts.

A main peak at 462-464 cm^{-1}, due to the triply degenerate F_{2g} active mode of the crystalline fluorite-type ceria lattice [19,40], features instead the

Raman spectrum of the M1C1-P4 sample (Figure 16) in agreement with the related HRTEM picture (Figure 3B) displaying the chaotic array of "stepped" crystalline ceria domains, mostly characterized by diffraction fringes of d-spacing of 0.31 nm and 0.27 nm of the <111> and <200> planes [19,40]. Although other crystalline phases are not clearly discernible, the Raman spectrum displays several other peaks due to various MnO_x crystalline species. The peak at ca. 390 cm^{-1} arises from the Mn-O bending, while the Mn-O stretching modes in the range 500-700 cm^{-1} mask the weak component at ca. 590 cm^{-1} due to the non-degenerate Raman LO mode of the ceria lattice [40].

Namely, the peak at 580 cm^{-1} along with the broad "hill" in the range 500-520 cm^{-1} are typical of the MnO_2 species [41], while the lines at 633 and 650 cm^{-1} are due to Mn_2O_3 and Mn_3O_4, respectively [42,43]. Although the latter are detected in Raman measurements of MnO_2 samples due to reduction/decomposition processes further to laser-induced heating phenomena, the weak power (~0.5 mW) used in this case allows to take them as a reliable proof of various oxidation states of Mn ions in the M1C1-P4 sample [19].

VI.3.6. Surface properties (XPS)

Furthermore, XPS measurements have been carried out to shed light into the effects of the preparation method and manganese loading on surface composition and dispersion of the calcined catalysts. In particular, the XPS data of the "redox-precipitated" catalysts in terms of the surface Mn/Ce atomic ratio (e.g., Mn 2p/Ce 3d) are compared with the bulk composition data (Table V.X) in Figure 17. A very accurate straight-line relationship is diagnostic of a constant degree of dispersion of Mn ions and, although a slope value (1.26) larger than one could signal some surface segregation of the active phase, this finding is consistent with a "monolayer" dispersion of the active phase. Considering the wide range of variation of the Mn loading (9-33 wt %), this represents a very remarkable characteristic of the new synthesis route. On the other hand, with a Mn/Ce surface value (0.42) threefold lower than the counterpart M1C1-R4 sample (Figure 7), XPS analysis provides evidence of a
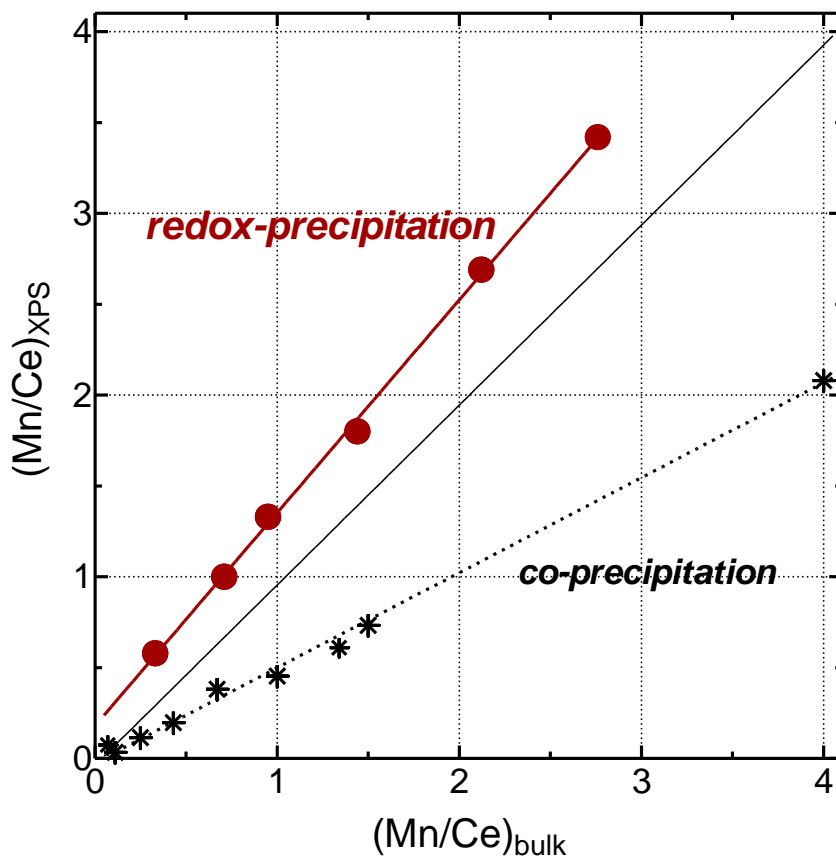
Figure 16. Surface XPS Mn/Ce ratio of redox-precipitated and co-precipitated catalysts (values taken from References [1,6] as a function of the bulk composition.

much lower dispersion of the active MnO_x phase in the counterpart M1C1-P4 system, a consequence of deeply different structure and morphology.

This is further confirmed by comparing such figures with literature data relative to the co-precipitated systems [1,6], from which it emerges a some three times higher surface concentration of the active phase at any Mn loading, that is attributable to a statistically homogeneous dispersion of Mn and Ce ions and lack of *clustering* phenomena (Figure 16). At variance, the overwhelming presence of crystalline MnO_x domains well explains the lower surface active phase exposure of co-precipitated systems [1,6,25].

Structure and dispersion of oxide species have a strong influence on the chemical state of surface atoms, as revealed by ESCA analyses of M1C1-R4 and M1C1-P4 catalysts. The spectra of Ce3d (A), Mn2p (B) and O1s (C) core levels are shown in Figure 17, while a summary of abundance and average oxidation number (AON) of Mn, Ce and O ions is reported in Table 1. The Ce3d spectrum of the M1C1-R4 sample displays mostly the six components (i.e., 881.7-888.1; 897.7-900.8; 907.3-916.1 eV) of Ce^{IV} species [44-46], while additional energy-transition states at 884.3 eV (v^l) and 903.3 eV (u^l), typical of Ce^{III} ions [44-46], are evident in that of the M1C1-P4 system. From the u^{III} transition (916.1 eV) area, an AON of Ce atoms equal to +3.9 and +3.7 is quoted for the M1C1-R4 and M1C1-P4 catalysts, respectively. The Mn2p region, monitoring the $2p^{1/2}$ and $2p^{3/2}$ *spin-orbit* transitions of ions with AON between +4 and +3 [47-49], shows consistent differences in BE position (≈ 0.2 eV) and *spin-orbit* split (≈ 0.1 eV), index of a higher AON also of Mn ions in the M1C1-R4 sample (Table 1). Abundance and AON of Ce and O (-2) atoms provide, thus, the following "normalized" surface stoichiometric ratios Mn:Ce:O=0.43:0.57:1.79 and Mn:Ce:O=0.29:0.71:1.76 for the M1C1-R4 and M1C1-P4 systems, respectively. In spite of a similar surface oxygen availability, then XPS data indicate a marked surface Mn enrichment accounting for the enhanced oxygen mobility and reducibility of redox-precipitated catalysts [15,16], though the O1s spectra (Fig. 6C) do not display significant effects of preparation method on types and population of oxygen species. Two resolved components at 529.2-529.3 and 531.3-531.8 eV in the spectra of both systems are attributable to lattice ions (O$_I$) and surface oxygen species (O$_{II}$), respectively [6,50]. The assignment of the O$_{II}$ peak is controversial as it has been somewhat related to hydroxyl-like groups (531-532 eV), oxide defects (529-530 eV), adsorbed mononuclear oxygen species (531-532 eV) and water molecules (533-534 eV). In particular, pointing that the BE of adsorbed $O_2^{\delta-}/O_2$ species falls in this range, some authors argued that the O$_{II}$ transition is diagnostic of oxygen *vacancies* across the ceria lattice [19]. On account of this, the higher relative intensity and downward shift (≈ 0.5 eV) of this component would match the greater Ce^{III} abundance of the M1C1-P4 catalyst (Table 1).
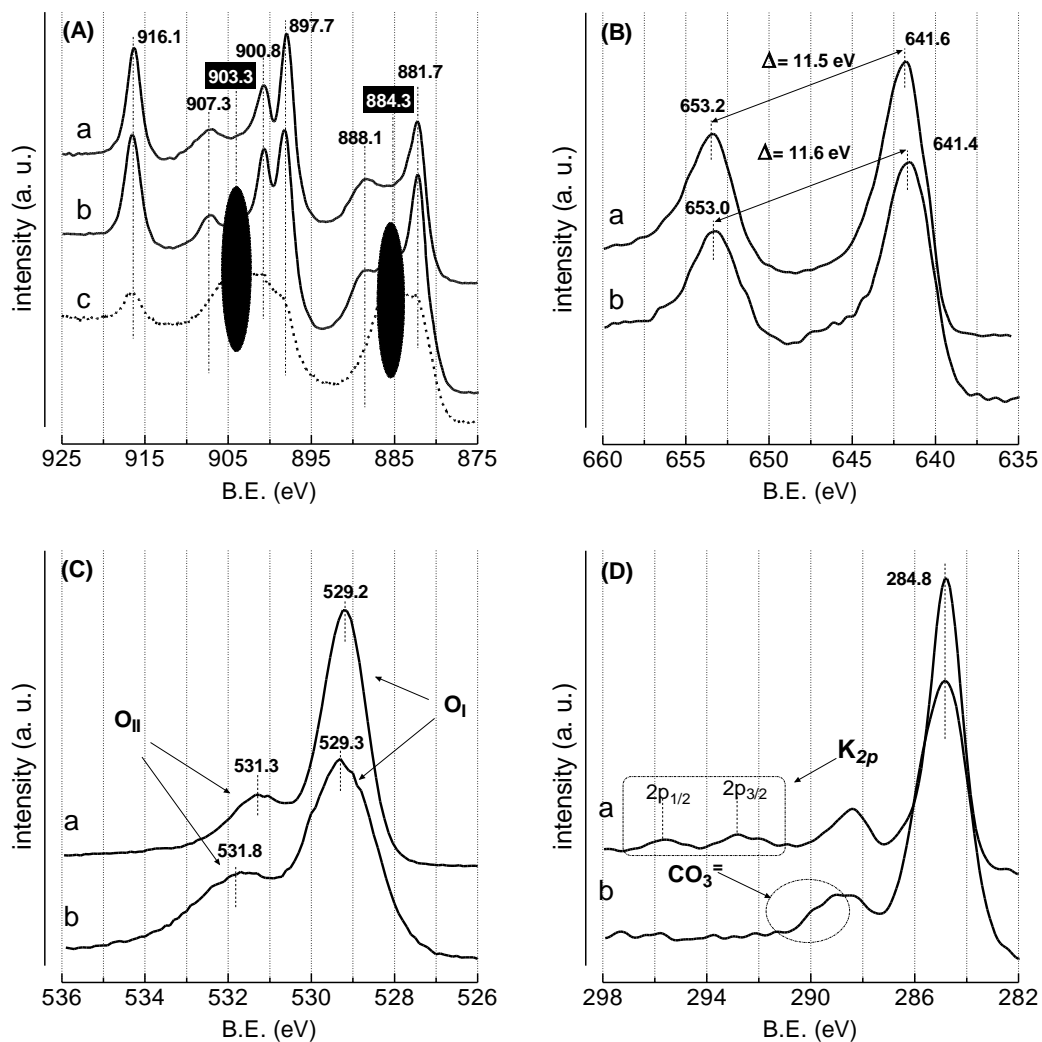
Figure 17. XPS analysis of the M1C1-R4 (a) and M1C1-P4 (b) catalysts. Spectra of Ce3d (A), Mn2p (B), O1s (C) and C1s – K2p (D) core levels. *Spectrum c in panel A refers to an in situ reduced CeO₂ sample.*

Table 1. XPS data of the calcined M1C1-R4 and M1C1-P4 catalysts. Surface atomic concentration, average oxidation number (AON) of Mn and Ce ions and "normalized" surface composition.

Catalysts	Atom conc. (%)				AON		"Normalized" surface composition
	(Mn)	(Ce)	(K)	(O)	Ce[a]	Mn[b]	
M1C1-R4	20.4	15.4	1.0	63.2	+3.9	+3.3	$Mn_{0.57}Ce_{0.43}O_{1.79}$
M1C1-P4	10.2	25.7	0.0	64.0	+3.7	+3.1	$Mn_{0.29}Ce_{0.71}O_{1.76}$

VI.3.7. Redox properties (TPR)

The redox properties of the studied catalysts have been probed by TPR measurements in the range 293-773K, the results being shown in Figure 18 with respect to the effects of Mn/Ce ratio (A), preparation method (B) and calcination temperature (C), while in Table 1 are summarized the values of the onset temperature of reduction ($T_{o,red}$), the peak maximum temperatures (T_M) and the extent of H_2 consumption. The reduction features of redox-precipitated $MnCeO_x$ catalysts with different Mn/Ce ratio (Figure 18A) show a broad reduction band featuring several poorly resolved maxima and shifting to lower temperatures at higher Mn/Ce ratios. This accounts for a regular growth of the extent of H_2 consumption in spite of a decrease in the H_2/Mn ratio (1.16→0.79) as can be seen in Table 2.
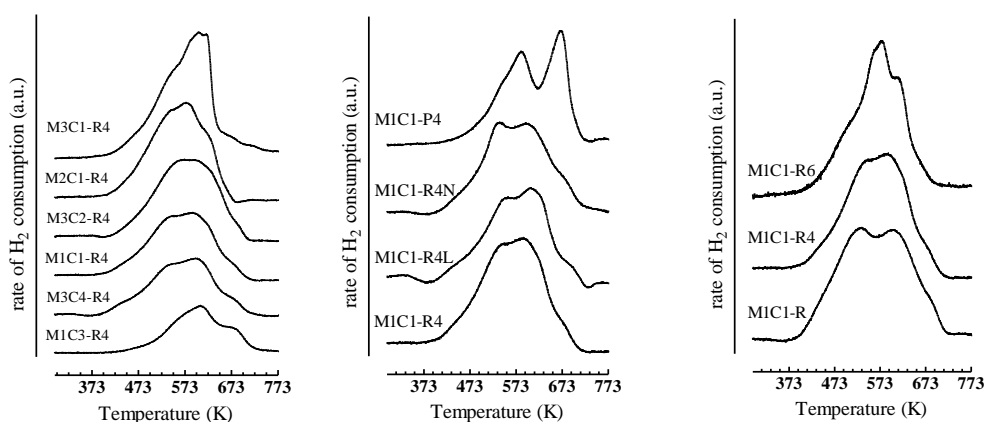
Figure 18. TPR of $MnCeO_x$ catalysts: A) Influence of the Mn/Ce ratio on the profile of redox-precipitated catalysts. B) Effect of the preparation method on the profile of the M1C1-4 system; C) Effect of the calcination temperature on the profile of the M1C1-R catalyst.

Looking at the influence of the preparation method on the TPR pattern of the M1C1-4 systems (Figure 18B) it emerges that the M1C1-P4 system features a fairly different spectrum consisting of two resolved peaks centered at 600 and 688K with an onset temperature of reduction of 400K, that accounts for a total hydrogen consumption equal to ca.3.3 mmol/g corresponding to a H_2/Mn ratio equal to 0.70. Very slight, if any, is the influence of the base used

Table 2. TPR data of MnCeO$_x$ redox catalysts.

| Catalyst	$T_{o,red}$	T_M	H_2 consumption	
	K	K	mmol/g$_{cat}$	H_2/Mn
M1C3-R4	390	586	1.94	1.16
M3C4-R4	375	591	2.95	0.93
M1C1-R4	365	591	3.27	0.85
M3C2-R4	365	599	3.78	0.77
M2C1-R4	375	573	4.60	0.79
M3C1-R4	383	600	5.46	0.79
M1C1-P4	400	588	2.71	0.70
M1C1-R4L	375	600	2.58	0.72
M1C1-R4N	375	590	3.08	0.86
M1C1-R	365	591	3.30	0.86
M1C1-R6	383	573	3.05	0.78

for the synthesis on the reduction pattern of the M1C1-R4 system in qualitative and quantitative terms. In fact, these spectra signal that the redox-precipitated catalysts miss the component at ca. 690K relative to crystalline MnO$_x$ particles (an incipient formation of these is likely to occur only for Mn/Ce>2) while the peak at 545K associated with the reduction of "isolated" Mn^{4+} ions is nearly absent in the spectrum of the co-precipitated system as the lower dispersion of the active phase [25,51,52].

Furthermore, the reduction patterns of the M1C1-R system calcined at different temperatures display some evident changes only for the M1C1-R6 system (Figure 18C). In particular, the decreasing trend of the first peak maximum and the growing intensity of the second one with rising calcination temperature suggests the occurrence of a reconstruction process leading to a

progressive sintering of the overall catalyst structure as timely probed by the strong SA decay (Figure 8). The consequent collapse in the catalyst structure implies the aggregation of "isolated" moieties into crystalline MnO_x species, evidenced also by the appearance of a sharp component on the right-side of the reduction maximum (Figure 18C).

VI.3.8. Redox properties (OSC)

Nevertheless, transient nature of the TPR technique, overlapping of surface and bulk processes and potential H_2 *spillover* phenomena onto ceria carrier [53] hinder a reliable assessment of the oxygen mobility and availability [54]. This prompted us to evaluate the oxygen storage capacity (OSC) of the representative M1C1-R4 and M1C1-P4 catalysts using CO as reductant [55].
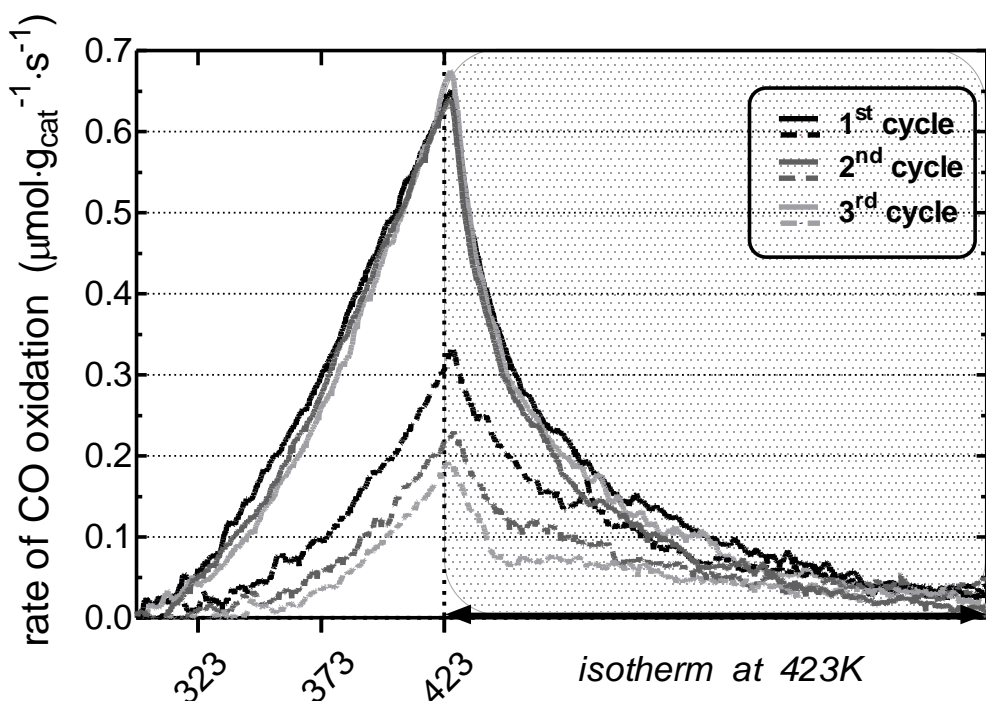

Figure 19. Rate of CO oxidation in absence of gas-phase oxygen of the M1C1-R4 (solid lines) and M1C1-P4 (dotted lines) catalysts in the range 293-423K and then in isotherm at 423K.

151

Figure 19 shows the CO oxidation patterns in the range 293-423K, while Table 3 summarizes the OSC values at 323, 373 and 423K per weight and SA unit. The M1C1-R4 sample features an onset oxidation temperature close to r.t. and reaction rates rising up to 0.65 µmol·g_{cat}^{-1}·s^{-1} at 423K (Figure 19). In parallel the OSC values rise from 4 (323K) to 200 µmolO2·g_{cat}^{-1} (423K), the last figure corresponding to a small fraction (<3.5%) of the overall oxygen availability.

Table 3. Oxygen storage capacity (OSC) of the M1C1-R4 and M1C1-P4 catalysts in the 323-423K range.

Catalyst	1st cycle			2nd cycle			3rd cycle		
	323	373	423	323	373	423	323	373	423
	(µmol$_{O2}$·g_{cat}^{-1}) /(µmol$_{O2}$·m_{cat}^{-2})			(µmol$_{O2}$·g_{cat}^{-1}) /(µmol$_{O2}$·m_{cat}^{-2})			(µmol$_{O2}$·g_{cat}^{-1}) /(µmol$_{O2}$·m_{cat}^{-2})		
M1C1-R4	4/0.03	48/0.31	198/1.29	4/0.03	45/0.29	175/1.13	5/0.03	49/0.32	186/1.21
M1C1-P4	0.5/0.005	10/0.01	104/1.03	0/0	7/0.07	68/0.67	0/0	5/0.05	56/0.55

This finding is substantiated by a "low" value of the relative Ea (43±4 kJ/mol), quoted from the relative Arrhenius plot in Figure 20, suggesting that the oxygen release process mostly concerns the catalyst surface without the significant contribution of bulk oxygen diffusion. In addition, unchanged oxidation rates (Figure 19) and OSC values denote an excellent catalyst stability in subsequent reaction cycles. In agreement with physico-chemical characterization data [13,16,17], the M1C1-P4 system features a much weaker oxidation strength probed by both a much higher (ca. 330K) onset oxidation temperature and slower CO oxidation rates in the whole range, accounting for an OSC rising from 0.01 (323K) to ca. 100 µmol$_{O2}$·g_{cat}^{-1} (423K). The last value corresponds to a fraction lower than 2% of the total oxygen availability, while a sharper dependence on temperature (Figure 20) signals a significantly higher energetic barrier (Ea, 62±3 kJ/mol) to oxygen abstraction.
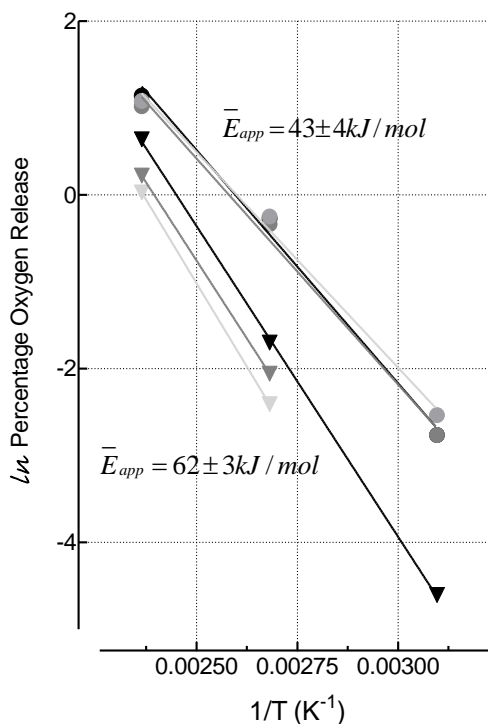
Figure 20. Arrhenius plot of the percentage of catalyst oxygen removed in OSC measurements between 323 and 423K.

Moreover, a progressive decay in the CO oxidation rate (Figure 19) matches the lower OSC values in the 2nd and 3rd cycles, without significant changes in E_a (Figure 20). Such different behavior still depend on the different structural features of the two system, since the very high dispersion of the M1C1-R4 catalyst and the consequent strong interaction between manganese ions and ceria matrix promote the electron-transfer from $O^=$ to Mn^{n+} ions (e.g., $Mn^{(n)+}-O^{2-} \rightarrow Mn^{(n-1)+}-O^-$) with the consequent easy formation of very reactive *electrophylic* oxygen species able to oxidize CO [54]. For opposite reasons, the presence of crystalline MnO_x phases depresses the OSC of the co-precipitated system resulting also in a poor stability under redox cycles [36].

VI.3.9. Redox and structural properties (XRD)

To shed further lights into this issue an XRD study of the M1C1-R4 (Figure 22A) and M1C1-P4 (Figure 22B) catalysts subjected to reduction treatments at 423 (a), 585 (b) and 720K (c) has been carried out. The first (423K) was chosen as the temperature of OSC measurements, while the second (585K) and third (720K) ones correspond to first maximum (T_{M1}) and final MnO_x reduction in TPR measurements [13,15], respectively. The XRD patterns of "untreated" samples substantiate the prevalently amorphous pattern of the redox-precipitated system (Figure 22A) in contrast to sharp diffraction lines typical of *cerianite* and *pyrolusite* (i.e., MnO_2) phases present in the co-precipitated one (Figure 22B) [13,15]. In both cases the reduction at 423K (profiles a) does not cause any detectable change, while the XRD patterns of samples reduced at 585K, bear evidences of different structural changes. In fact, beside an initial appearance of cerianite peaks, index of an incipient phase-segregation [17], the diffractogram of the M1C1-R4 sample (Figure 22A, b) displays small, though detectable, peaks at 34.9° and 40.6 of the *cubic* MnO species [JCPDS 7 230].

Whereas the M1C1-P4 system shows the lines of the Mn_2O_3 phase (18°, 36.2° and 37.6°), those relative to MnO_2 (37.3° and 45.8°) being no longer visible. These data suggest that the first TPR maximum of the M1C1-R4 system monitors the reduction of "isolated" Mn^{4+} ions to MnO, while for the M1C1-P4 one it is related to the step-wise reduction of the crystalline MnO_2 phase to Mn_2O_3 [13,16,17].

Finally, at 720K, in concomitance with a full reduction of the active phase to MnO, the cerianite and MnO peaks become easily distinguishable in the XRD patterns (profiles c) of both systems [6-9,13,31,38]. Therefore, XRD data and above E_a values reveal that the superior activity and stability of the redox-precipitated system relies on the full reversibility of the surface redox cycle involving isolated Mn^{4+} ions ($Mn^{4+} \leftrightarrows MnO$), while their strong interaction with ceria matrix hinders the sintering leading to the formation of crystalline MnO_x species. On the other hand the ongoing irreversible reduction of MnO_2
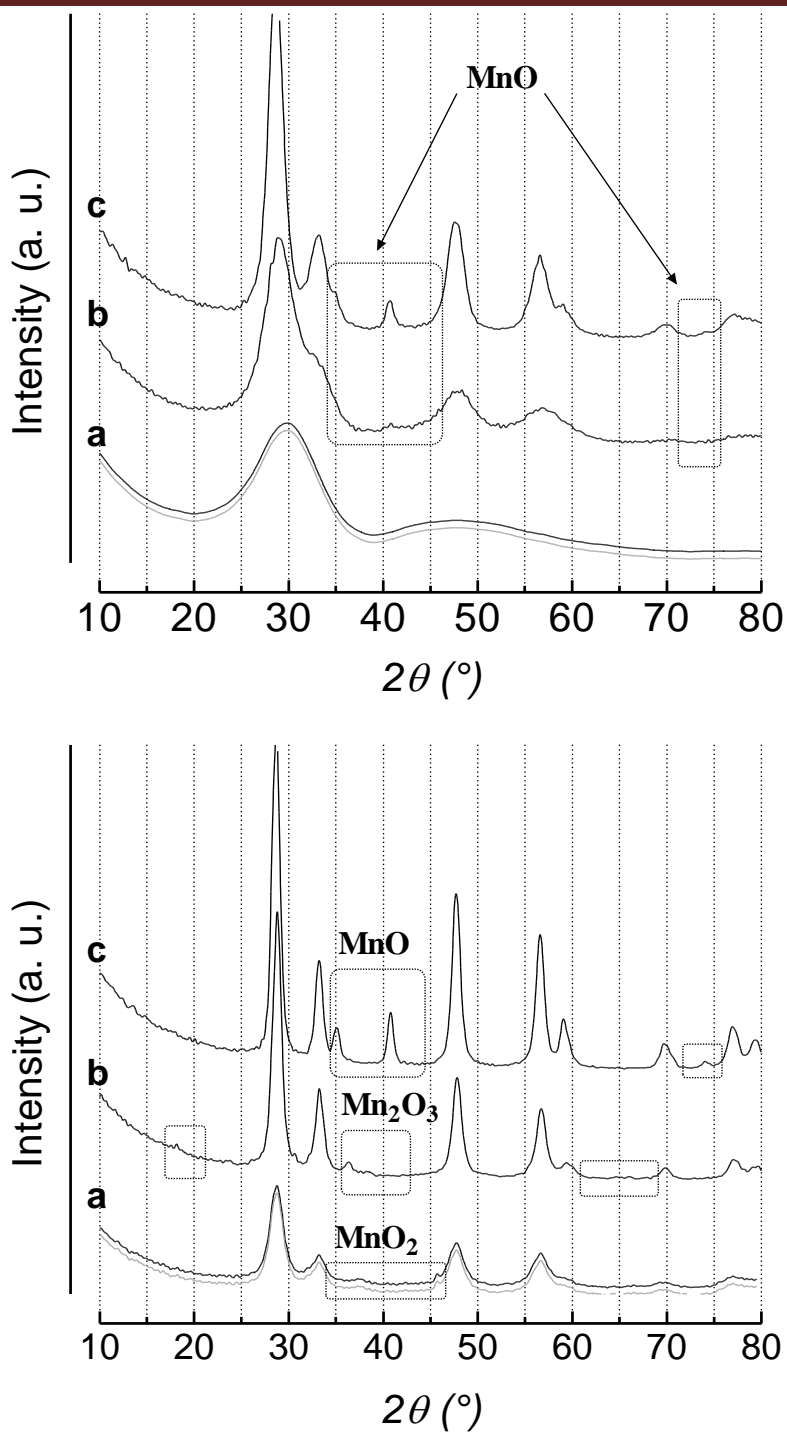
Figure 22. XRD patterns of the M1C1-R4 (A) and M1C1-P4 (B) catalysts reduced at 423 (a); 585 (b) and 720K (c). The diffractograms of "untreated" samples (grey lines) are shown for reference.

particles to crystalline Mn_2O_3 species explains the lower and decreasing OSC of the M1C1-P4 catalyst [36].

VI.3.10. Catalytic oxidation pattern and structure-activity relationships

CO oxidation activity measurements in the range 373-423K were performed to address the influence of structural and redox properties on the catalytic activity of the $MnCeO_x$ system. Kinetic data of CO oxidation are summarized in Table 4 in terms of reaction rate and average Mn site time yield (sty,s^{-1}), referred to the bulk composition (Table 4).
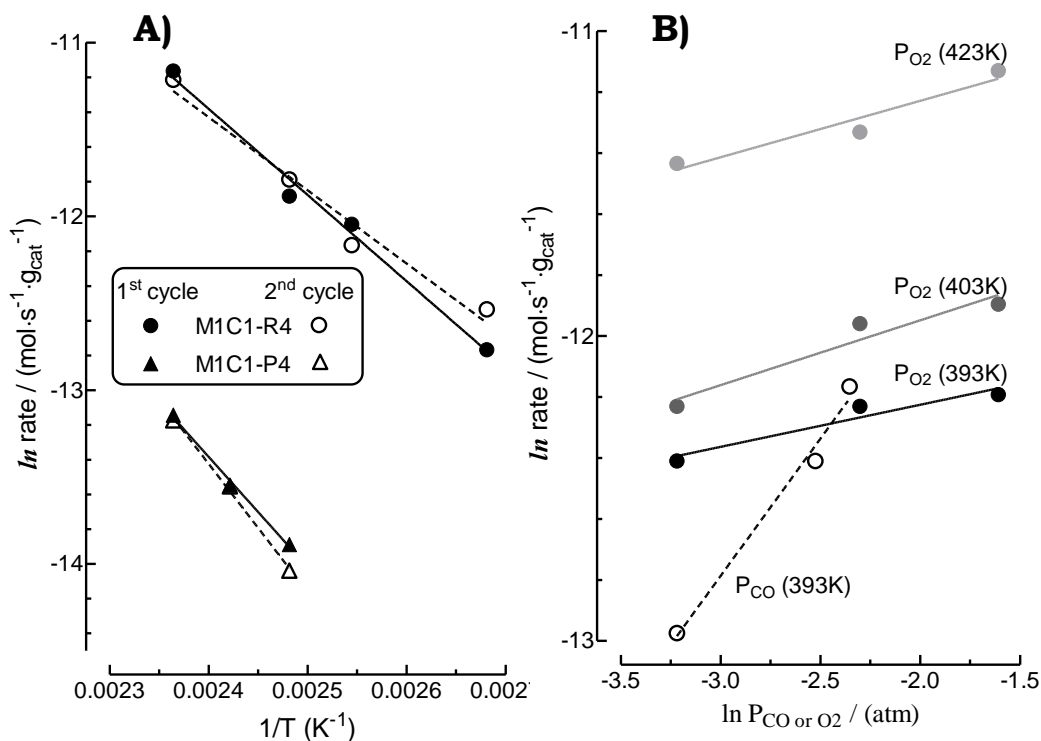
Figure 21. (A) Arrhenius plots (373-423K) of CO oxidation on the M1C1-R4 and M1C1-P4 catalysts;. (B) kinetic dependence of the CO oxidation rate of the M1C1-R4 catalyst on CO and O_2 partial pressure at 393K.

156

The M1C1-R4 catalyst exhibits a noticeable activity in the range 373-423K with reaction rate values rising from ca. 3 to 15 $\mu mol \cdot g_{cat} \cdot s^{-1}$, that compare with those of Co_3O_4-CeO_2 [55] and Au/CeO_2 catalysts [51]. Much lower reaction rate values (Table 4) confirm a significantly lower activity of the M1C1-P4 catalyst, though this is not only consequence of the different active sites availability. In fact, while both the surface specific rate and *sty$_{Mn}$* values are much lower than the ca. three times lower active phase dispersion, the Arrhenius plots (Figure 21A) account for average E_a values equal to 35-41 and 53-61 kJ/mol for M1C1-R4 and M1C1-P4 catalysts, respectively. Noteworthy, comparable differences in CO oxidation E_a (18-20 kJ/mol) were previously ascribed to a high dispersion of Mn ions and a very effective MnO_x-CeO_2 interaction that, besides enhancing the oxidation strength, hinders the formation of crystalline MnO_x (x≤1.5) phases on CeO_2-promoted MnO_x/SiO_2 catalysts. Further, Ea values very close to those found for the OSC suggest that the surface reduction of the catalyst (CO + σ-O→CO_2 + σ) is the rate determining step of CO oxidation in comparison to a much easier oxygen incorporation rate onto surface reduced active sites (σ + ½ O_2→σ-O) [51]. Experimental reaction orders on CO and O_2 pressure (Figure 21B) equal to 0.9 and 0.14, respectively, substantiate in fact that the oxidation activity of the $MnCeO_x$ system depends on the efficiency of the electron-transfer process from oxygen to manganese ions leading to the formation of e*lectrophylic* oxygen species [51].

Finally, rate values more than one order of magnitude greater than in absence od gas-phase oxygen (Table 4) indicate that CO oxidation entails the direct participation of gas-phase oxygen. Therefore, the occurrence of a "push-pull" redox mechanism accounts for a (quasi)simultaneous proceeding of the surface reduction and oxidation steps [56]. Nevertheless the much faster rate of the surface oxidation step is substantiated by reaction orders for both catalysts close to 1 and 0 with respect to P_{CO} and P_{O2}, respectively (Figure 21B).

Table 4. Kinetic data of CO oxidation in the range 373-423K on the M1C1-R4 and M1C1-P4 catalysts.

| Sample	T	1st cycle		sty_{Mn}	2nd cycle		sty_{Mn}
		reaction rate			reaction rate		
	(K)	($\mu mol \cdot g_{cat}^{-1} \cdot s^{-1}$)	($\mu mol \cdot g_{cat}^{-1} \cdot s^{-1}$)	(s^{-1})	($\mu mol \cdot g_{cat}^{-1} \cdot s^{-1}$)	($\mu mol \cdot g_{cat}^{-1} \cdot s^{-1}$)	(s^{-1})
	373	2.9	18.8	7.6E-4	3.3	21.4	9.7E-4
	393	5.9	38.3	1.6E-3	5.4	35.1	1.4E-3
M1C1-R	403	6.9	44.8	1.9E-3	7.6	49.4	2.0E-3
	413	n.d.	n.d.	n.d.	n.d.	n.d.	n.d.
	423	14.2	92.2	3.8E-3	13.5	87.7	3.6E-3
	403	0.9	8.9	2.4E-4	0.8	7.9	2.1E-4
M1C1-P	413	1.3	12.8	3.4E-4	1.3	12.9	3.4E-4
	423	2.0	19.8	5.1E-4	1.9	18.8	4.9E-4

158

## VI.4. Catalytic behavior in the CWAO of phenol.

VI.4.1. Effect of manganese loading

The CWAO activity data at 373K in two consecutive reaction runs of 1 hour of the M1C1 system prepared *via* the redox-precipitation (M1C1-R4) and co-precipitation (M1C1-P4) methods are shown in Figure 22 in terms of phenol and TOC conversion. The M1C1-R4 catalyst feature a superior performance than the M1C1-P4 one both in the first and second runs, ensuring a complete removal of both phenol and TOC in less than 15 min and 45 min, respectively. On the other hand, the M1C1-P4 system enables a quasi complete elimination of phenol and TOC in the first run only after 1 hour of reaction time, and a partial elimination of phenol (ca. 80%) and TOC (ca. 70%) in the second run.

Then, the effect of the Mn/Ce ratio on the CWAO activity of the redox-precipitated system is shown in Figure 23.
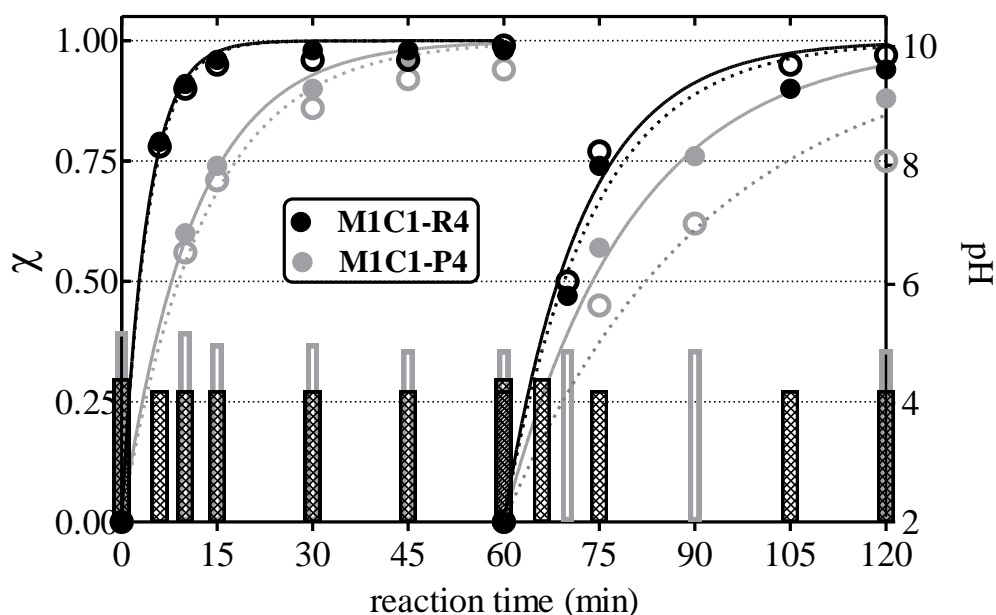
Figure 4. Effect of the preparation method on the CWAO activity of the M1C1 catalysts calcined at 673K: phenol (full symbols) and TOC (open symbols) conversion and pH of the reacting solution vs. reaction time.
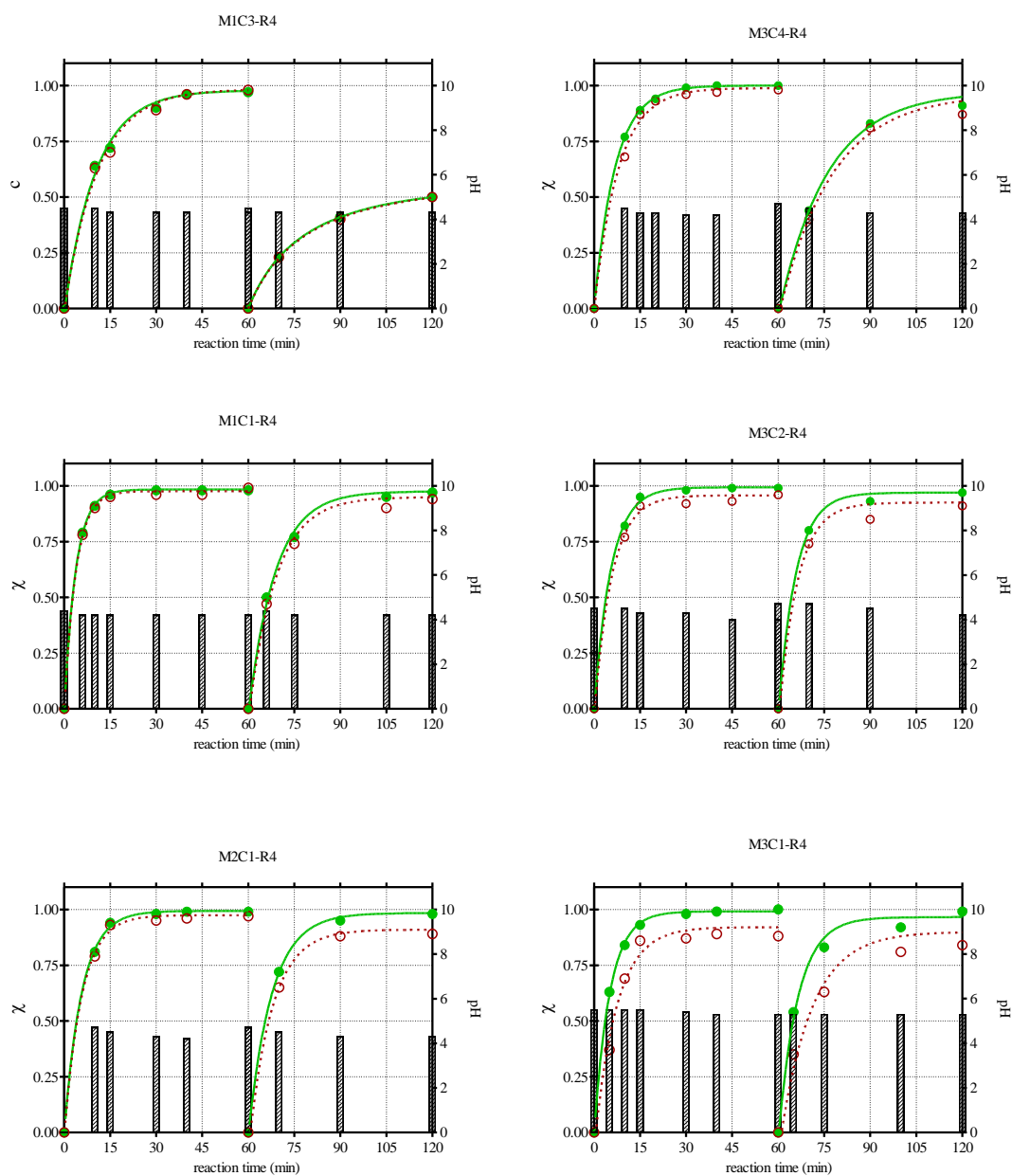
Figure 23. Effect of the Mn/Ce ratio on the CWAO activity of the redox-precipitated catalysts calcined at 673K: phenol and TOC conversion and pH of the reacting solution vs. reaction time.

All the systems feature a noticeable CWAO activity, leading to a complete and simultaneous removal of substrate and TOC in the first reaction cycle,

160

though a composition-effect emerges from time required by the various systems for water purification, mostly in the second reaction cycle.

The calculated values of the kinetic constant referred to catalyst weight ($L \cdot g_{cat}^{-1} \cdot h^{-1}$) and surface area ($L \cdot m_{cat}^{-2} \cdot h^{-1}$) [13], along with the percentage weight loss recorded by TG-DSC analyses on the various "used" samples, are compared in Table 5. In spite of a general decrease in activity, the catalysts with Mn/Ce>1 ensure a complete elimination of substrate and TOC also in the second cycle (Figure 23), except for the systems with Mn/Ce<1 attaining only a partial removal after 1 hour of reaction time.

Table 5. CWAO of phenol at 373K. Kinetic constants of phenol and TOC removal.

Catalyst	1st cycle		2nd cycle	
	k_{PhOH}	k_{TOC}	k_{PhOH}	k_{TOC}
	($L \cdot g^{-1} \cdot h^{-1}$)		($L \cdot g^{-1} \cdot h^{-1}$)	
M1C3-R4	1.1	1.0	0.2	0.2
M3C4-R4	1.8	1.5	0.7	0.6
M1C1-R4	3.0	2.9	1.3	1.1
M3C2-R4	2.1	1.9	1.2	1.0
M2C1-R4	2.0	1.9	1.1	0.8
M3C1-R4	2.4	1.9	1.1	1.0
M1C1-P4	1.1	0.9	0.6	0.4
M1C1-R4L	2.3	2.1	1.2	1.1
M1C1-R4N	2.0	1.9	0.3	0.3
M1C1-R	3.3	3.1	1.3	1.1
M1C1-R6	1.4	1.3	0.9	0.8

The kinetic constants plotted against the Mn/Ce ratio provide, then, a volcano-shaped relationship, indicating the value of 1 as the optimum catalyst composition for the Mn/Ce system (Figure 24). In comparison to redox-precipitated catalysts the co-precipitated system features a much lower activity, well evident from Figure 24A. Considering that the removal of the substrate and TOC depends on the adsorption at the catalyst surface [51,52], such finding surmises a correlation with the textural properties of the catalysts. This is evident from Figure 24B, showing an optimum value in APD

comprised between 10 and 15 nm to ensure the faster rate of phenol and TOC adsorption. Because of intraparticle diffusion resistances, it is likely that a pore diameter smaller than ca. 10 nm hinders the phenol adsorption, resulting yet in a slight release of intermediates, proved by very close values of the kinetic constant of phenol and TOC removal. On the other hand, a pore size diameter larger than 10 nm allows a fast adsorption of phenol implying yet an easier release of intermediates that accounts for an increased gap between k_{phen} and k_{TOC} values (Figure 24).
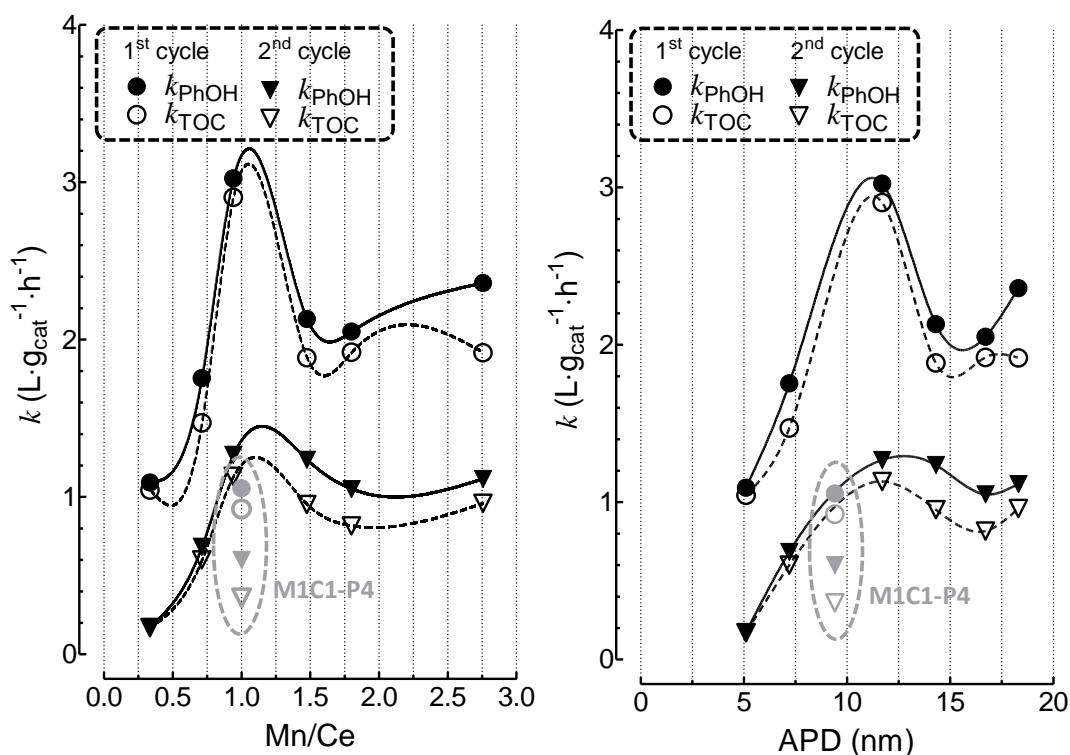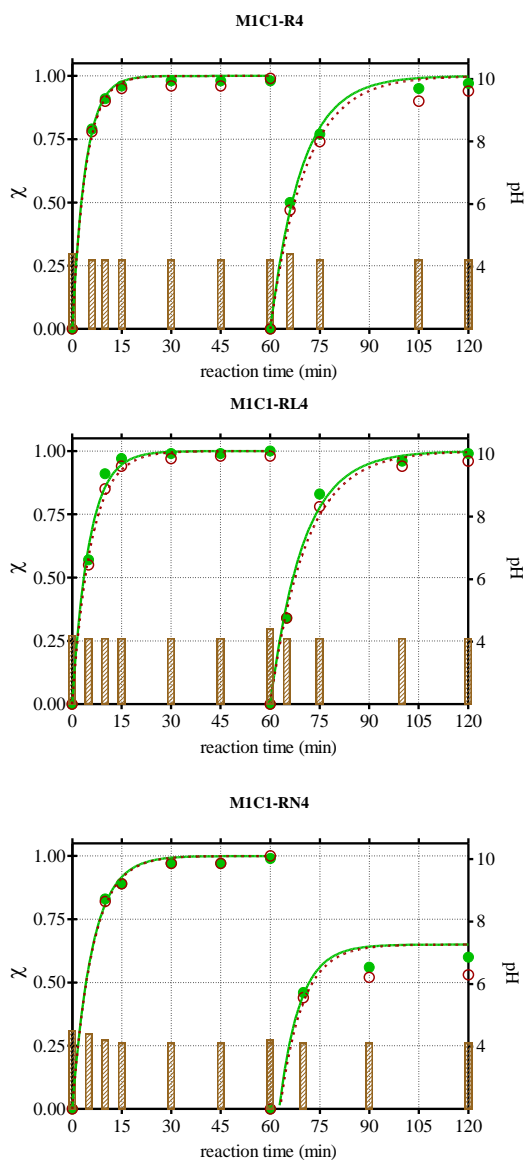

Figure 24. A) Relationships between the kinetic constant of phenol and TOC conversion in the first and second reaction cycles and Mn/Ce ratio; B) Relationships between the kinetic constant of phenol and TOC conversion in the first and second reaction cycles and average pore diameter.

VI.4.2. Effect of synthesis parameter

Such findings are substantiated by the CWAO data of the M1C1-R4 system obtained using various types of bases.

Figure 25. Effect of the type of base used for the synthesis and the CWAO activity of the M1C1-R4 catalyst: phenol and TOC conversion and pH of the reacting solution vs. reaction time.

Data shown in Figure 25 display a similar activity in the first and second reaction cycles for catalysts prepared using KOH and LiOH, whilst that obtained using NH_4OH is considerably less active, mostly in the second reaction cycle when it attains a plateau of ca. 50% in the elimination of phenol and TOC.

Also in this case, a direct relationship between the kinetic constants and pore diameter (Figure 26) suggests the fundamental role of the textural properties on the CWAO pattern of the $MnCeO_x$ system.
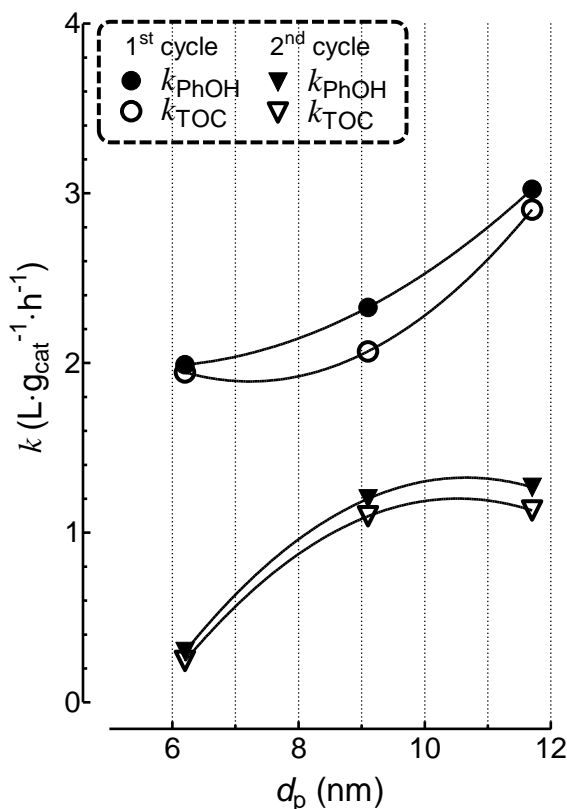

Figure 26. Relationhipss between the kinetic constant of phenol and TOC conversion in the first and second reaction cycles and average pore diameter of the M1C1-R4 catalyst (see Figure 25).

VI.4.3. Effect of calcination temperature

Since the calcination temperature affects both the textural properties and redox pattern it is expected that it has remarkable consequences on the

CWAO pattern of the M1C1-R system, as confirmed by the activity data shown in Figure 27.

The reactivity of the system is not significantly affected for a calcination temperature in the range 373-673K, whilst the M1C1-R6 system displays a considerably activity loss that is evidently related to both the marked SA decay and the considerable broadening of the APD (Figure 27).
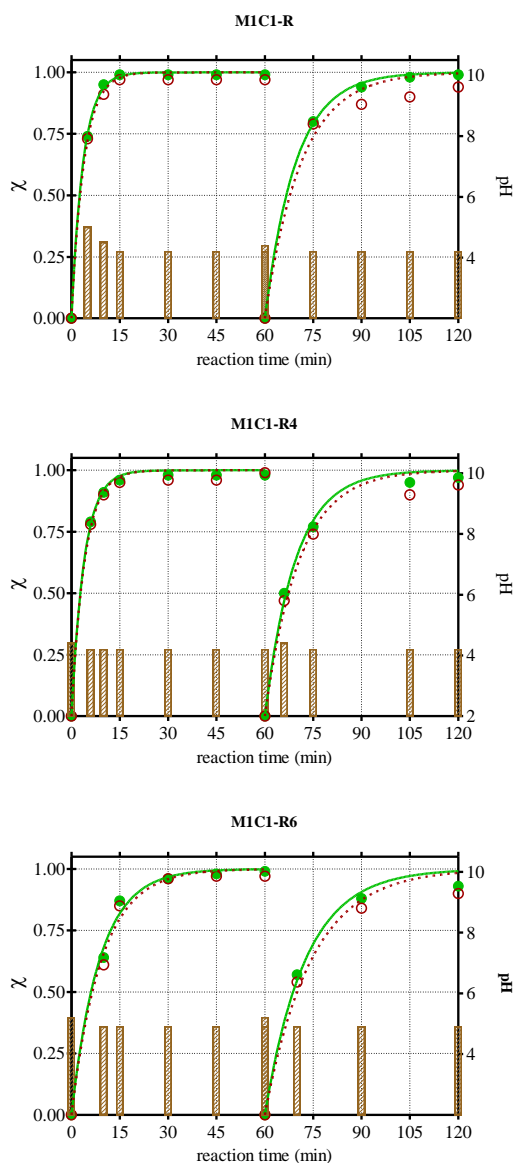

Figure 9. Effect of the calcination temperature on the CWAO activity of the M1C1-R catalyst: phenol and TOC conversion and pH of the reacting solution vs. reaction time.

VI.4.4. CO_2 selectivity

We further evaluated the carbon dioxide selectivity by bubbling the outlet reactor stream into a $BaOH_2$ solution. The CO_2 selectivity obtained a the end of each testing is never higher than 4.0%, even though it represents a very high improvement respect to the 0.5% value reported in a previous work, relative to a coprecipitated system [13]. In particular, as can be seen from Figure 28 where the CO_2 selectivity is reported for each sample, the mineralization efficiency depends on the manganese loading, increasing progressively from a minimum of 1.2% for the M1C3-R4 catalyst to a maximum of 3.4% for the M3C1-R4 one.

An opposite effect is observable for the calcination temperature, as the dried sample shows the best performance, while the M1C1-R6 catalyst seems to be totally inactive in mineralizing the substrate under the adopted reaction conditions. The catalysts prepared with different bases showed practically
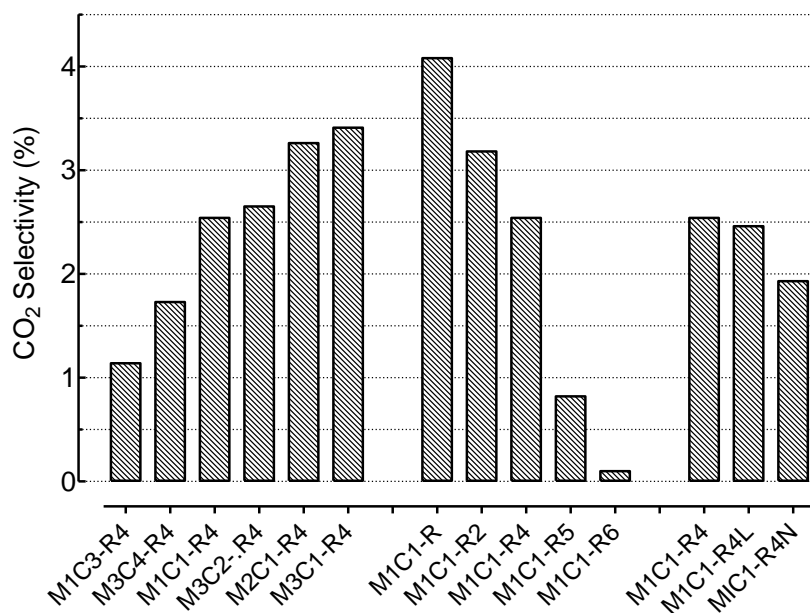
Figure 28. Overview of the CO_2 selectivity of the various catalysts in the CWAO of phenol at 373K.

similar CO_2 selectivity, the only exception being the M1C1-R4N sample, which gets also a minor phenol and TOC abatement. The mild temperature adopted to carry out the CWAO, corresponding to the most common employed in literature [1-22], lay down in correspondence to the onset reduction temperature of the redox-precipitated catalysts. Then, the CO_2 selectivity should be related to the redox properties of the catalysts [13], since an easier catalyst reducibility implies a more effective electron-transfer between Mn^{n+} and O^{2-} ions (i.e., $Mn^{n+}-O^{2-} \rightarrow Mn^{(n-1)+}-O^-$) favoring the generation of *electrophylic* oxygen species (O_2^-, O_2^{2-}, O^-, etc.) which drive the total oxidation [24]. In fact, the CO_2 selectivity values of the different catalysts are directly associated to the relative extent of H_2 consumption recorded by TPR measurements.
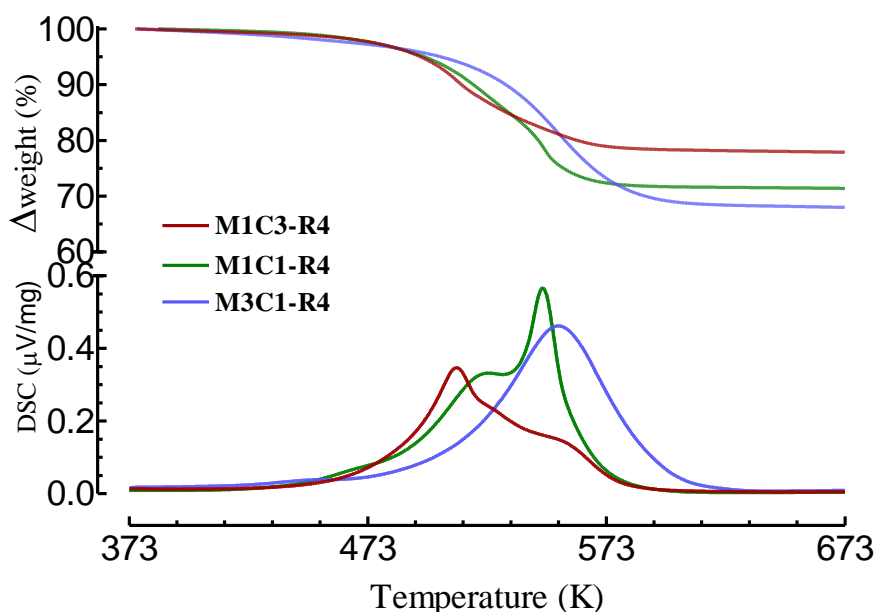

Figure 29. TGA analyses performed on M1C3-R4, M1C1-R4 and M3C1-R4 catalysts recovered after CWAO of phenol at 150°C and 10atm.

Probatory evidences of the quasi unique substrate adsorption on the catalyst surface are given by TGA analyses of representative "used" samples. A weight loss corresponding, in any case, to the amount of phenol converted

during the two reaction cycles is evident from Figure 29. In fact, the less active M1C3-R4 sample, which converted only 50% of phenol during the second cycle, shows a weight decrease of 21% against 27-29% for the M1C1-R4 and M3C1-R4 ones. The slightly higher weight loss displayed by the more selective M3C1-R4 catalyst, coupled with a more elevated temperature necessary for the complete oxidation, could be attributed to an incipient oxidation/degradation of the substrate over the catalyst surface, which lead to the presence of high molecular weight compounds, with some oxygen atoms inserted in the C-C chain, on the catalyst surface.

Selectivity data on CO_2 production can be related to redox properties of the $MnCeO_x$ samples, as shown on Figure 30 where the H_2 consumption calculated from TPR measurements (Table 2) is plotted against mineralization selectivity. Catalyst with different characteristics, as calcination treatment or synthesis procedure, does not present the same relationship. In fact, these catalysts, at a glance, have got diverse surface exposure and the dried sample shows the highest selectivity, while the M1C1-R6 one is not able to produce the carbon dioxide. On the other hand the co-precipitated system, as expected, shows lower oxidative activity, due to its poorer overall features.
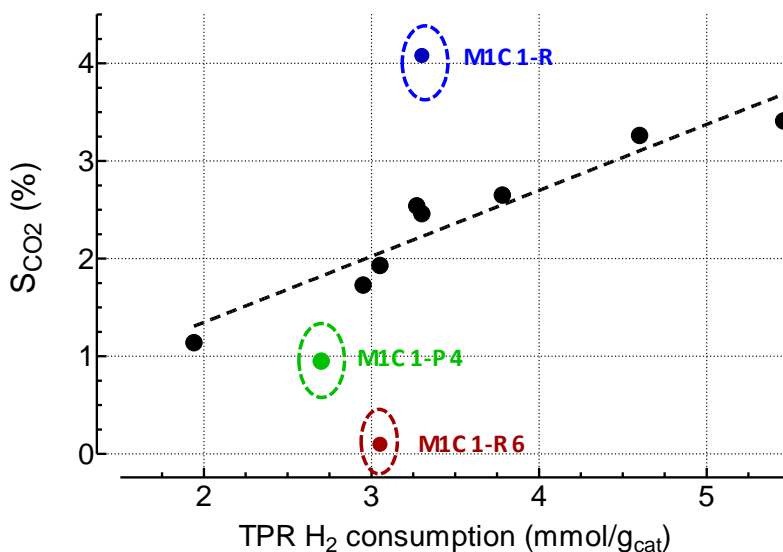
Figure 30. Relationship between H_2 consumption (from TPR data) and CO_2 selectivity.

VI. 5. Effect of temperature on the CWAO of phenol

Notwithstanding the good results both in terms of improvement of textural and redox features and of CWAO activity, last evidences confirm the reaction mechanism proposed at the end of section V also for the novel redox-precipitated system. In fact, though the reaction proceed with a very clean path due to the quasi absence of both phenol and intermediates into the reacting solution, evident also by the transparency of solutions periodically withdrawn for HPLC analyses (test conducted with the co-precipitated catalyst present a yellowish color in the very initial reaction minutes), the CO_2 selectivity is yet low with a value of 5% for the most efficient sample (M1C1-R4, Figure 28).
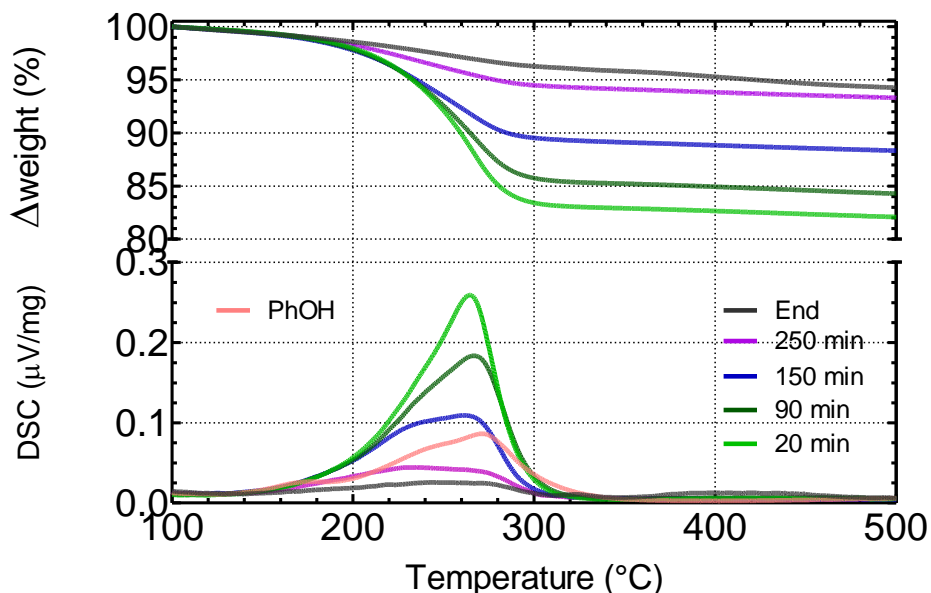
**Figure 30.** TGA-DSC analyses of samples withdrawn from the reactor at different reaction time. TGA analysis of fresh M1C1-R4 catalyst adsorbed with 5%wt phenol is reported for reference.

Effective confirmation of the proposed reaction path come out from TGA analyses of samples periodically withdrawn from the reactor during a CWAO test conducted at 150°C and 1.4MPa for 6 hours. Higher reaction temperatures

would promote the mineralization and the amount of carbonaceous species initially adsorbed on the catalyst surface progressively diminishes along with reaction time.

Figure 30 confirm our expectation and, as a consequence, definitively asses the above proposed reaction mechanism which state that the phenol rapidly adsorb on the catalyst surface in consequence of its surface exposure. The subsequent slow oxidization to CO_2 by activated oxygen species present on the catalyst surface, the amount of which depending on the catalyst redox features, represent the rate determining step of the overall reaction.

Catalytic wet oxidation at temperatures ranging from 110 to 150°C allows to shed further lights on the mineralization capacity of the $MnCeO_x$ system. As expected, the "redox-precipitated" catalyst present the better selectivity at each temperature while the co-precipitated present an appreciable CO_2 productivity only at 130°C. Anyway, the former sample presents a faster kinetics with a descending rate just after 2 hours of reaction time, due to the quasi substrate consumption at the catalyst surface, as shown on Figure 31.
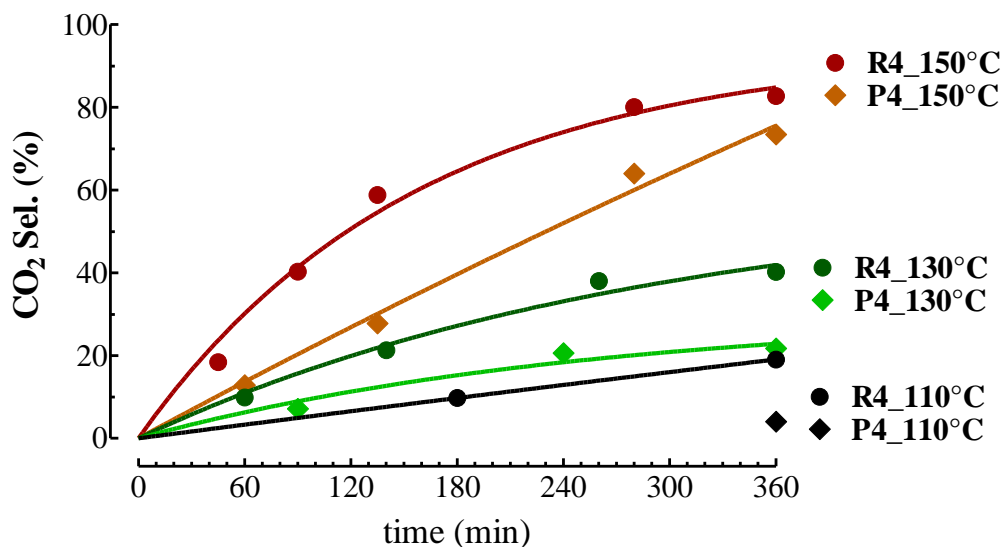
Figure 31. CWAO of phenol at Temperatures in the range 110-150°C in the presence of "redox" and co-precipitated catalysts.

Finally, Arrhenius plot of kinetic values derived from experimental data exposed on Figure 31 gives an activation energy for the CO_2 production equal to 75KJ/mol, as shown on Figure 32.
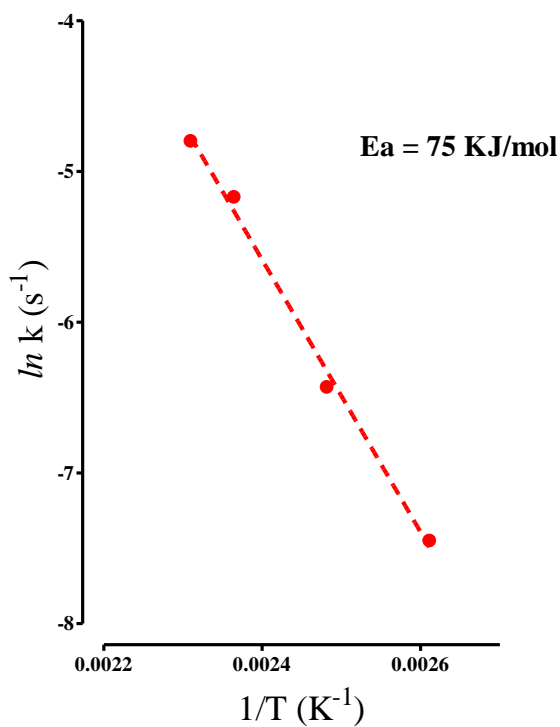
Figure 32. Arrhenius plot of the CWAO of phenol on redox-precipitated catalyst.

VI.6. References

[1]. F. Larachi, *Top. Catal.* **33** (2005) 109.

[2]. S.K. Bhargava, J. Tardio, J. Prasad, K. Foger, D.B. Akolekar, S.C. Grocott, *Ind. Eng. Chem. Res.* **45** (2006) 1221.

[3]. A. Cybulski, *Ind. Eng. Chem. Res.*, **46**, (2007) 4007.

[4]. S. Imamura, *Ind. Eng. Chem. Res.* **38** (1999) 1743.

[5]. Yu.I. Matatov-Meytal, M. Sheintuch, *Ind. Eng. Chem. Res.* **37** (1998) 309.

[6]. H.Chen, A. Sayari, A. Adnot, F. Larachi, *Appl. Catal. B: Environmental*, **32** (2001) 195.

[7]. S. Hamoudi, F. Larachi, A. Sayari, *J. Catal.,* **177 (**1998) 247.

[8]. S.T. Hussain, A. Sayari, F. Larachi, *Appl. Catal. B: Environmental*, **34** (2001) 1.

[9]. S.T. Hussain, A. Sayari, F. Larachi, *J. Catal.* **201** (2001) 153

[10]. I. Iliuta, F Larachi, *Chem. Eng. Process.* **40**, (2001) 175.

[11]. M. Abecassis-Wolfovich, M.V. Landau, A. Brenner, M. Herskowitz, *Ind. Eng. Chem. Res.* **43** (2004) 5089.

[12]. M. Abecassis-Wolfovich, R. Jothiramalingam, M.V. Landau, M. Herrskowitz, B. Viswanathan, *Appl. Catal. B* **59** (2005) 91.

[13]. F. Arena, J. Negro, G. Trunfio, A. Parmaliana, *Ind. Eng. Chem. Res.* **46** (2007) 6724.

[14]. F. Arena, A. Parmaliana, G. Trunfio, *Sci. Tec. Catal.* **172** (2007) 489.

[15]. F. Arena, G. Trunfio, J. Negro, L. Spadaro, *Appl. Catal. B* **85** (2008) 40.

[16]. F. Arena, G. Trunfio, J. Negro, B. Fazio, L. Spadaro, *Chem. Mater.* **19** (2007) 2269.

[17]. F. Arena, G. Trunfio, J. Negro, L. Spadaro, *Mater. Res. Bull.* **43** (2008) 539.

[18]. F. Arena, G. Trunfio, J. Negro, L. Spadaro, *Appl. Catal. B* **59** (2008).

[19]. F. Arena, G. Trunfio, B. Fazio, J. Negro, L. Spadaro, *J. Phys. Chem. C* accepted for publication.

[20]. S.-K. Kim, S.-K. Ihm, *Top. Catal.* **33** (2005) 171.

[21]. S-K Kim, S-K Ihm, *Ind. Eng. Chem. Res.* **41** (2002) 1967.

[22]. A.M.T. Silva, R.R.N. Marques, R.M. Quinta-Ferreira, *Appl. Catal. B* **47** (2004) 269.

[23]. S. Imamura, I. Fukuda, S. Ishida, *Ind. Eng. Chem. Res.* **27 (4)** (1988) 718.

[24]. A.F.J Santiago, J.F. Sousa, R.C. Guedes, C.E.M. Jerônimo, M. Benachour, *J. Hazard. Mat. B* **2006**, *38*, 325

[25]. G.Y. Adachi, T. Masui, In *Catalysis by Ceria and Related Materials*; Trovarelli, A., Ed.; Imperial College Press: London, U.K., 2002; Vol. 3, p 51.

[26]. S.T. Kolaczkowski, P. Pluciuski, F.J. Beltran, F.J. Rivas, D.B. Melurgh, *Chem. Eng. J.*, **73** (1999) 149.

[27]. I.M. Kolthoff, E.B. Sandell, E.J. Mehan, S. Bruckenstein, *Quantitative Analytical Chemistry*, vol. 1 (p. 268), Piccin Edition, Padua, ITALY, (1973).

[28]. L.-X. Yang, Y.-J. Zhu, G.-F. Cheng, *Mater. Res. Bull.* **2007**, *42*, 159.

[29]. S. Liang, F. Teng, G. Bulgan, R. Zong, Y. Zhu, *J. Phys. Chem. C* **2008**, *112*, 5307.

[30]. Y. Liu, M. Luo, Z. Whei, Q. Xin, P. Ying, C. Li, C. *Appl. Catal. B* **2001**, *29*, 61.

[31]. A. Gil, L.M. Gandía, S.A Korili, *Appl. Catal. A* **2004**, *274*, 229.

[32]. W.B. Li, W.B. Chu, M. Zhang, J. Hua, *Catal. Today* **2004,** *93-95*, 205.

[33]. L. Lamaita, M.A. Peluso, J.E. Sambeth, H.J. Thomas, *Appl. Catal. B* **2005,** *61,* 114.

[34]. I. Barrio, I. Legórburu, M. Montes, M.I. Domínguez, M.A. Centeno, J.A. Odriozola, *Catal. Lett.* **2005,** *101*, 151.

[35]. R. Cracium, *Sol. St. Ion.*, **110** (1998) 87.

[36]. R. Cracium, *Catal. Lett.*, **55** (1998) 25.

[37]. G. Qi, R.T. Yang, *J. Catal.*, **217** (2003) 434.

[38]. D. Terribile, A. Trovarelli, C. de Leitnburg, A. Primavera, G. Dolcetti, *Catal. Today*, **47** (1999) 133.

[39]. S. Tsunekawa, R. Sivamohan, S. Ito, A. Kasuya, T. Fukuda, *Nanostruct. Mater.*, **11** (1999) 141.

[40]. C. Burda, X.B. Chen, R. Narayanan, M. El-Sayed, M. *Chem. Rev.* **2005**, *105*, 1025.

[41]. Z.L. Wang, X. Feng, *J. Phys. Chem. B* **2003**, *107*, 12563.

[42]. A. Bumajad, M.I. Zaki, J. Eastoe, L. Pasupulety, *Langmuir* **2004,** *20*, 11223.

[43]. J.R. McBride, K.C. Hass, B.D. Poindexter, W.H. Weber, *J. Appl. Phys.* **1994**, *76*, 2435.

[44]. F. Buciuman, F. Patcas, R. Craciun, D.R.T. Zahn, *Phys. Chem. Chem. Phys.* **1999**, *1*, 185.

[45]. M.C. Bernard, A. Hugot-Le Goff, B. Vu Thi, S.C. de Torresi, *J. Electrochem. Soc.* **1993**, *140*, 3065.

[46]. C. Julien, M. Massot, S. Rangan, M. Lemal, D. Guyomard, *J. Raman Spectrosc.* **2002**, *33*, 223.

[47]. D.R. Mullins, S.H. Overbury, D.R. Huntley, *Surf. Sci.* **1998**, *409*, 307.

[48]. J.Z. Shyu, W.H. Weber, H.S. Gandhi, *J. Phys. Chem.* **1998**, *92*, 4964.

[49]. F. Larachi, J. Pierre, A. Adnot, A. Bernis, *Appl. Surf. Sci.* **2002**, *195*, 236.

[50]. M. Romeo, K. Bak, J. El Fallah, F. le Normand, L. Hilaire, *Surf. Interf. Anal.* **1993**, *20*, 508

[51]. A. Bielañski, J. Haber, In: *Oxygen in Catalysis.* New York, New York: Marcel Dekker, Inc(1991).

[52]. G. Blanco, M.A. Cauqui, J.J. Delgado, A. Galtayries, J.A. Perez-Omil, J.M. Rodriguez-Izquierdo, *Surf. Int. Analys.* 36 (2004). 752.

[53]. M.I. Zaki, C.Z. Kappenstein, *Phys. Chem.* **1992**, *176*, 97.

[54]. P. Bera, A.Gaten, M.S. Hegdé, L. Spadaro, F. Frusteri, F. Arena, *J. Phys. Chem. B* **2003**, *107*, 6122.

[55]. D. Duprez, C. Descorme, in Catalysis by Ceria and Related Materials (A. Trovarelli, Ed.), Imperial College Press, London, UK, 7 (2002) 243.

[56]. Arena, F.; Famulari, P.; Trunfio, G.; Bonura, G.; Frusteri, F.; Spadaro, L. *Appl. Catal. B* **2006**, *66*, 81.

Conclusions

On the basis of literature overwiew, the Catalytic Wet Air Oxidation represents to date the most promising alternative among the various technologies, for an effective detoxification of industrial wastewaters streams, because of its high versatility in terms of COD load and feed rate. However, the lack of an adequate catalyst formulation hinders the applicability on an industrial scale of the CWAO process.

On account of the above consideration, the work described in this PhD Thesis has been devoted to a careful assessment of the reaction mechanism in the presence of both homogeneous and heterogeneous catalysts with the aim of developing a new effective and low costly heterogeneous catalytic system that could open real perspectives to large scale CWAO applications. Then, the main results of my research activity in the field of CWAO can be summarized as follows:

- The poor reproducibility of blank test results depends upon the leaching of Fe^{3+} ions further to reactor-shield corrosion phenomena.
- Homogeneous catalysts drive an unselective homogeneous free-radical reaction path, while a classical surface L-H mechanism greatly promotes the CWAO efficiency of the heterogeneous $MnCeO_x$ system.
- The formation of common acidic intermediates and the low intrinsic activity of solid catalysts likely explain the assumption of a homogeneous radical path accounting for the CWAO pattern of both homogeneous and heterogeneous systems.
- A fast surface adsorption of the substrate accounts for a high water decontamination efficiency of the $MnCeO_x$ system, while the combustion of adsorbed species is the rate limiting step *(r.l.s.)* determining the selectivity pattern and the catalyst stability against fouling phenomena and indicating that the CWAO of phenol proceeds via a classic heterogeneous "redox" reaction path.
- Both textural and redox properties affect the performance of the title system in the CWAO of phenol.

- The new redox-precipitation route allows to obtain highly dispersed $MnCeO_x$ systems with much improved physico-chemical properties in comparison to conventional co-precipitated systems.

- Irrespective of manganese loading (in the range 9-33 wt %), the redox precipitation route ensures larger surface area exposure and dispersion of the active phase.

- The monolayer dispersion of the active phase enhances the redox behavior and the surface affinity to oxygen of redox-precipitated $MnCeO_x$ catalysts in comparison to conventional coprecipitated systems.

- The monolayer dispersion of the active phase prompts an easy reduction of the catalyst, markedly promoting the oxygen storage capacity of the system in the range 323-423K.

- The molecular patterning of redox-precipitated catalysts greatly enhance the low temperature CO oxidation activity, resulting also in a very high stability under redox reaction conditions.

- The reducibility of the active phase determines the rate of electron-transfers from oxygen to manganese ions and the consequent formation of electrophylic oxygen species, playing thus a fundamental role on the catalytic oxidation pattern of the $MnCeO_x$ system.

- The redox-precipitated catalysts exhibit a superior performance in the CWAO of phenol under mild reaction conditions both in terms of activity and CO_2 selectivity.

- An optimum catalyst composition (Mn/Ce, 1) and APD ensures a superior efficiency in the removal of both phenol and TOC, while the mineralization selectivity relies on the redox properties of the catalyst.

- Structural, redox and catalytic features of redox-precipitated systems are slightly affected by the calcination treatment in the range 373-673K, while at 873K a marked structural rearrangement has a strongly negative effect on the CWAO performance.

- The molecular dispersion of the active phase prompts an easy reduction of the active phase speeding-up the oxidation rate of surface adsorbed C-containing intermediates, which is the *r.l.s.* of the CWAO of phenol.

- The absence of any intermediate into the reacting solution during reaction time and the high catalysyt stability make the new system "clean" and suitable for the development of the process at industrial scale.

Biographical note

Name: Giuseppe TRUNFIO

Date of birth: 08/02/1975

Education:

28/03/2003, MSC, Università di Messina. Title of the Thesis: *"Activity and stability of Ni-based catalyst for the pre-reforming process"*

Publications:

- Arena F., Trunfio G., Fazio B., Negro J., Spadaro L., *J. Phys. Chem. C,* 113 (7) (2009) 2822.
- Arena F., Trunfio G., Negro J., Spadaro L., *Appl. Catal. B,* 85 (2008) 40.
- Arena F., Trunfio G., Negro J., Spadaro L. *Mat. Res. Bull.,* 43 (2008) 539.
- F. Arena, A. Parmaliana, Trunfio G. (2008). In: Science and Technology in Catalysis 172: 489-492. (vol. 172, pp. 489-492). TOKYO: Elsevier (JAPAN).
- Arena F., Trunfio G., Negro J., Fazio B., Spadaro L. *Chem. Mater.,* *19 (*2007) *2269.*
- Arena F, Negro J, Parmaliana A, Spadaro L, Trunfio G. *Ind. Eng. Chem. Res.,* *46 (*2007)*6724.*
- Arena F.; Alongi E.; Famulari P.; Parmaliana A.; Trunfio G. *Catal. Lett.,* *107 (*2006) 39.

Contributions in Congresses:

- F. Arena, G. Trunfio, J. Negro, B. Fazio, L. Spadaro. (2008) *14th ICC.* Seoul, Korea, 13-18/07/2008.
- F. Arena, G. Trunfio, J. Negro, L. Spadaro. (2008) *14th ICC.* Seoul, Korea, 13-18/07/2008.
- Trunfio G., Negro J, Spadaro L, Arena F. (2008) *3rd International Symposium on Environment.* Athens, Greece, 21-24/05/2008.
- F. Arena, J. Negro, A. Parmaliana, L. Spadaro, Trunfio G. (2006) *MCEE 2006.* Venice, Italy, 4-6/10/2006.

- F. Arena, Trunfio G., J. Negro, L. Spadaro, A. Parmaliana. (2006) *SCI2006*. Florence, Italy, 10-15/09/2006.
- Arena F., Parmaliana A., Trunfio G. (2006) *TOCAT5*. Tokyo, Japan. 21-27/07/2006.